uOttawa

L'Université canadienne
Canada's university

FACULTÉ DES ÉTUDES SUPÉRIEURES ET POSTOCTORALES

uOttawa

L'Université canadienne
Canada's university

FACULTY OF GRADUATE AND POSDOCTORAL STUDIES

Yun Li

AUTEUR DE LA THÈSE / AUTHOR OF THESIS

Ph.D. (Physics)

GRADE / DEGREE

Department of Physics

FACULTÉ, ÉCOLE, DÉPARTEMENT / FACULTY, SCHOOL, DEPARTMENT

Development of the Distributed Brillouin Sensor with High Spatial and Frequency Resolution

TITRE DE LA THÈSE / TITLE OF THESIS

Xiaoyi Bao

DIRECTEUR (DIRECTRICE) DE LA THÈSE / THESIS SUPERVISOR

Liang Chen

CO-DIRECTEUR (CO-DIRECTRICE) DE LA THÈSE / THESIS CO-SUPERVISOR

Andrzei Czajkowski

Heather Logan

Zbigniew Stadnik

Chang-Qing Xu (McMaster University)

Gary W. Slater

Le Doyen de la Faculté des études supérieures et postdoctorales / Dean of the Faculty of Graduate and Postdoctoral Studies

Development of the Distributed Brillouin Sensor with High Spatial and Frequency Resolution

by

Yun Li

Thesis submitted to the
Faculty of Graduate and Postdoctoral Studies
In partial fulfillment of the requirements for the Degree of

Doctor of Philosophy

Ottawa-Carleton Institute for Physics
University of Ottawa
Ottawa, Canada

Your file Votre référence
ISBN: 978-0-494-65567-2
Our file Notre référence
ISBN: 978-0-494-65567-2

To my family

Abstract

This thesis includes studies of improving the performance of the distributed fiber optic sensor based on Brillouin scattering, especially focusing on spatial resolution and frequency resolution.

A novel distributed Brillouin sensor based on offset locking of two distributed feedback lasers has been developed. With offset locking technique, the beat frequency of two lasers can not only be locked together but also be tuned over a wide range of more than 1GHz. Moreover, a lock-in amplifier has been applied to lock the bias drift of the electro optic modulator, which ensures the probe pulse stability and constant signal-to-noise ratio during the sensing measurement. With the offset locking based distributed Brillouin sensor, a 1m spatial resolution and 0.5°C temperature resolution has been achieved.

High spatial and frequency resolution Brillouin sensor with phase locking technique has been studied. A theoretical model dealing with laser source phase locking has been derived. Simulation and experimental results have been used to prove the ability of improving the spatial and frequency resolution with phase locking technique.

Improving the spatial and frequency resolution with different pulse pair technique has been explored. This technique can obtain high spatial resolution (<1m) and high frequency resolution (<35MHz linewidth) simultaneously along several kilometer long sensing fiber, which is a promising candidate in the field of structure health monitoring. The ultimate measurement accuracy with different pulse pair Brillouin optical time domain analysis technique has been investigated and it is determined by the combination of the system bandwidth, system signal-to-noise ratio, absolute pulse width, pulse width difference, and the rise/fall time of the pulse.

A Brillouin optical time domain analysis sensor based on optical differential parametric amplification technique has been proposed and realized to obtain high spatial and frequency resolution at the same time without increasing the measurement time. A new theoretical model dealing with optical differential parametric amplification technique has been derived. An experiment is successfully realized to validate the proposal in a polarization maintaining fiber with a spatial resolution of 0.5 m and a strain accuracy of 6 με.

Statement of Originality

This work contains no material which has been accepted for the award of any other degree or diploma in any University or other tertiary institution and, to the best of my knowledge and belief, contains no material previously published or written by another person, except where due reference has been made in the text.

I give consent to this copy of my thesis, when deposited in the University Library, being available for loan and photocopying.

SIGNED: .....

DATE: .....

Supervisors: Dr. Xiaoyi Bao and Dr. Liang Chen

Acknowledgements

It is my pleasure to take this opportunity to thank all the people who have helped me over the past few years.

First of all, I would like to thank my supervisor Dr. Xiaoyi Bao, who invited me to join her group as a graduate student and gave me the chance to do research in fiber optic sensors. I am grateful for the interest she shows in my progress and for the guidance she gave me. She is more than a supervisor, her diligence and persistence in research has set an example for me. Also I would like to thank Dr. Liang Chen. He gave me lots of directions in my theoretical and numerical study of Brillouin sensor. His critical and thoughtful approach to problems was always instructive.

Many thanks to my colleagues in Fiber Optics Group at University of Ottawa. Your comments and suggestions have greatly benefited me. Special thanks to Evgueni A. Ponomarev, Lufan Zou, Fabien Ravet, Jeffry Snoddy, Wenhai Li, and Yongkang Dong for their kind help and valuable suggestions in developing distributed Brillouin sensors.

I could not forget my friends, Ziyi and Wei. They were with me whenever I got

confused, lost and disappointed. I would like to express my hearty appreciation to them.

I am deeply indebted to my family in China, especially my parents and grandparents. Their enduring love and understanding give me the strength to overcome the challenges of taking the Ph.D study. To them, I dedicate this thesis.

I cannot end without thanking Bo, my husband. No words can describe my feelings, gratitude and appreciation to him. His continual love, support, encouragement, tolerance and patience made this work possible.

Contents

List of Figures

List of Tables

List of Acronyms

AOM:	Acoustic-Optic Modulator
BG:	Brillouin Gain
BL:	Brillouin Loss
BOFDA:	Brillouin Optical Frequency Domain Analysis
BOTDA:	Brillouin Optical Time Domain Analysis
BOTDR:	Brillouin Optical Time Domain Reflectometer
CW:	Continuous Wave
DBS:	Distributed Brillouin Sensor
DFB:	Distributed Feedback laser
DPP:	Differential Pulse width Pair
EDFA:	Erbium Doped Fiber Amplifier
EM:	Electromagnetic
EMI:	Electromagnetic Interference
EOM:	Electro-Optic Modulator
ER:	Extinction Ratio
ESA:	Electrical Spectrum Analyzer
FBG:	Fiber Bragg Grating
FUT:	Fiber Under Test

FWHM:	Full Width at Half Maximum
GPIB:	General Purpose Interface Bus
IFFT:	Inverse Fast Fourier Transform
ODPA:	Optical Differential Parametric Amplification
OSA:	Optical Spectrum Analyzer
OTDA:	Optical Time Domain Analysis
OTDR:	Optical Time Domain Reflectometer
PID:	Proportional-Integral-Derivative
PM:	Polarization Maintaining
PMF:	Polarization Maintaining Fiber
SBS:	Stimulated Brillouin Scattering
SHM:	Structural Health Monitoring
SNR:	Signal-to-Noise Ratio
SOP:	State of Polarization

Chapter 1

Introduction

Over the past decades, distributed fiber optic sensors based on Brillouin scattering have been developed and widely applied to the health monitoring of various civil structures such as dams, bridges, and pipe lines. In order to identify the early crack and deformation of the civil structures, high spatial resolution and high strain and/or temperature resolution are required. This thesis focuses on developing a distributed fiber optic sensor based on Brillouin scattering for structure health monitoring applications with high measurement accuracy, which can detect small strain (a few $\mu\varepsilon$) and/or temperature change (less than 1°C) over sections of a few centimeters along tens-of-kilometer long fiber.

This chapter introduces the background, motivation, and contribution of the research work. Section 1.1 compares the state of the art of the distributed sensing technologies that are based on Brillouin scattering and illustrates the motivation of developing high performance Brillouin sensors. Section 1.2 focuses on the contributions we made to improve the spatial resolution and the strain and/or temperature resolution of distributed Brillouin sensors. Section 1.3 presents the thesis outline.

1.1 Background and Motivation

In industrialized countries, many public civil structures, such as bridges, dams, underground power cable, and oil pipelines, are overused, leading to accelerated aging. For example, more than 150,000 bridges in the United States and over 40% of the bridges in Canada are over 40 years old. A significant percentage of them are structurally or functionally deficient, which means that they require costly rehabilitation and replacement [Lounis 2007]. In order to eliminate the risk of catastrophic structural failure, determining when the structure needs to be repaired or reinforced is then crucial. Thus, a new field, known as structural health monitoring (SHM), is currently developing in civil, mechanical, and aerospace engineering. SHM is able to continually monitor structural physical properties such as strain, pressure, vibration, and so on. Further, it can be implemented to identify early signs of potential problems, allowing for prevention of disasters and repair of the damage.

Distributed fiber optic sensor technology is one of the most promising candidates among the numerous sensor technologies that are adopted for SHM. This is due to its inherent fiber optic properties such as light in weight, small in size, non-corrosive, and the immunity to electromagnetic interference [Kersey 1996, Agrawal 2002, Culshaw 2004, Thévenaz 2006]. Fiber optic sensors can measure the structural physical properties with a certain spatial resolution at any position along a single optical fiber, and the gauge

length can be as short as tens of meters over tens-of-kilometer sensing length [Alasaarela 2002]. In applications where monitoring is required at a large number of points or on a continuum, distributed fiber optic sensors are particularly suitable.

Brillouin scattering can be used to perform distributed sensing in fibers. In Brillouin scattering, the incident light is backscattered by acoustic phonons in the fiber and the backscattered light experiences a Doppler frequency shift that is related to the speed of the acoustic waves in the fiber. The frequency shift depends on the change of outside physical conditions, such as strain and temperature; therefore, these conditions can be measured by analyzing the Brillouin loss or gain spectrum of the fiber. Distributed Brillouin sensors have attracted more and more attention in the past two decades because of the low input power requirement (a few mW), the high sensitivity to both strain and temperature, and the large measurement range from –270°C to 800°C for temperature [Fellay *et al.* 2001, Li *et al.* 2003b] and from a few με to 20,000 με for strain [DeMerchant 2000]. A variety of Brillouin sensor configurations have been developed, which are introduced as follows.

The first kind of distributed sensor based on Brillouin scattering was reported by Horiguchi and his colleagues [Horiguchi *et al.* 1989a, Horiguchi *et al.* 1989b, Horiguchi et al. 1989c] and it was named Brillouin optical time domain analysis (BOTDA). With the BOTDA technique, a 3°C temperature resolution and a 100m spatial resolution were demonstrated on a 1.2km long optical fiber by Horiguchi *et al.* using NTT's (Nippon Telephone and Telegraphs, Tokyo, Japan) BOTDA system [Kurashima *et al.* 1990].

Adopting the Brillouin loss technique rather than the Brillouin gain technique, Bao *et al.* further increased the measurement capability of Brillouin sensor to 51km sensing length with a 5m spatial resolution and a 1°C temperature resolution [Bao *et al.* 1993a, Bao *et al.* 1993b, Bao *et al.* 1995].

A second configuration known as the Brillouin optical time domain reflectometer (BOTDR) was introduced by a research laboratory of NTT in 1992 [Kurashima *et al.* 1992, Kurashima *et al.* 1993]. In the BOTDR configuration, the spontaneous Brillouin scattering light rather than the Brillouin amplification signal was detected. Because the output signal from the BOTDR sensor was proportional to the intensity of the scattered light and the local oscillator signal, a high signal-to-noise ratio (SNR) can be achieved. The BOTDR technique has the advantage of requiring access to only one end of the sensing fiber; but it has the drawback that the spontaneous Brillouin signal is much weaker than the amplified Brillouin signal of the BOTDA technique. Further, because more signals need to be collected to do average to achieve a satisfactory SNR, the measurement time of the BOTDR sensor is longer than that of the BOTDA sensor.

Niklès *et al.* at the Metrology Lab (MET-EPFL) of the Swiss Federal Institute of Technology, Switzerland developed a distributed Brillouin sensor consisting of a single laser [Niklès, *et al.* 1994]. In their configuration, the Stokes wave was generated by diverting part of the pump signal and then modulated by a sinusoidal modulation at the Brillouin frequency that was applied on electro-optic modulator (EOM). Both pump and probe were pulsed signals that propagate back and forth through the sensing fiber. The

pump pulse provided gain to the probe pulse during its forward propagation and amplified the probe pulse during its way back. The advantage of this configuration is that only a few optical components are required, only one laser source is needed, and a single fiber end is accessed. But the cost of this configuration is comparable to that of the BOTDA sensor with two lasers due to the high power tunable microwave generators for the EOM.

However, it is hard to achieve a high spatial resolution and a high frequency resolution simultaneously in distributed Brillouin sensors with either BOTDA or BOTDR techniques discussed above. Normally, in a distributed Brillouin sensor if the receiver is fast enough to respond to the launched pulse with duration τ, the spatial resolution Δl is determined by the optical pulse width τ according to $\Delta l = \frac{1}{2}\tau \cdot \upsilon$, where υ is the light velocity inside the sensing fiber [Horiguchi *et al.* 1995]. Thus, the smaller the optical pulse width, the higher the spatial resolution can be achieved. The strain and/or temperature resolution of a distributed Brillouin sensor is determined by the frequency resolution, the accuracy of the Brillouin frequency shift. The frequency resolution is determined by the linewidth and SNR of the measured Brillouin spectrum. According to Ref [Horiguchi *et al.* 1995], the Brillouin spectrum is accurately approximated by a Lorentzian function with a central frequency υ_B and a full width at half maximum (FWHM) $\Delta\upsilon_B$. The linewidth and SNR determine the minimum detectable frequency change according to $\delta\upsilon_B = \frac{\Delta\upsilon_B}{\sqrt{2}(SNR)^{\frac{1}{4}}}$, where SNR is the electrical

signal-to-noise power ratio [Horiguchi *et al.* 1995]. The minimum detectable changes of strain ($\delta\varepsilon$) and temperature (δt) are expressed as $\delta\varepsilon = \frac{\delta\upsilon_B}{C_s\upsilon_B(0)}$ and $\delta t = \frac{\delta\upsilon_B}{C_t\upsilon_B(t_r)}$, where $\upsilon_B(0)$ is the Brillouin frequency without strain, $\upsilon_B(t_r)$ is the Brillouin frequency at reference temperature, t_r is the reference temperature, and the proportional coefficients of strain and temperature are found to be $C_s = 4.6\mu\varepsilon^{-1}$ and $C_t = 9.4\times10^{-5}K^{-1}$ for single mode fiber. Thus, the narrower the linewidth of the Brillouin spectrum and the higher the SNR, the higher is the frequency resolution. However, there is a tradeoff between the spatial resolution and the frequency resolution [Horiguchi *et al.* 1995, Fellay *et al.* 1997]. The spatial resolution can be improved by using a short pulse, while a short pulse will give a broad Brillouin spectrum, which induces poor frequency resolution. Moreover, a short pulse gives weak Brillouin interaction, resulting in lower SNR. Maximum spatial resolutions of 1m are typical in the Brillouin sensors using BOTDA or BOTDR techniques. Although some progress has been made toward further improvement of the spatial resolution [Bao *et al.* 1999, Brown *et al.* 1999, Brown *et al.* 2005, Zou et al. 2005, Koyamada *et al.* 2007], they have the shortcomings of inducing gain saturation problem or having poor frequency resolution. Hence, it is difficult to achieve a high spatial resolution and a high frequency resolution simultaneously with either BOTDA or BOTDR techniques discussed above. Therefore, other techniques such as frequency domain analysis and correlation based methods are introduced.

The distributed fiber optic sensor based on Brillouin optical frequency domain analysis (BOFDA) was developed to reduce the electrical noise generated at the detection and amplification stage by Lehrstuhl für Allgemeine Elektrotechnik und Elektrooptik (AEEO) at Ruhr-University, Germany [Garus *et al.* 1996, Garus *et al.* 1997]. The BOFDA sensor was based on the measurement of a complex baseband transfer function that relates the amplitudes of counter propagating pump and the Stokes waves along a fiber length. Because of the averaging effect of the discrete inverse Fourier transform, the BOFDA sensor has higher SNR and dynamic range than a BOTDA sensor. However, its measurement time is relatively long, because high spatial resolution and long sensing range can only be achieved by increasing the frequency sweeping range and the step size respectively.

The Brillouin optical correlation domain analysis (BOCDA) technique was introduced to improve the spatial resolution of the distributed Brillouin sensor by Hotate *et al.* at the University of Tokyo [Hotate *et al.* 1999, Hotate *et al.* 2000, Hotate *et al.* 2001, Hotate *et al.* 2002, Hotate *et al.* 2003]. It used the simultaneously frequency-modulated lightwaves rather than the pulsed lightwaves to locally excite stimulated Brillouin scattering (SBS). SBS was generated at a position where the two lightwaves were highly correlated [Hotate *et al.* 2002, Song *et al.* 2006]. Recently, a Brillouin Optical Correlation Domain Reflectometry (BOCDR) configuration was also proposed to realize the measurement with only one end access [Mizuno *et al.* 2008, Mizuno *et al.* 2009]. This BOCDA/BOCDR technique can detect dynamic strain and its

spatial resolution is high (~1cm); however, it has comparatively short sensing range (hundreds of meters) and long measurement time (over hours). Because there can be only one correlation peak along the whole sensing fiber in order to obtain the correct spatial information, the sensing range is limited by the distance between two correlation peaks. The long measurement time is due to the frequency modulation of both the probe modulator and the laser source.

In SHM, an excellent sensor is expected to have the strengths of all the above techniques: good strain and/or temperature measurement accuracy, high spatial resolution, long sensing length, fast measurement time, and cost effectiveness. However, none of the existing Brillouin sensors can achieve these goals. Thus, more research is needed. In this thesis, we will show our study on improving the spatial resolution and strain and/or temperature resolution in a long length Brillouin sensor.

1.2 Thesis Contributions

In this thesis, we propose and develop BOTDA sensors with offset locking method, different pulse width pair method, and optical differential parametric amplification method respectively. BOTDA sensors with high spatial resolution and high strain and/or temperature resolution are successfully realized by the above techniques.

Firstly, we propose utilizing offset locking method to lock the beat frequency of

two DFB lasers and then build a BOTDA system. In this distributed Brillouin sensor based on offset locking technique, an optical phase locked loop is realized to lock and tune the beat frequency of the two laser sources. With the optical phase locked loop, not only the beat frequency but also the phases of the two lasers are locked together. Thus, a highly coherent Brillouin interaction can be obtained in the offset locking based Brillouin sensor. Narrow linewidth and high SNR Brillouin spectrum can be obtained due to the high efficiency of coherent Brillouin interaction. Moreover, a lock-in amplifier is utilized to stabilize the base of the probe pulse generated by EOM. This stabilizing process ensures the minimum pulse distortion when the sensing fiber is tens-of-kilometer long, prevents the probe power variation, and further increases the SNR. Narrow linewidth and high SNR of the Brillouin spectrum makes the sensing measurement with high frequency resolution possible. A 1m spatial resolution and a narrow Brillouin spectrum linewidth, which is ~60MHz for 10ns probe pulse and is less than hundreds of MHz spectrum linewidth obtained in other BOTDA sensors, can be obtained in this cost effective offset locking based distributed Brillouin sensor, where only a few optical components are used.

In order to detect small strain and/or temperature changes that occur on a short length, a Brillouin fiber sensor should have high spatial resolution, narrow spectrum linewidth, and high SNR. The 1m spatial resolution with narrow Brillouin spectrum linewidth (~60MHz for 10ns probe pulse) and high SNR (37dB) achieved by our offset locking based Brillouin sensor are much better than those (1m, hundreds of MHz

linewidth) obtained by other BOTDA sensors [Fellay et al. 1997, Horiguchi et al. 1995]. In our offset locking based BOTDA sensor, phase locking technique is adopted to lock two lasers, while other BOTDA sensors use frequency locking technique to lock the two lasers. This Brillouin spectrum linewidth narrowing phenomenon in offset locking based Brillouin sensor is caused by the phase locking of the laser sources. Nevertheless, little theoretical work has been done to compare the performance of distributed Brillouin sensors with phase locking with that with frequency locking. In this context, we have derived a general model of Brillouin scattering inside an optical fiber, which introduces a randomly varying phase to account for the laser source phase locking. The randomly varying phase has a de-correlation time associated with the inverse laser linewidth of the input optical fields. With this new model, we have obtained simulation results matching with the experimental results and proved that narrow Brillouin spectrum can be realized with phase locking technique.

A trade-off exists between the spatial resolution and the frequency resolution in distributed Brillouin sensors. As stated above, the spatial resolution is determined by the pulse width, and it can be improved by using a short pulse; however, the short pulse will give a broad Brillouin spectrum. Furthermore, the shorter pulse gives the weaker Brillouin signal and subsequently results in a lower SNR. These limitations prohibit us from obtaining a high spatial resolution and a high frequency resolution simultaneously. In this thesis, a different pulse width pair (DPP)-BOTDA technique for high spatial and high frequency resolution sensing proposed by our group will be elaborated. The

OPP-BOTDA sensor employs two separate long pulses (a few tens of nanoseconds) with a small pulse-width difference (a few nanoseconds) to map the differential Brillouin gain spectrum of the sensing fiber, which can be obtained by subtracting the two Brillouin spectra. The spatial resolution of the DPP-BOTDA sensor is determined by the pulse width difference of the two separate long pulses. The ultimate spatial and frequency resolution in the DPP-BOTDA sensor is also investigated experimentally and theoretically. It is found that in the DPP-BOTDA sensor high spatial resolution, high frequency resolution along with high SNR can be achieved by utilizing pulse pairs that have large absolute pulse width, small pulse width difference, and short pulse rise/fall time.

The DPP-BOTDA technique provides two major advantages over conventional BOTDA techniques. The first one is the stronger signal intensity and thus the better SNR because of the differential Brillouin signal detected. The second one is the simultaneous obtaining of narrow linewidth Brillouin spectrum (a few tens of MHz) and high spatial resolution (< 1m) because of two long pulses used. However, the DPP-BOTDA sensor has the disadvantage that the measurement time is twice of the conventional BOTDA sensor. In this thesis, for the first time to the best of our knowledge, a Brillouin sensor that is based on optical differential parametric amplification (ODPA) is proposed. In the ODPA-BOTDA sensor, two long pulses with a small pulse width difference at the Stokes and anti-Stokes frequencies interact respectively with continuous wave (CW) sensing wave through two

counter-propagating acoustic waves, and create Brillouin gain and loss at the same position simultaneously. At the overlapping region of the two long pulses, the gain and loss can cancel each other out when they are well balanced, which can achieve the effect similar to that gained by the subtraction process in the DPP-BOTDA sensor. However, in the ODPA-BOTDA sensor the "subtraction" process is realized in the optical field via optical differential parametric amplification. This sensor has the same advantages as the DPP-BOTDA sensor, while the measurement time and noise is reduced by half due to the one time measurement with respect to the two times needed in the DPP-BOTDA sensor. In addition, both the DPP-BOTDA sensor and the ODPA-BOTDA sensor use photodetector to collect the data. While the higher the signal intensity, the easier the photodetector will get saturated because of its limited dynamic range. Because the DPP-BOTDA sensor detects the normal Brillouin signal directly, it will be easier for the photodetector to become saturated with large signal when the sensing length is long. While in the ODPA-BOTDA sensor, the signals have been subtracted in the optical field before reaching the photodetector, it is less likely for the photodetector to become saturated in the ODPA-BOTDA sensor than in the DPP-BOTDA sensor. With this ODPA technique, high spatial resolution (50cm) and narrow Brillouin spectrum linewidth (52MHz for 20/15ns pulse pair) can be realized simultaneously.

1.3 Thesis Outline

This thesis contains seven chapters and is organized as follows.

Chapter 2 presents the physics of the Brillouin scattering. We start from the nonlinear optical phenomenon, go through the physics of light scattering, and then discuss the spontaneous Brillouin scattering and the stimulated Brillouin scattering separately. The polarization and phase effects in Brillouin scattering are also addressed.

Chapter 3 describes the offset locking based distributed Brillouin sensor. The configuration of the offset locking based distributed Brillouin sensor and the sensor's working principle are presented.

Chapter 4 studies the Brillouin spectrum narrowing with the phase locking method. A theoretical model dealing with optical source phase locking is presented and the theoretical calculation results are compared with the experimental results.

Chapter 5 focuses on building high spatial and frequency resolution Brillouin sensor with the different pulse width pair method. The working principle and experimental results of the DPP-BOTDA sensor are given and the ultimate resolution of DPP-BOTDA is also discussed.

Chapter 6 proposes a high spatial and frequency resolution Brillouin sensor with the optical differential parametric amplification method. Not only the working principle is illustrated, but also a new theoretical model dealing with ODPA-BOTDA

is derived. Moreover, an ODPA-BOTDA setup has been successfully developed to achieve high spatial and frequency resolution.

Finally, chapter 7 concludes all the work we have done and suggests some possible future directions.

Chapter 2

Physics of Brillouin Scattering

Improving the performance of the distributed Brillouin sensor requires understanding the physics of the Brillouin scattering. The present chapter is dedicated to the study of the principles of the Brillouin scattering and to the building of the foundations of our research. This chapter is organized as follows. Section 2.1 introduces the basics of the nonlinear optical phenomenon. Section 2.2 gives the physics of the light scattering. Section 2.3 and section 2.4 illustrate the spontaneous and stimulated Brillouin scattering. Section 2.5 shows the foundations of our research, the polarization and phase matching effect in Brillouin scattering.

2.1 Nonlinear Optical Phenomenon

Nonlinear optics is the study of the interaction between medium and intense optical fields. The response of any dielectric medium to light becomes nonlinear for intense electromagnetic fields and optical fibers are no exception. Nonlinear effects in dielectrics, such as optical fibers, originate from the aharmonic motion of bound electrons under the influence of an applied electric field. As a consequence, the total

polarization $\vec{P}$ induced by electric dipoles is nonlinearly related with the electric field $\vec{E}$ and can be expressed in a more general relation [Agrawal 2007]:

$$\vec{P} = \varepsilon_0 \left(\chi^{(1)} \cdot \vec{E} + \chi^{(2)} : \vec{E}\vec{E} + \chi^{(3)} \vdots \vec{E}\vec{E}\vec{E} + \ldots \right) \tag{2.1.1}$$

Where ε_0 is the vacuum permittivity and $\chi^{(j)}$, which is a tensor of rank $j+1$, is the j^{th} order susceptibility. The linear susceptibility $\chi^{(1)}$ represents the main contribution to $\vec{P}$, whose effects include refraction and birefringence. The second order susceptibility $\chi^{(2)}$ is responsible for nonlinear effects such as second-harmonic generation and sum-frequency generation. However, $\chi^{(2)}$ vanishes for media that has inversion symmetry at the molecular level, such as optical fiber. Hence, the lowest order nonlinear effects in optical fiber comes from the third-order susceptibility $\chi^{(3)}$ and it is related with the phenomenon such as third-harmonic generation, Raman scattering, and Brillouin scattering.

2.2 Light Scattering

When light travels through matter, which may be in the form of solid, liquid or gas, various scatterings can occur. The scatterings are caused by fluctuations or excitations of the optical properties of the medium. The polarization vector $\vec{P}$ that is used to describe the response of a homogeneous and isotropic dielectric medium to an electric field $\vec{E}$ is defined as:

$$\vec{P} = \varepsilon_0 \chi \vec{E} \tag{2.2.1}$$

where ε_0 is the vacuum dielectric constant and χ is the medium susceptibility. The scattering is evoked by the medium dielectric constant fluctuation $\Delta\varepsilon$, which then induces a small polarization $\vec{P_s}$. We can decompose the displacement vector $\vec{D}$ of the scattered field into its scattered field $\vec{E_s}$ and input field $\vec{E_{in}}$ as [Ravet 2007]:

$$\vec{D_s} = \varepsilon_0 \varepsilon \vec{E_s} + \Delta\varepsilon \vec{E_{in}} \tag{2.2.2}$$

A perturbed wave equation can be applied to describe the scattered wave as the following:

$$\nabla^2 \vec{E_s} - \left(\frac{n}{c_0}\right)^2 \frac{\partial^2 \vec{E_s}}{\partial t^2} = \mu_0 \frac{\partial^2 \vec{P_s}}{\partial t^2} \tag{2.2.3}$$

where c_0 is the light velocity in vacuum, n is the refractive index, and μ_0 is the magnetic permeability of the vacuum.

The scattering phenomenon governed by the third-order susceptibility $\chi^{(3)}$ is elastic when no energy is exchanged between the electromagnetic field and the dielectric medium. The scattering process is said to be inelastic when the optical field transfers part of its energy to the nonlinear medium [Agrawal 2007].

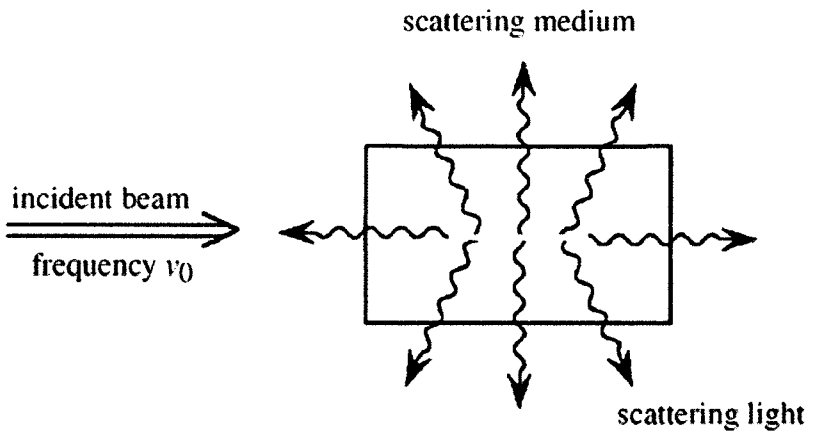

(a)

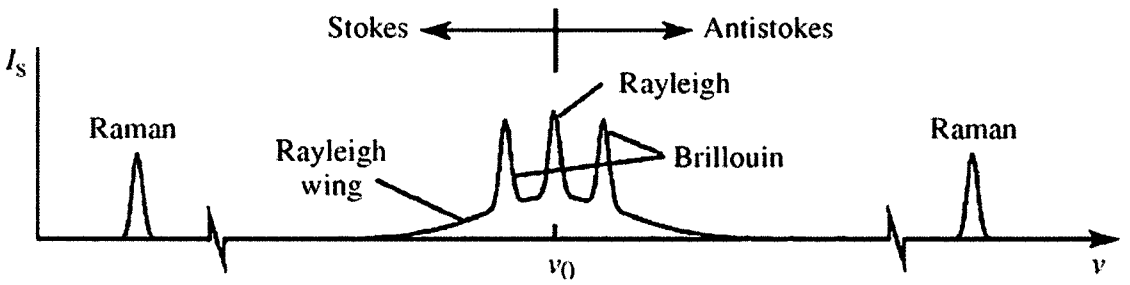

(b)

Fig 2.2.1: Spontaneous light scattering (a) Experimental setup (b) Typical observed spectrum [Boyd 2008]

Under the most general condition, the light scattering is a random, statistical process with scattering over a wide angular direction as shown in Fig. 2.2.1(a). The frequency spectrum of the scattered light in a particular direction is indicated as in Fig. 2.2.1 (b) [Boyd 2008], which includes Raman, Brillouin, Rayleigh, and Rayleigh-wing scattering. Those that are shifted to lower frequencies are known as the Stokes

components and those that are shifted to higher frequencies are known as the anti-Stokes components. The central peak is called Rayleigh scattering and it originates from non-propagating density fluctuations and can be referred to as scattering from entropy fluctuations. Because no frequency shift is induced between the incident field and scattered field, Rayleigh scattering is known as elastic scattering. Those next to the central Rayleigh peak are called Brillouin scattering components and they originate from light interaction with propagating density waves (or acoustic phonons). When the light is scattered by molecular vibrations, we call it Raman scattering. Raman scattering can also be described as the scattering of light from optical phonons. Because of the frequency shift between the incident light field and scattered light field, both Brillouin and Raman scattering are called inelastic scattering. There is another scattering that is called Rayleigh-wing scattering. It comes from the fluctuations in the orientation of anisotropic molecules. For molecules with an isotropic polarizability tensor, there is no Rayleigh-wing scattering. [Boyd 2008]

The light scattering is known as spontaneous when the optical properties of the medium do not change. Normally, the spontaneous light scattering happens at low light intensity level and is caused by the quantum mechanical or thermal fluctuations of the medium. The light scattering is called stimulated when the optical properties of the medium are altered. The stimulated light scattering happens at high light intensity and the material fluctuation is induced by the presence of the incident light itself [Damzen *et al.* 2003].

2.3 Spontaneous Brillouin Scattering

Since light scattering results from fluctuations in the optical properties of a material medium, at present, we will express the dielectric constant of the medium in terms of two independent thermodynamic variables: density ρ and temperature T as the following [Boyd 2008]:

$$\Delta\varepsilon = \left(\frac{\partial\varepsilon}{\partial\rho}\right)_T \Delta\rho + \left(\frac{\partial\varepsilon}{\partial T}\right)_\rho \Delta T \tag{2.3.1}$$

Because density fluctuations affect the dielectric constant more strongly than temperature fluctuations, the second term of (2.3.1) can usually be ignored [Fabelinskii 1968] and the error is estimated to be of the order of 2%. If we choose the entropy s and pressure p as two independent thermodynamic variables, the variation in density $\Delta\rho$ can be represented as [Boyd 2008]:

$$\Delta\rho = \left(\frac{\partial\rho}{\partial p}\right)_s \Delta p + \left(\frac{\partial\rho}{\partial s}\right)_p \Delta s \tag{2.3.2}$$

The first term of (2.3.2) is adiabatic density fluctuations and it is the origin of the Brillouin scattering. The second term of (2.3.2) corresponds to isobaric density fluctuations and it is the origin of Rayleigh-center scattering. For Brillouin scattering, the dielectric fluctuation can be written as:

$$\Delta\varepsilon = \left(\frac{\partial\varepsilon}{\partial\rho}\right)_T \left(\frac{\partial\rho}{\partial p}\right)_s \Delta p = \frac{\gamma_e}{\rho_0}\left(\frac{\partial\rho}{\partial p}\right)_s \Delta p \tag{2.3.3}$$

The electrostrictive constant γ_e is defined as [Boyd 2008]:

$$\gamma_e = \left(\rho \frac{\partial \varepsilon}{\partial \rho} \right)_{\rho=\rho_0} \tag{2.3.4}$$

where ρ_0 is the average density of the material. The pressure wave (or acoustic wave) propagation equation is given by [Fabelinskii 1968]:

$$\frac{\partial^2 \Delta p}{\partial t^2} - \Gamma' \nabla^2 \frac{\partial \Delta p}{\partial t} - \upsilon^2 \nabla^2 \Delta p = 0 \tag{2.3.5}$$

Here υ denotes the velocity of sound and Γ' is a damping parameter.

The phenomenon of Brillouin scattering originates from light interaction with a propagating pressure wave (or acoustic wave). Next, we will consider how light is scattered out of a beam by these pressure waves (or acoustic waves). Adopt the general expression for incident optical field as [Boyd 2008]:

$$\vec{E}_0(z,t) = \vec{E}_0 e^{i(\vec{k}\bullet\vec{r}-\omega t)} + c.c. \tag{2.3.6}$$

where $\vec{k}$ is the wave vector of the incident optical field and ω is its frequency. The pressure wave (or acoustic wave) is expressed as [Boyd 2008]:

$$\Delta p = \Delta p_0 e^{i(\vec{q}\bullet\vec{r}-\Omega t)} + c.c. \tag{2.3.7}$$

here $\vec{q}$ is the wave vector of the pressure wave and Ω is the pressure wave frequency. The scattered field obeys the driven wave equation [Boyd 2008]:

$$\nabla^2 \overline{E} - \frac{n^2}{c^2} \frac{\partial^2 \overline{E}}{\partial t^2} = \frac{1}{\varepsilon_0 c^2} \frac{\partial^2 \overline{P}}{\partial t^2} \tag{2.3.8}$$

According to equations (2.2.1), (2.3.1), (2.3.3), the polarization $\overline{P}$ of the medium can be written as [Boyd 2008]:

$$\vec{P}(\vec{r},t) = \varepsilon_0 \left(\frac{\partial \varepsilon}{\partial \rho}\right)\left(\frac{\partial \rho}{\partial p}\right)_s \Delta p(\vec{r},t)\vec{E}_0(z,t) = \varepsilon_0 \gamma_e C_s \Delta p(\vec{r},t)\vec{E}_0(z,t) \qquad (2.3.9)$$

where C_s is the adiabatic compressibility and γ_e is the electrostrictive constant defined in (2.3.4). Substituting equation (2.3.9) and (2.3.7) into equation (2.3.8), after simplifying, we can get the scattered field wave equation as the following [Boyd 2008]:

$$\begin{aligned} \nabla^2 \vec{E} - \frac{n^2}{c^2}\frac{\partial^2 \vec{E}}{\partial t^2} = -\frac{\gamma_e C_s}{c^2}[(\omega-\Omega)^2 \vec{E}_0 \Delta p_0^* e^{i(\vec{k}-\vec{q})\cdot\vec{r}-i(\omega-\Omega)t} \\ +(\omega+\Omega)^2 \vec{E}_0 \Delta p_0^* e^{i(\vec{k}+\vec{q})\cdot\vec{r}-i(\omega+\Omega)t} + c.c.] \end{aligned} \qquad (2.3.10)$$

There are two terms on the right hand side of equation (2.3.10). The first term leads to Stokes scattering and the second term leads to anti-Stokes scattering. Let us look at the Stokes scattering first. The wave vector $\vec{k}'$ and frequency ω' of the Stokes scattering component are:

$$\vec{k}' = \vec{k} - \vec{q} \qquad (2.3.11)$$

$$\omega' = \omega - \Omega \qquad (2.3.12)$$

$\vec{k}$ and ω are the wave vector and frequency of the incident optical field and they are related as:

$$\omega = \frac{\left|\vec{k}\right| c}{n} \qquad (2.3.13)$$

$\vec{q}$ and Ω are the wave vector and frequency of the acoustic wave and they are related as:

$$\Omega = \left|\vec{q}\right| \upsilon \qquad (2.3.14)$$

$\vec{k}'$ and ω' are the wave vector and frequency of the scattered optical field and they are related as:

$$\omega' = \frac{\left|\vec{k}'\right| c}{n} \tag{2.3.15}$$

The following Fig. 2.3.1 is an illustration of the Stokes scattering and it demonstrates the relationship between the wave vector of the acoustic wave and those of the incident and scattered optical wave [Boyd 2008]. According to Fig. 2.3.1 (b),

$$\left|\vec{q}\right| \cong 2\left|\vec{k}\right| \sin(\frac{\theta}{2}) \tag{2.3.16}$$

θ is the scattering angle between the incident and Stokes fields, and we assume $\left|\vec{k}\right| \approx \left|\vec{k}'\right|$. After substituting relation (2.3.13) and (2.3.14) into (2.3.16), we can obtain the Stokes shift as:

$$\Omega = 2\left|\vec{k}\right| \upsilon \sin(\frac{\theta}{2}) = 2n\omega \frac{\upsilon}{c} \sin(\frac{\theta}{2}) \tag{2.3.17}$$

It shows that the Stokes frequency shift Ω is dependent on the scattering angle. The only relevant directions inside an optical fiber are the forward and backward directions. Thus, Ω equals zero for forward scattering and is maximum for backward scattering ($\theta = \pi$). The maximum Stokes shift is:

$$\Omega_{\max} = 2n \frac{\upsilon}{c} \omega \tag{2.3.18}$$

In optical fiber, the typical Stokes shift is around 11GHz for 1550nm lightwave.

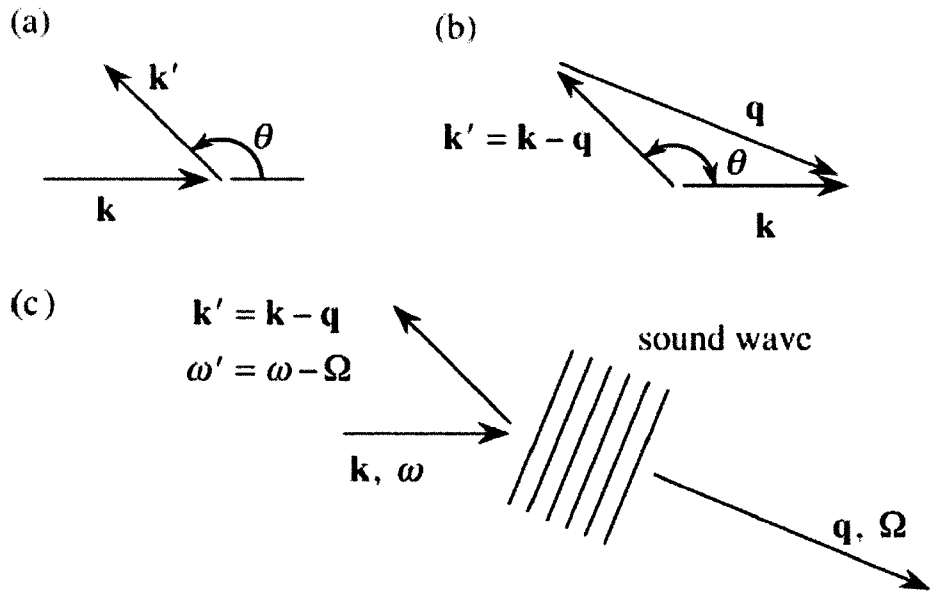

Fig. 2.3.1: Illustration of Stokes scattering [Boyd 2008]

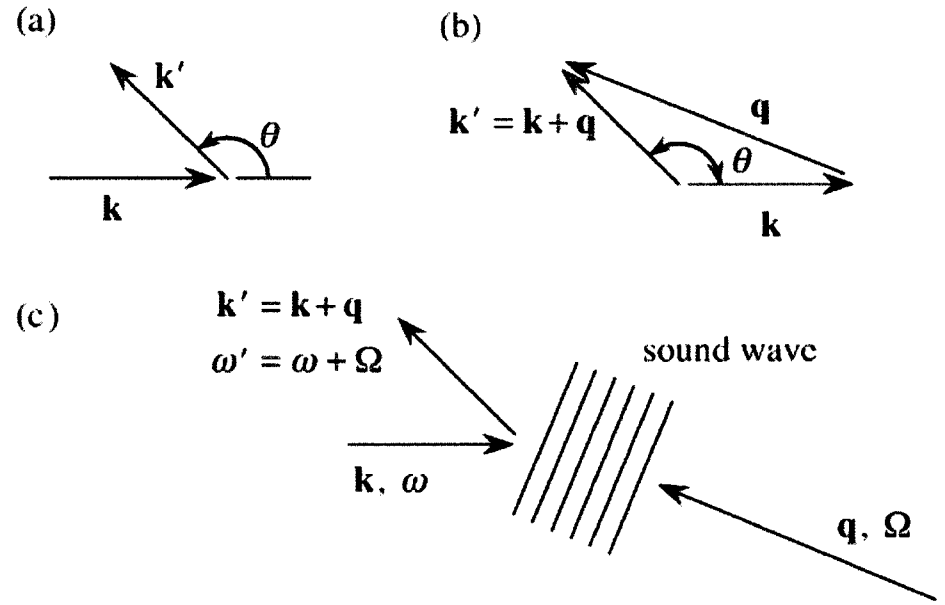

Fig. 2.3.2: Illustration of Anti-Stokes scattering [Boyd 2008]

The anti-Stokes scattering is quite similar to the Stokes scattering. The wave

vector and frequency of the anti-Stokes component are:

$$\vec{k}' = \vec{k} + \vec{q} \tag{2.3.19}$$

$$\omega' = \omega + \Omega \tag{2.3.20}$$

Similar as before, $\omega = \frac{\left|\vec{k}\right| c}{n}$, $\Omega = \left|\vec{q}\right| \upsilon$, and $\omega' = \frac{\left|\vec{k}'\right| c}{n}$. As illustrated in Fig. 2.3.2, because of $\left|\vec{k}\right| \approx \left|\vec{k}'\right|$, the acoustic wave vector can be expressed as:

$$\left|\vec{q}\right| \cong 2\left|\vec{k}\right| \sin(\frac{\theta}{2}) \tag{2.3.21}$$

Consider the relation (2.3.13) and (2.3.14), we have:

$$\Omega = 2\left|\vec{k}\right| \upsilon \sin(\frac{\theta}{2}) = 2n\omega \frac{\upsilon}{c} \sin(\frac{\theta}{2}) \tag{2.3.22}$$

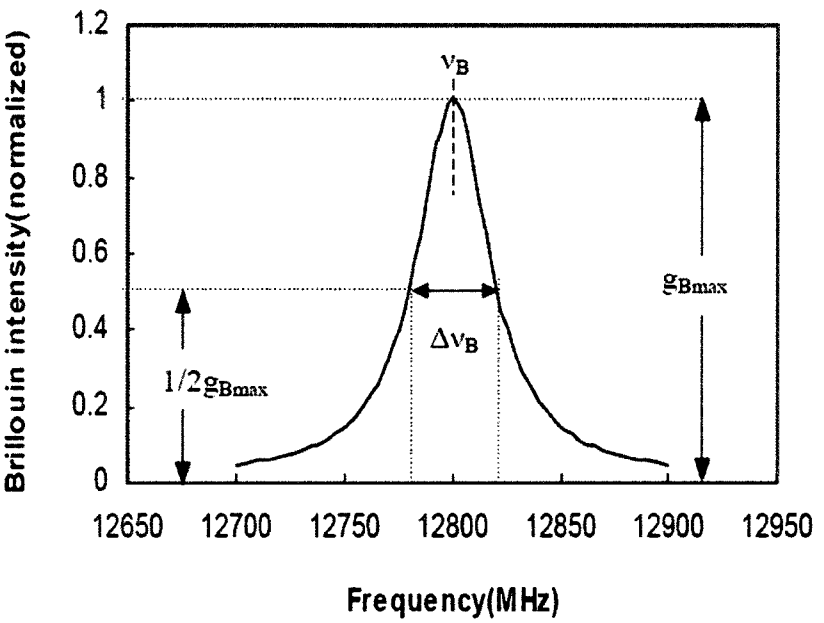

Fig. 2.3.3: A Lorentzian shaped Brillouin spectrum [Yu 2006]

If we include the exponential decay of the acoustic wave into the above analysis, we will find that the scattered radiation exhibits a frequency broadening. The line shape is Lorentzian with the FWHM given by:

$$\delta\omega = 4\Gamma' \left|\vec{k}\right|^2 \sin^2(\frac{\theta}{2}) = 4n^2\Gamma' \frac{\omega^2}{c^2} \sin^2(\frac{\theta}{2}) \qquad (2.3.23)$$

Fig. 2.3.3 shows a typical Brillouin spectrum with the maximum gain coefficient normalized to 1. The FWHM of this spectrum is around 33MHz, which is a value broadly quoted in many related literature.

2.4 Stimulated Brillouin Scattering

As described in section 2.2, if the fluctuations in the optical properties of a material system that cause the light scattering are induced by thermal or quantum mechanical zero-point effects, the scattering process is said to be spontaneous. However, if the fluctuations are excited by the presence of the optical field, the scattering is called stimulated [Boyd 2008]. In spontaneous scattering regime, the amount of scattering is proportional to the incident intensity. While in the stimulated scattering regime, an exponential amplification of the scattered light can be expected as there is very strong interaction between light fields and the material [Damzen *et al.* 2003]. In previous section, we assume that the incident optical fields are so weak that

the optical properties of the material system are not altered; and thus the spontaneous Brillouin scattering results from the density variations that are present in thermal equilibrium. In this section, we will describe the stimulated Brillouin scattering caused by induced density variations of a material system under an incident optical field with sufficient intensity.

Stimulated Brillouin scattering (SBS) was first experimentally observed by Chiao *et al.* in 1964 [Chiao *et al.* 1964]. There are two different physical mechanisms that account for the density variation of the material, which is the origin of the Brillouin scattering [Boyd, 2008]. One is electrostriction, which can be understood as the tendency of materials to become denser in the presence of an electric field. The other one is optical absorption, that is, the absorption and subsequent thermalization of the optical energy leading to temperature and hence density variations inside the medium. Because SBS induced by optical absorption can only occur in lossy optical medium, here we only focus on the electrostriction induced SBS, which is the normal case in optical fiber.

The potential energy of a material subject to an electric field with strength E is given by [Ravet 2007, Boyd 2008]:

$$U = \frac{1}{2}\varepsilon_0 \varepsilon E^2 \tag{2.4.1}$$

where ε is the dielectric constant of the material and ε_0 is the permittivity of vacuum. With the change of the density of the material, the change of the dielectric constant will be:

$$\Delta\varepsilon = \left(\frac{\partial\varepsilon}{\partial\rho}\right)\Delta\rho \tag{2.4.2}$$

As a consequence, the field energy density will change by the amount:

$$\Delta u = \frac{1}{2}\varepsilon_0 \Delta\varepsilon E^2 = \frac{1}{2}\varepsilon_0 E^2 \left(\frac{\partial\varepsilon}{\partial\rho}\right)\Delta\rho \tag{2.4.3}$$

The work done per unit volume which compresses the material is given by:

$$\Delta w = p_{st}\frac{\Delta V}{V} = -p_{st}\frac{\Delta\rho}{\rho} \tag{2.4.4}$$

This work should be equal to the change in energy according to the first law of thermodynamics. By equating (2.4.3) and (2.4.4), we can find the electrostrictive pressure as [Ravet 2007, Boyd 2008]:

$$p_{st} = -\frac{1}{2}\varepsilon_0 \rho\left(\frac{\partial\varepsilon}{\partial\rho}\right)E^2 = -\frac{1}{2}\varepsilon_0\gamma_e E^2 \tag{2.4.5}$$

When E denotes an optical field, the electrostrictive pressure should be written as:

$$p_{st} = -\frac{1}{2}\varepsilon_0\gamma_e\left\langle \vec{E}\bullet\vec{E}\right\rangle \tag{2.4.6}$$

where the angular brackets denote a time average over an optical period. The negative pressure implies that the total pressure is reduced at high field strength, the material tends to be compressed at these regions, and the density would be increased. The change in the density can be written as:

$$\Delta\rho = -\rho C p_{st} \tag{2.4.7}$$

where $C = \frac{1}{\rho}\left(\frac{\partial\rho}{\partial p}\right)$ denotes the compressibility. Because $\Delta\chi = \Delta\varepsilon\cdot\varepsilon_0$

and $\Delta\varepsilon = \left(\frac{\partial\varepsilon}{\partial\rho}\right)\Delta\rho$, by combining (2.4.6), (2.4.7), the change of the susceptibility can be given by:

$$\Delta\chi = \frac{1}{2}\varepsilon_0^2 C\gamma_e^2 \left\langle \vec{E}\bullet\vec{E} \right\rangle \tag{2.4.8}$$

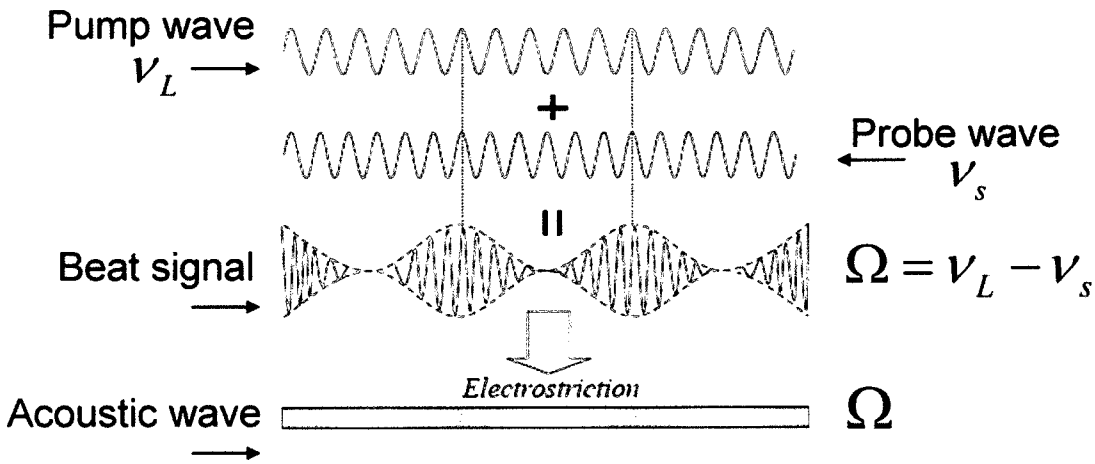

Fig. 2.4.1: Generation of the acoustic wave [Yu 2006]

The stimulated Brillouin scattering is caused by the density variations induced by the incident optical fields. Such kind of SBS inside an optical fiber with two input lightwaves pump and probe is illustrated in Fig. 2.4.1, where pump light with frequency ν_L and probe light with frequency ν_s are counter propagating inside an optical fiber. The beat frequency of pump and probe equals the frequency Ω of the acoustic wave, hence the beat signal from the beating of the pump and probe wave enhances the thermally generated acoustic wave through the electrostriction effect. The acoustic wave varies the refractive index along the fiber, thus scatters the pump wave

through Bragg diffraction, and increases the probe wave. The beating of the pump wave and probe wave tends to increase the acoustic wave, whereas the beating of the pump wave and acoustic wave tends to increase the probe wave. As a result, the probe wave will get amplified and the pump wave will be depleted by such a positive feedback.

The stimulated Brillouin scattering can be considered as the interaction of pump and probe wave through acoustic wave. The formal theoretical description of the SBS inside an optical fiber will be given as the following. Assume the pump wave and acoustic wave are propagating in the positive direction of the fiber and the probe wave is propagating in the negative direction of the fiber. The total optical field inside the optical fiber can be represented as:

$$\vec{E}(z,t) = \vec{E}_1(z,t) + \vec{E}_2(z,t) \tag{2.4.9}$$

where $\vec{E}_1(z,t) = \vec{A}_1(z,t)e^{i(k_1 z - \omega_1 t)} + c.c.$ is the pump wave and $\vec{E}_2(z,t) = \vec{A}_2(z,t)e^{i(-k_2 z - \omega_2 t)} + c.c.$ is the probe wave. The acoustic wave can be described in terms of the material density distribution:

$$\tilde{\rho}(z,t) = \rho_0 + [\rho(z,t)e^{i(qz - \Omega t)} + c.c.] \tag{2.4.10}$$

Here $\Omega = \omega_1 - \omega_2$, $q = 2k_1$, and ρ_0 is the mean density of the fiber. The spatial and temporal evolution of the optical fields can be described by the wave equation [Boyd 2008]:

$$\frac{\partial^2 \vec{E}_1}{\partial z^2} - \frac{n^2}{c^2}\frac{\partial^2 \vec{E}_1}{\partial t^2} = \frac{1}{\varepsilon_0 c^2}\frac{\partial^2 \vec{P}_1}{\partial t^2}$$
$$\frac{\partial^2 \vec{E}_2}{\partial z^2} - \frac{n^2}{c^2}\frac{\partial^2 \vec{E}_2}{\partial t^2} = \frac{1}{\varepsilon_0 c^2}\frac{\partial^2 \vec{P}_2}{\partial t^2} \qquad (2.4.11)$$

The source terms in the above equation are the nonlinear polarization and they are given by [Boyd 2008]:

$$\vec{P}_1 = \vec{p}_1 e^{i(k_1 z - \omega_1 t)} + c.c.$$
$$\vec{P}_2 = \vec{p}_2 e^{i(-k_2 z - \omega_2 t)} + c.c. \qquad (2.4.12)$$

where $\vec{p}_1 = \frac{\varepsilon_0 \gamma_e}{\rho_0}\rho \vec{A}_2$ and $\vec{p}_2 = \frac{\varepsilon_0 \gamma_e}{\rho_0}\rho^* \vec{A}_1$. The material density obeys the acoustic wave equation [Boyd 2008]:

$$\frac{\partial^2 \rho}{\partial t^2} - \Gamma' \nabla^2 \frac{\partial \rho}{\partial t} - \upsilon^2 \nabla^2 \rho = \nabla \cdot \vec{f} \qquad (2.4.13)$$

The source term of the acoustic wave equation is the divergence of the force per unit volume and it is given by:

$$\nabla \cdot \vec{f} = \varepsilon_0 \gamma_e q^2 [\vec{A}_1 \vec{A}_2^* e^{i(qz - \Omega t)} + c.c.] \qquad (2.4.14)$$

for the fields given by (2.4.9). If we substitute (2.4.9), (2.4.12) into (2.4.11), introduce (2.4.10), (2.4.14) into (2.4.13), consider the loss of the material, and make the slowly-varying amplitude approximation, we can obtain the following equations:

$$\frac{\partial \vec{A}_1}{\partial z}+\frac{n}{c}\frac{\partial \vec{A}_1}{\partial t}=\frac{i\omega\gamma_e}{2nc\rho_0}\rho\vec{A}_2-\frac{\alpha}{2}\vec{A}_1$$

$$-\frac{\partial \vec{A}_2}{\partial z}+\frac{n}{c}\frac{\partial \vec{A}_2}{\partial t}=\frac{i\omega\gamma_e}{2nc\rho_0}\rho^*\vec{A}_1-\frac{\alpha}{2}\vec{A}_2 \qquad (2.4.15)$$

$$-2i\Omega\frac{\partial\rho}{\partial t}+(\Omega_B^2-\Omega^2-i\Omega\Gamma_B)\rho-2iq\upsilon^2\frac{\partial\rho}{\partial z}=\varepsilon_0\gamma_e q^2\vec{A}_1\vec{A}_2^*$$

where $\Gamma_B=q^2\Gamma'$ is the Brillouin linewidth and α is the attenuation factor of the material. Because the phonon propagation distance is very short (<10μm), $\frac{\partial\rho}{\partial z}$ term of the third equation of (2.4.15) can be neglected. Thus, we can obtain the three wave coupled equations as the following:

$$\frac{\partial \vec{A}_1}{\partial z}+\frac{n}{c}\frac{\partial \vec{A}_1}{\partial t}=\frac{i\omega\gamma_e}{2nc\rho_0}\rho\vec{A}_2-\frac{\alpha}{2}\vec{A}_1$$

$$-\frac{\partial \vec{A}_2}{\partial z}+\frac{n}{c}\frac{\partial \vec{A}_2}{\partial t}=\frac{i\omega\gamma_e}{2nc\rho_0}\rho^*\vec{A}_1-\frac{\alpha}{2}\vec{A}_2 \qquad (2.4.16)$$

$$-2i\Omega\frac{\partial\rho}{\partial t}+(\Omega_B^2-\Omega^2-i\Omega\Gamma_B)\rho=\varepsilon_0\gamma_e q^2\vec{A}_1\vec{A}_2^*$$

The above three wave coupled equations describe completely the interaction between the pump and probe wave through acoustic wave. In the following chapters, all the theoretical models we used are derived based on the above three wave coupled equations.

2.5 Polarization and Phase Matching Effect in Brillouin Scattering

As described in section 2.4, the origin of the stimulated Brillouin scattering is the acoustic wave generated by the beating of the pump and probe waves. Thus, the interaction is strongly and inherently dependent on the state of polarization (SOP) of the pump and probe waves. In polarization maintaining (PM) fibers, the gain of the stimulated Brillouin scattering is the maximum for pump and probe waves with parallel linear polarization states that are aligned to one of the principal axes of the PM fiber. The gain equals zero for pump and probe waves with orthogonal linear polarization states aligned to the principal axes of the PM fiber. The gain is half for pump and probe with linear polarization states launched to 45° of the principal axis of the PM fiber. In a single mode optical fiber, the situation is more complicated due to the residual fluctuating birefringence [Deventer *et al.* 1994, Thévenaz *et al.* 2008]. At one point along the single mode fiber, the Brillouin interaction is most efficient when the electric fields of the pump and signal are aligned, for example, their vectors trace parallel ellipses and are in the same sense of rotation. Conversely, if the two ellipses are again similar, but traced in opposite senses of rotation, with their long axes being orthogonal to each other, the Brillouin interaction at that point averages to zero over an optical period that is defined as the time when lightwave propagates through one wavelength. As the pump and probe waves counter-propagate along the fiber, residual birefringence of the fiber changes the states of polarization of both the pump and probe waves in a random fashion, it is impossible for the counter propagating pump and probe waves to have both the same polarization ellipse and the same sense of rotation along the entire fiber. Thus, the

Brillouin gain is fluctuating because of such polarization change. Consequently, in the presence of birefringence, the overall signal gain depends on the birefringent properties of the fiber and on the input states of polarization of both pump and probe signal. [Agrawal 2007, Walker *et al.* 2008, Zadok *et al.* 2008].

However, most previous work related to the polarization properties of the Brillouin interaction was restricted to CW signals [Deventer *et al.* 1994, Zadok *et al.* 2008, Galtarossa et al. 2008]. The work with pulse signals has so far been poorly exploited, especially for optical pulses whose durations are shorter than the phonon relaxation time (~10ns). In single mode fiber, as long as the pulse width is larger than or comparable to the light propagating time through the characteristic beat length of the fiber, which is typically from several meters to tens of meters, it is possible to maximize the Brillouin signal everywhere due to the average effect of different SOPs of the pump and probe waves. However, for pulse whose width is shorter than the characteristic beat length of the fiber, there is no such average effect because the Brillouin interaction length of the pump and probe waves is even shorter than the SOPs evolution length of the pump and probe waves. In the PM fiber, the situation is different from that in the single mode fiber. Because the characteristic beat length of the PM fiber is normally a few centimeters, when an optical field propagates in a PM fiber, its SOP changes very fast. The CW or the broad pulse wave has a narrow spectral linewidth that corresponds to a few frequency components; while the pulsed signal, especially narrow (1-2ns) pulse, has a broad spectral linewidth that corresponds to

more frequency components than the CW or the broad pulse wave. Each frequency component inside the linewidth represents a different SOP. The SOP evolution for different frequency components in the PM fiber is different. Because the Brillouin interaction is dependent on the SOPs of the two light waves, the Brillouin interaction with CW or broad pulse is different from the Brillouin interaction with short pulse. Because in the distributed Brillouin sensor with high spatial resolution, short pulsed signals are widely adopted, it is worth to study the SBS attributes with short pulsed signals.

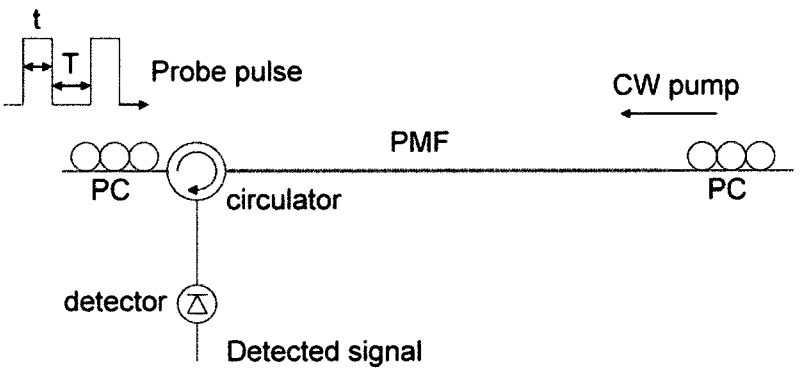

Fig. 2.5.1: Schematic diagram of Brilloun scattering with double probe pulses (PC: polarization controller, PMF: polarization maintaining fiber, CW: continuous wave).

Some experiments were performed to address the relationship between the Brillouin gain spectrum and the SOPs of the optical pulses whose duration were even shorter than the phonon relaxation time (~10ns) inside an optical fiber. As shown in Fig. 2.5.1, a PM fiber was chosen as the testing fiber. Two probe pulses were sent to one

side of the PM fiber and the CW pump was sent to the other side of the PM fiber. The pulse widths t of the two probe pulses were 2ns and the separation T of the two pulses was 1.5ns, which was less than the pulse widths of the two probe pulses. Different SOP combinations of the two probe pulses were adopted and the measured Brillouin spectra for different cases are shown in the following Fig. 2.5.2. When the SOPs of the two probe pulses are the same and the SOP of the pump and the SOPs of the probe pulses are all aligned to one of the principal axes of the PM fiber, the Brillouin gain is the maximum among all the cases as in Fig. 2.5.2 case (a). When the SOPs of the two probe pulses are the same and are aligned to one of the principal axes of the PM fiber while the SOP of the CW pump is not aligned to any principal axes of the PM fiber, the Brillouin gain spectrum is shown in case (b). The Brillouin gain in case (b) is smaller than that in case (a). Comparing Fig. 2.5.2 case (a) with Fig. 2.5.2 case (b), it is found that although the Brillouin gain decreases for un-parallel SOPs between the pump and the probe, the profile of the Brillouin spectrum in case (a) is similar to the Brillouin spectrum in case (b). When the SOPs of the two probe pulses are orthogonal and are not aligned to the same principal axis of the PM fiber as the pump wave, the measured Brillouin spectrum is given in Fig. 2.5.2 case (c) and is very noisy.

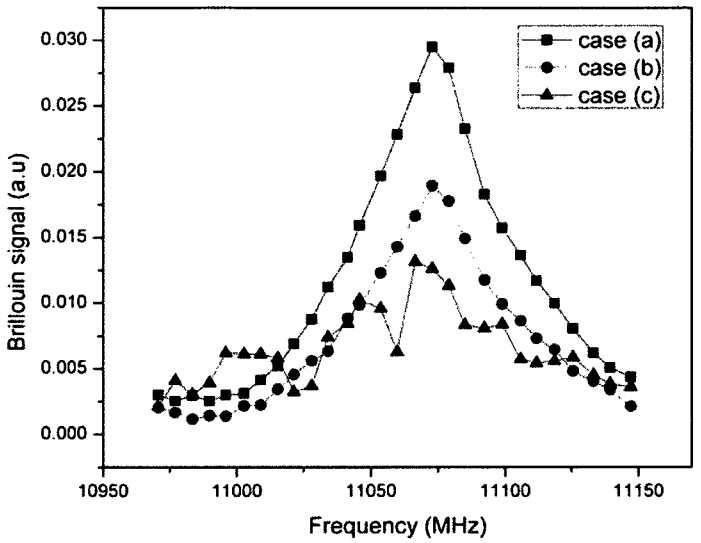

Fig. 2.5.2: Brillouin spectra for double pulse width different SOP, pulse width t=2ns, pulse separation T=1.5ns.

Case (a) the SOPs of two pulses were the same and aligned with the SOP of the pump wave,
Case (b) the SOPs of two pulses were the same and not aligned with the SOP of the pump wave,
Case (c) the SOP of two pulses were orthogonal and not aligned with the SOP of the pump wave

The SOPs of the pump and probe waves are aligned to the same principal axis of the PM fiber in neither Fig. 2.5.2 case (b) nor Fig. 2.5.2 case (c); however, the Brillouin spectrum in (b) is very smooth while the Brillouin spectrum in (c) is very noisy. The difference between Fig. 2.5.2 case (b) and Fig. 2.5.2 case (c) is related to the SOPs of the two probe pulses and the phonon fields they generated. Due to the very short separation, which is even shorter than the phonon lifetime, between the two probe pulses, when the second probe pulse interact with the pump wave, the phonon field generated by the interaction between the first probe pulse and the pump wave has not been totally attenuated and the phonon field generated by the first probe pulse will be

interfered by the phonon field generated by the second probe pulse. When the SOPs of the two probe pulses are the same, as in case (b), the phonon fields generated by the two probe pulses also has the same phase relation when they interact with the CW pump and these two phonon fields can be added together coherently. When the SOPs of the two probe pulses are orthogonal, as in case (c), the phonon field generated by the first probe pulse and the phonon field generated by the second probe pulse will also have orthogonal phase relation when they interact with CW pump. The orthogonal phase relation implies that the first phonon field is not in phase with the second phonon field and the Brillouin interaction that involves the first phonon field will be interfered by the Brillouin interaction that involves the second phonon field due to the phase mismatch between these two phonon fields. Thus, the measured Brillouin spectrum by those two probe pulses is very noisy. Furthermore, this time domain interference of the Brillouin interaction between the first phonon field and the second phonon field is related with the time separation between the two probe pulses. If the time separation between the two probe pulses is much greater than the phonon lifetime, there would not be any interference between the two phonon fields because the phonon field generated by the first probe pulse has been attenuated completely before the appearance of the phonon field generated by the second probe pulse. Thus, the Brillouin spectrum is very smooth. The smaller the pulse separation, the severer the interference between the Brillouin interaction involving the first pulse and the Brillouin interaction involving the second pulse is. Table 2.5.1 proves the above statement. As shown in Table 2.5.1, the

SNR of the Brillouin spectrum increases from 17dB to 26dB when the separation between the two consecutive probe pulses increases from 1.5ns to 20ns.

Table 2.5.1: The SNR of the Brillouin spectrum for double pulse with different separation, pulse width t=2ns, the SOPs of the two pulses are orthogonal.

	Separation (ns)	SNR (dB)
Case (a)	1.5	17
Case (b)	4	20
Case (c)	20	26

Based on the above investigation, it is found that the relationship between the SOPs of the pump and probe waves and the Brillouin spectrum is actually related to the disturbance caused by the generated phonon field. In order to get efficient Brillouin scattering, all the phonon fields generated by the probe and pump waves must have the same SOPs in order to keep all the phonon fields being phase matched together; thus, the time domain disturbance of the phonon field could be avoided.

2.6 Conclusion

In conclusion, nonlinear optics studies the interaction between medium and

intense optical fields. When light travels through matter, various scatterings, which are caused by fluctuations or excitations of the optical properties of the medium, can occur. The spontaneous Brillouin scattering arises from the interaction between a light wave and an acoustic wave. The acoustic wave can be considered as a propagating grating that diffracts the incident wave and induces the periodic variation of the material density and consequently the refractive index change. The diffracted wave experiences a frequency shift with an amount proportional to the acoustic velocity inside the material due to the Doppler Effect. The stimulated Brillouin scattering arises from the electrostriction caused by the incident optical fields. When two counter-propagating lightwaves are present inside the fiber, the beat of these two waves can induce the density and refractive index variation caused by electrostriction. The acoustic wave inside the fiber is enhanced when the beat frequency of the two lightwaves matches with the frequency of the acoustic wave. The scattered Stokes wave can be increased by the enhanced acoustic wave. The positive feedback between the acoustic wave and scattered Stokes wave leads to Stimulated Brillouin scattering. Since SBS originated from the mixing of the two lightwaves, the efficiency of this effect is polarization dependent.

Chapter 3

Distributed Brillouin Sensor Based on Offset Locking of Two DFB Lasers

As described in Chapter 1, the application of optical fiber sensors has attracted much attention in recent years due to the need for health monitoring of civil structures. Different types of distributed fiber sensor have been developed for temperature and strain monitoring over tens-of-kilometer long fiber [Kurashima *et al.* 1990, Bao *et al.* 1993a, Bao *et al.* 1993b, Niklès *et al.* 1996]. Based on the stimulated Brillouin scattering phenomenon, counter-propagating pump and probe lasers were used to measure the Brillouin gain [Kurashima *et al.* 1990] or loss spectrum [Bao *et al.* 1993]. The temperature or strain could then be determined by measuring the Brillouin frequency shift that is linearly related to the temperature or the strain applied to the fiber [Kurashima *et al.* 1990, Bao *et al.* 1993a, Bao *et al.* 1993b, Niklès *et al.* 1996]. This made it possible to monitor large structures, such as dam, bridge, and pipeline, with sub-meter spatial resolution using highly frequency-stabilized lasers [Brown *et al.* 1999, Bao *et al.* 2001]. However, for the development and the application of a cost effective distributed Brillouin sensor, the need of one or two highly stabilized laser sources with large tuning range and fast tuning ability is still a major limiting factor. In

order to solve this problem, several schemes have already been proposed as follows.

Ultra fast EOMs were used to produce the frequency shift from a single laser source [Niklès *et al.* 1996, Izumita *et al.* 1996]. Although this approach only used a single laser source, the cost of the microwave generator, power amplifier, and special optical modulator increased the overall cost of the system. The approach in Ref [Brown *et al.* 1999, DeMerchant 2000] involved a frequency counter to lock and tune the beat frequency of two stabilized lasers (Nd-YAG lasers). Because of the frequency counter and two stabilized lasers used, the system cost was comparable to that in Ref [Niklès *et al.* 1996, Izumita *et al.* 1996]. Recently, a new technique that used laser injection locking, which required the carrier laser (so called slave laser) frequency to be locked on one of the master laser side modes, was proposed [Thévenaz *et al.* 2004] for the distributed Brillouin sensor system. The spatial resolution of the distributed Brillouin sensor based on injection locking technique was on the order of meters, which was limited by the phonon lifetime. Although the injection locking method was simple and did not need highly frequency stabilized lasers, it had the disadvantage of requiring that the locked frequency be equal to one of the master laser side modes, which limited the frequency locking range. Moreover, in order to map out the Brillouin spectrum, the tuning of the laser frequency in the injection-locking configuration was through changing the microwave generator frequency that applied to the slave laser. Care must be taken to ensure that the frequency scan range did not exceed the locking range, which limited the tuning range. In addition, the change of the tuning frequency

had an impact on the laser (slave) power stability. Also, a power change of the master laser would affect the master laser side modes and had a direct effect on the slave laser, and it took time for the slave laser to re-establish the stabilized frequency condition after each tuning step, limiting the tuning speed and sensing time. This same principle is also applicable to the highly stabilized laser frequency tuning that is achieved inside the laser cavity. The frequency tuning speed of the highly stabilized laser sets the minimum time for the stabilization and frequency sweeping of the distributed sensor system.

In this chapter, we will describe an offset locking based distributed Brillouin sensor that adopts a different technique to lock and tune the frequency [Li *et al.* 2008b]. The frequency stabilization technique, that made use of laser heterodyne source and optical delay line, was used to stabilize the frequency of millimeter-wave sub carrier that was adopted as the basis for the implementation of a fiber-radio system [Doi *et al.* 2001]. We found that the characteristics of this offset locking technique for two DFB lasers could meet the requirements of a Brillouin based distributed sensor system that should have wide tuning range, less than 1 MHz frequency fluctuation, and millisecond or less response time. Moreover, the frequency tuning was achieved externally from the lasers; hence the tuning did not affect the laser power output and the tuning and signal processing time were shorter than that of the sensors that achieved the frequency tuning inside the laser cavity. Furthermore, in order to make the sensor system simple and cost effective, a hardware proportional-integral-derivative (PID) controller

[Astrom 1995] was used to lock the beat frequency that made the tuning of the laser frequency much faster (μs), while Doi *et al.* used a software control method with milliseconds response [Doi *et al.* 2001]. We then implemented the offset locking technique with a hardware controller in a Brillouin sensor system rather than the software control method in Ref [Doi *et al.* 2001]. A fast measurement time of a few minutes over frequency sweeping range of ≥1 GHz at frequency step of 1-2 MHz has been achieved. With offset locking technique, the phase of the pump and probe waves are locked together and the acoustic wave that originates from the beating of the pump and probe waves is also in phase with the pump and the probe waves. When the pump, probe, and acoustic waves are all in phase, they generate coherent Brillouin scattering with maximum Brillouin gain within the linewidth of the natural Brillouin spectrum through the optical field adding; while outside the linewidth of the natural Brillouin spectrum, the Brillouin amplification is much weaker because the phase and frequency matching conditions between the pump and probe waves are not both fulfilled due to the limited phase locking bandwidth. As a result, narrow linewidth and high SNR Brillouin spectrum can be obtained due to the coherent Brillouin interaction. Moreover, a lock-in amplifier was adopted to stabilize the base of the probe pulse generated by EOM, which ensured the minimum pulse distortion for sensing lengths of kilometers, prevented probe power variation, and further increased the SNR.

This chapter is organized as the following. Section 3.1 describes the working principle and the setup of the offset locking based distributed Brillouin sensor, and

especially focuses on the offset locking sub-system and EOM bias stabilization sub-system. Section 3.2 presents the sensor performance.

3.1 Sensor Development

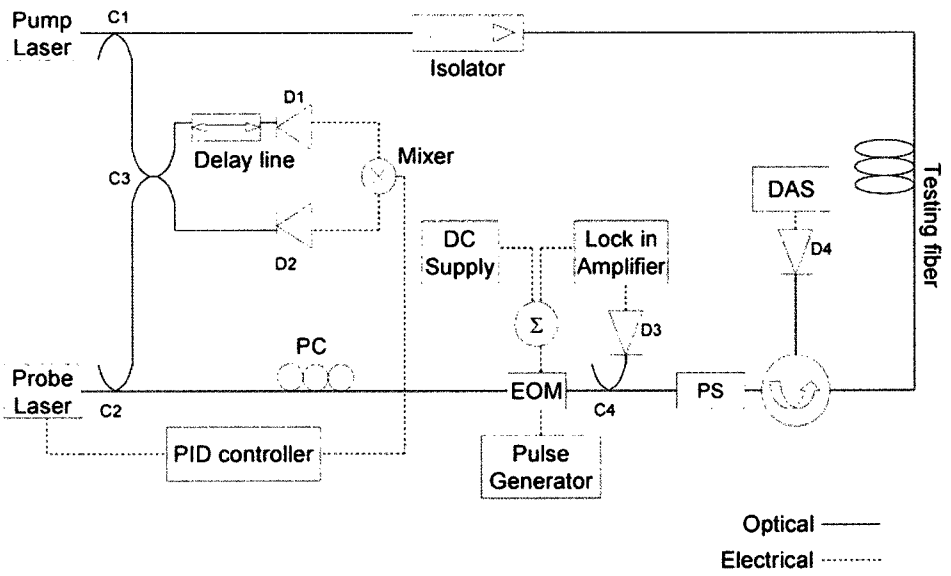

Fig. 3.1.1: Experimental setup.
C: coupler (1-2: 95/5, 3: 50/50, 4: 99/1), D: detector,
EOM: electro-optical modulator, PC: polarization controller,
PS: polarization scrambler, DAS: data acquisition system.

The offset locking based distributed Brillouin sensor setup is shown in Fig. 3.1.1. The light sources are two DFB lasers operating at 1550 nm and the beat frequency is locked using the offset locking method. One of the DFB lasers launches a CW pump beam, while the other DFB laser is modulated by an EOM to produce an optical pulse that works as the probe beam. By tuning the frequency difference between the pump

and probe beams, the depletion in the pump power via the Brillouin loss process can be monitored using an alternating current (AC) coupled photo detector over a range of beat frequencies to measure the Brillouin spectra. The AC detector is required to remove the large direct current (DC) offset of CW power.

In section 3.1.1 and section 3.1.2, the working principle of the offset locking sub-system and EOM bias stabilization sub-system will be described separately. These two sub-systems are two crucial parts in realizing high sensing performance.

3.1.1 Offset Locking Sub-system Description

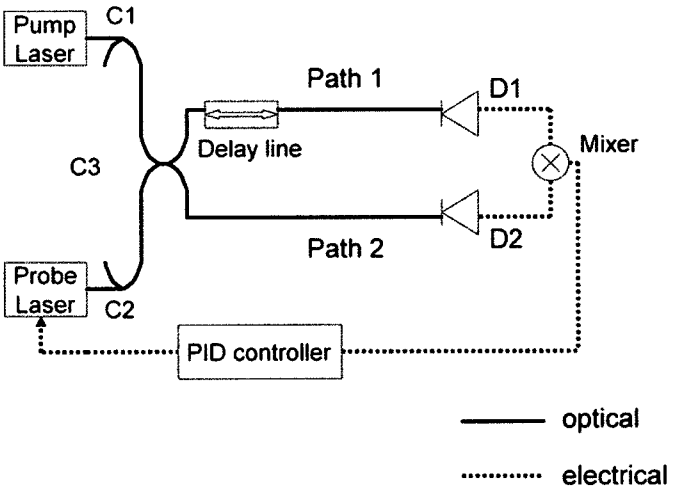

Fig. 3.1.2: Offset locking sub-system
C: coupler (1-2: 95/5, 3: 50/50), D: detector.

DFB lasers have broad bandwidth and large frequency fluctuations because of the very short photon lifetime in semiconductor laser resonators, a few picoseconds

compared with the conventional laser's tens of nanoseconds photon lifetime. Hence, the beat frequency of two DFB lasers cannot be locked using a frequency counter. In our distributed Brillouin sensor, the locking of the beat frequency is realized by offset locking the DFB lasers at various frequencies. The offset locking sub-system is shown in the Fig 3.1.2. Part of the output of the DFB lasers are first combined together and then split into two paths, one of which contains an optical delay line that is used to change the phase difference between the two paths. In the path that has no optical delay, the optical field can be written as:

$$X = E_{01}\cos(\omega_1 t + \phi_{01}) + E_{02}\cos(\omega_2 t + \phi_{02}) \tag{3.1.1}$$

where E_{01} and E_{02} are the optical amplitude of the two lasers, ω_1 and ω_2 are the optical frequencies of the two lasers, ϕ_{01} and ϕ_{02} are the optical phases of the two lasers. In the path that contains an optical delay line, the optical field can be written as:

$$Y = E_{01}\cos(\omega_1 t + \phi_{01} - \omega_1 \Delta t) + E_{02}\cos(\omega_2 t + \phi_{02} - \omega_2 \Delta t) \tag{3.1.2}$$

Δt is the time delay of the two paths. The optical signals of the two paths are converted to electrical signals by two photodiodes. The converted electrical signal can be considered as the following:

$$X^2 \propto \frac{1}{2}E_{01}^2 + \frac{1}{2}E_{02}^2 + E_{01}E_{02}\cos[(\omega_1 - \omega_2)t + (\phi_{01} - \phi_{02})] \tag{3.1.3}$$

$$Y^2 \propto \frac{1}{2}E_{01}^2 + \frac{1}{2}E_{02}^2 + E_{01}E_{02}\cos[(\omega_1 - \omega_2)t + (\phi_{01} - \phi_{02}) - (\omega_1 - \omega_2)\Delta t] \tag{3.1.4}$$

And then the converted signals are combined by a mixer, which is used as a phase comparator. The output signal from the mixer is given by:

$$V \propto \frac{1}{2} E_{01}^2 E_{02}^2 \cos[(\omega_1 - \omega_2)\Delta t] \tag{3.1.5}$$

It is a DC signal that is proportional to $\cos(\Omega\Delta t)$, where $\Omega = \omega_1 - \omega_2$. This DC signal can then be fed back to a PID controller circuit to lock the phase difference of ΩΔt between the two DFB lasers, as shown in the following Fig.3.1.3. The set point of the PID controller can be chosen at one of the zero crossing. Then, the difference between the measured phase difference and the set point is sent to the PID controller. The output from the PID controller is used to adjust the frequency of one of the DFB lasers via a current controller, in order to make ΩΔt constant.

The locking and tuning of the beat frequency of the two lasers can be fulfilled as follows: 1) when delay time Δt is fixed, the phase difference ΩΔt can be locked by the PID controller at a specific beat frequency Ω of the two DFB lasers; 2) For a new beat frequency Ω, the phase difference ΩΔt will be locked through PID via new Δt.

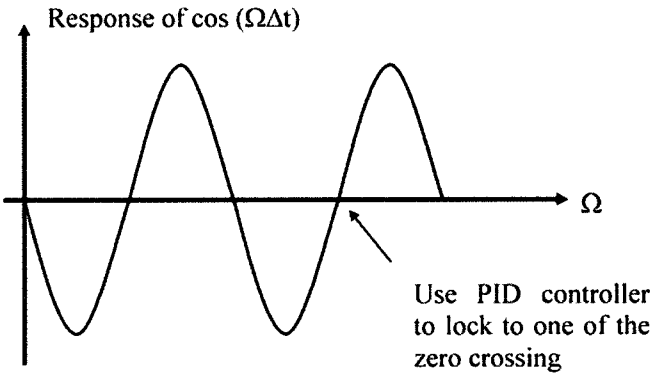

Fig. 3.1.3: Response curve of cos (ΩΔt) vs. Ω at the output of mixer.

3.1.2 EOM Bias Stabilization

The spatial information of the temperature or strain change is obtained by sending a probe pulse produced by an EOM to the testing fiber. The output pulse from the EOM always contains a DC base that is beneficial for short fiber length and centimeter resolution in reducing the Brillouin spectrum linewidth for better measurement accuracy through coherently adding the interaction between the DC base and the pump wave to the interaction between the pulse and the pump wave [Afshar 2003, Lecoeuche 1999]. While this DC base is harmful for long sensing length and meter spatial resolution in inducing the prolonged phonon lifetime and gain saturation problem [Bao *et al.* 2006]. Moreover, a critical problem with the EOM pulsing system is that the DC base does not stay constant but slowly drifts during the measurement time due to the charging effects or the variations in the temperature, wavelength, optical power, and polarization, even with a stabilized bias voltage [Jungerman *et al.* 1990, Li *et al.* 2003a]. The drifting DC base of the EOM induces pulse energy fluctuation and distorted Brillouin spectrum with reduced SNR and high measurement error.

In order to avoid this problem, in our distributed Brillouin sensor the EOM bias is locked at the minimum DC level by a lock-in amplifier [Meade 1983] as shown in Fig.3.1.1. The output DC voltage from the lock-in amplifier is proportional to the amplitude of the input signal and also depends on the phase difference between the

input signal and the reference signal from the lock-in amplifier. The output DC voltage and the reference signal from the lock-in amplifier that provides a small modulation on top of the optical pulse are fed into the bias port of the EOM along with the EOM bias power supply. Once the DC base of the optical pulse drifts away, the modulation amplitude will grow larger. The phase of the reference signal is set in such a way that a positive drift of the DC base will produce a negative output from the lock-in amplifier and vice versa. Thus, the drift is corrected by the output of the lock-in amplifier. This EOM bias locking method maintains the highest extinction ratio of the probe pulse, minimizes Brillouin gain saturation over long sensing fiber, and provides constant SNR. It should be noted that although the lock-in amplifier method is only capable of locking the pulse base to the minimum of the EOM transfer curve, the minimum pulse base level can be effectively increased by increasing the reference modulation amplitude. However, the increase of the pulse base level is accompanied by a significant increase in the measurement noise of the distributed Brillouin sensor because more noises are added to the probe pulse by increasing the reference modulation amplitude.

3.2 Sensor Performance

The experimental results shown in this section prove the effectiveness of offset locking technique in the distributed Brillouin sensor system. The beat signal could be

stabilized at a frequency of 10880.8 MHz for tens of minutes, which was much longer than the data acquisition time. The shift of this beat frequency was less than 250 kHz with a standard deviation of 50 kHz, which was much smaller than an unlocked frequency fluctuation that was tens of MHz. The following Fig.3.2.1 shows the relationship between the beat frequency and the optical time delay. The beat frequency tuning range is ~1 GHz and is limited by the delay time of the optical delay line.

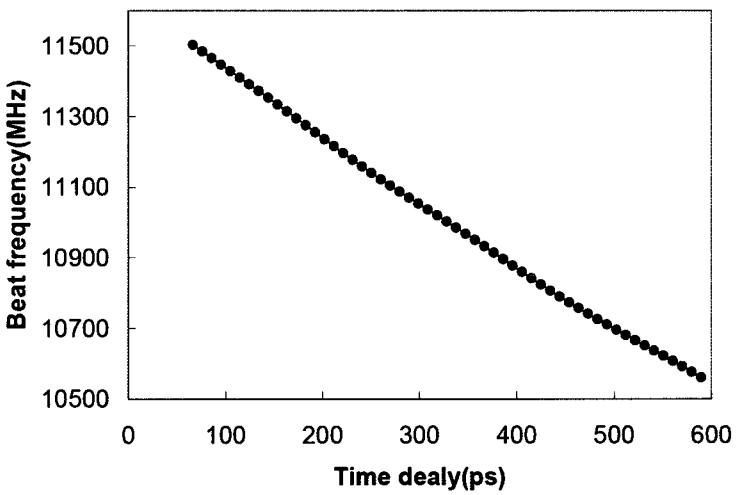

Fig. 3.2.1: Relationship between beat frequency and optical time delay.

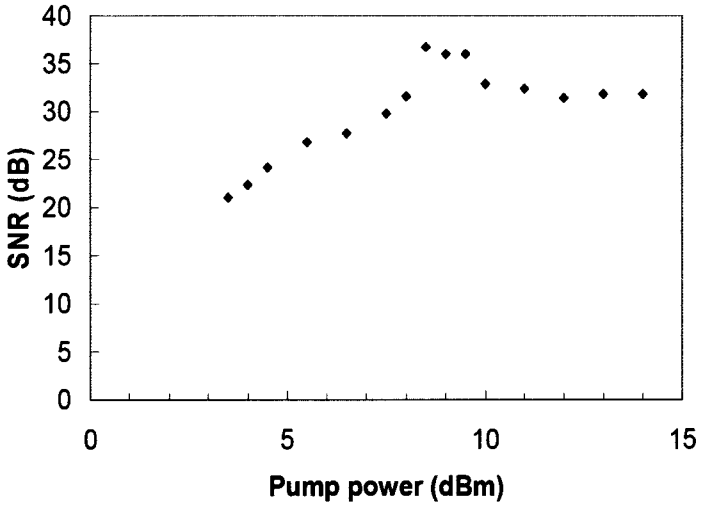

Fig. 3.2.2: SNR vs. Pump power.

The Brillouin spectra were measured using an optical pulse of 10 ns, which corresponds to a spatial resolution of 1m. As shown in Fig. 3.2.2. the pump power was set at 9 dBm in order to get an SNR better than 32 dB, which meant that the frequency uncertainty was 0.6 MHz that was equivalent to 0.5 °C temperature resolution. Further increase of the optical power would reduce the temperature or strain resolution due to the Brillouin gain saturation, as the pulse would be contaminated along the sensing fiber due to the distorted Brillouin spectrum [Bao *et al.* 2006]. To compensate the distortion, the location correlation method must be used to fit the Brillouin spectrum at each location to recover the Brillouin spectrum.

Table. 3.2.1: Central frequency, FWHM and SNR of Brillouin spectrum along the fiber with and without using lock-in amplifier

Lock In Amplifier	Central frequency of Brillouin spectrum (MHz)	FWHM of Brillouin spectrum (MHz)	SNR of Brillouin spectrum (dB)	Extinction Ratio(electrical) of pulse (dB)
off	10878.70 ± 4.65	58.99 ± 6.22	31.82 ± 3.60	35.30 ± 0.61
on	10878.80 ± 2.35	59.55 ± 2.25	26.64 ± 4.63	35.80 ± 0.06

The improvement of the EOM bias locking is shown in Table 3.2.1. Apparently the increased SNR leads to less variation of the Brillouin frequency and the FWHM of Brillouin spectra along the fiber, which indicates higher temperature or strain accuracy. The following Fig.3.2.3 shows how the peak frequency of the Brillouin spectrum changes with local temperature. The solid circles show the spectrum of the fiber at room temperature (23 °C) while the blank circles represent the spectrum of 1m sensing fiber immersed in ice-water (0 °C). The solid and dashed lines are the results of data reconstruction [Ravet et al. 2006]. It is found that the central frequency shifts by 27 MHz in ice water, which corresponds to the temperature change of 23 °C. The spectrum has no distortion and fits well with a Lorentzian shape.

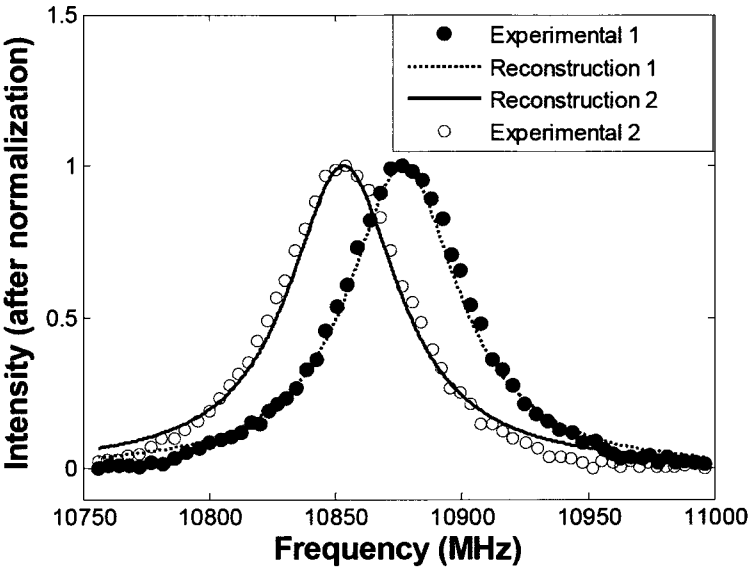

Fig. 3.2.3: The shift of the Brillouin spectrum when environmental temperature changes.
Experimental 1 and Reconstruction 1: T=23 °C
Experimental 2 and Reconstruction 2: T=0 °C

3.3 Conclusion

In conclusion, our distributed Brillouin sensor with offset locking technique has the following characteristics. Firstly, the offset locking technique provides three advantages for the distributed Brillouin sensors: 1) it changes the beat frequency through slightly changing the laser current by 10^{-5}A that is correspondent to 0.03% of the DFB laser's driving current; the tiny laser current change has no impact on the laser mode stability and has very low intensity fluctuation; 2) the beat frequency of the two lasers can be locked to any value in a wide range at high speed through simply adjusting the external optical delay line with minimum disturbance to the laser cavity,

which has no impact on laser frequency and power stability, and the frequency tuning can be done in micro-seconds that is limited by electronics; while in stabilized laser systems, the fast tuning is provided by the piezoelectric transducer (PZT) for <100 MHz range and the large frequency tuning is provided by thermal tuning, which makes the whole frequency tuning process last tens of minutes; 3) it can lock the phase difference between two lasers [Bao *et al.* 2005] well enough to gain coherent Brillouin interaction between the pump and probe beams. Hence, the linewidth of the Brillouin spectrum for a 10 ns pulse is less than 60 MHz for a pulse extinction ratio of ~30 dB. Secondly, because of the bias drift of the EOM, a lock-in amplifier is used to lock the DC level of the optical pulse at the minimum level. This locking process ensures the minimum pulse distortion for kilometers long sensing length, which prevents probe power variation, increases the SNR, and decreases the variation of the Brillouin frequency shift and the FWHM of Brillouin spectra along the fiber by half. Thirdly, in order to minimize the Brillouin spectrum distortion at kilometers-long fiber length, the pump power must be limited to below 10 mW to avoid Brillouin gain saturation. This allows us to achieve over 32 dB SNR for 10 ns pulses over 2-km-long fiber; and the Brillouin frequency measurement accuracy is 0.6 MHz, which is equivalent to 0.5 °C temperature resolution or 8 με strain resolution. Finally, to reduce the polarization dependence of the Brillouin gain spectrum, a polarization scrambling rate of 12.5 kHz is used.

The offset locking based distributed Brillouin sensor with cheap and widely

adopted devices described in this chapter presents a simple frequency locking method, large tuning range, high SNR, and fast tuning speed. The spatial resolution obtained with this system so far is 1 m with 0.5°C temperature resolution. The offset locking technique is therefore promising for the future development of distributed Brillouin sensors.

Chapter 4

High Spatial and Frequency Resolution Brillouin Sensor with Phase Locking Technique

As introduced in chapter 1, the strain and temperature measurement accuracy of the Brillouin sensor is limited by the linewidth and SNR of the Brillouin spectrum that determine the frequency resolution [Horiguchi *et al.* 1995]. The linewidth of the Brillouin spectrum in the distributed Brillouin sensor with the BOTDA technique is affected by the extinction ratio (ER) [Lecoeuche *et al.* 2000, Zou et al. 2005] and duration of the optical pulse wave [Bao *et al.* 1999, Smith *et al.* 1999, Bao *et al.* 2006]. As the pulse duration is reduced and the pulse spectrum becomes comparable to or greater than the linewidth of the natural Brillouin spectrum, the Brillouin gain decreases and the resultant Brillouin spectrum is a convolution of the pulse spectrum with the natural Brillouin spectrum [Smith *et al.* 1999]; thus, the linewidth of the Brillouin spectrum is increased. The desired Brillouin spectrum should be as narrow as possible for better frequency resolution, which means long duration pulse should be used. However, to obtain a spatial resolution on the order of centimeters, the pulse duration should be a few nanoseconds, which means the linewidth of the resultant Brillouin spectrum will be hundreds of MHz. Based on the theoretical calculation

results in Ref [Lecoeuche *et al.* 2000] and the experimental results in Ref [Zou *et al.* 2005], by increasing the DC base of the pulse, the acoustic wave created by the short pulses can be the same order of magnitude as the steady state acoustic wave created by the DC base, provided that the ER is less than 20 dB and the fiber length is from hundreds of metres to kilometres. Eventually, the linewidth of the Brillouin spectrum in the pulse-CW interaction is comparable to that of the steady-state interaction. Furthermore, when the ER is 20 dB for 8~10 ns pulse, the linewidth of the Brillouin spectrum increases to 80 MHz or more [Lecoeuche *et al.* 2000], which is much broader than the linewidth (35 MHz) of the natural Brillouin spectrum. Thus, with ER above 20 dB, the linewidth of the Brillouin spectrum will be above 100 MHz for pulses having a few nanoseconds duration.

The distributed Brillouin sensor described in chapter 3 uses offset locking technique to lock and tune the beat frequency of the two DFB lasers. The linewidth of the measured Brillouin spectrum in offset locking system for 10ns probe pulse with more than 20dB ER is around 60MHz. Normally the linewidth of the Brillouin spectrum for 10ns pulse with greater than 20dB ER is greater than 100MHz as described above [Lecoeuche *et al.* 2000]. The narrow Brillouin spectrum obtained in offset locking Brillouin sensor is caused by the phase locking of the light sources, which will be elaborated in detail in this chapter. In section 4.1, the laser source phase locking and frequency locking techniques will be described and the difference between the two locking method will be explained. In section 4.2, the spectral narrowing

phenomenon due to the phase locking of pump and probe waves is analyzed by incorporating a randomly varying phase for the input optical fields using three-wave coupled wave equations. The randomly varying phase has a de-correlation time associated with the inverse laser linewidth, and the narrowed linewidth corresponds to negligible phase noise. In section 4.3, the distributed Brillouin sensor with phase locking technique will be compared with the system with only frequency locking technique. Moreover, the characteristics of light sources' phase locking technique will be discussed in this section.

4.1 Phase Locking vs. Frequency Locking

In order to compare the impacts of laser source phase locking and laser source frequency locking on the performance of distributed Brillouin sensors, the phase locking and frequency locking techniques will be described and the difference between the two locking methods will be explained.

In the distributed Brillouin sensor with two laser sources, to get efficient Brillouin interaction and high signal intensity, the beat frequency of the two laser sources should match with the resonant Brillouin frequency of the fiber. The beat signal of the two laser sources can be written as:

$$E = A\cos(\omega_{beat}t + \varphi_{beat}) \tag{4.1.1}$$

In equation (4.1.1), if only ω_{beat} is locked while φ_{beat} drifts, it is called laser source frequency locking. If both ω_{beat} and φ_{beat} are locked, then it is called laser source phase locking because the phase term is locked. A phase locked loop is normally adopted to lock the phase term of the beat signal. In a phase locked loop, the phase difference between two laser sources are first detected by a phase detector, and then a feedback circuit is used to synchronously correct the phase drift of the beat signal. While in the frequency locking technique such as the injection locking, usually, the frequency of one laser source is forced to follow the frequency drift of the other laser source simply by adjusting the driving current or the length of the laser cavity, there is no feedback loop to synchronously correct the phase drift of the beat signal.

The difference between the impacts of the laser source phase locking and those of the laser source frequency locking on the efficiency of the Brillouin scattering will be illustrated in the following. In the laser source phase locking, such as that used in the offset locking based distributed Brillouin sensor described in chapter 3, firstly, the lightwaves from two laser sources were combined together to achieve the beat signal of the two laser sources; then, a phase comparator was adopted to detect the phase difference of these two lightwaves; after that, a PID feedback circuit was used to synchronously correct the drift of this phase difference by adjusting the current source of one of the laser sources. In other words, in the phase locking technique, the frequency difference between the two laser sources was converted to phase difference between the two laser sources by using a phase detector and a phase locked loop was

adopted to lock this phase difference. Once this phase difference was locked, both the frequency difference and the phase difference of the two laser sources were constant and the Brillouin interaction between these two laser sources was highly coherent. The highly coherent Brillouin scattering ensured that the Brillouin spectrum had high gain and narrow linewidth. While in the laser source frequency locking, such as that used in the injection locking based distributed Brillouin sensor [Thévenaz *et al.* 2004], there was no phase detector to convert the frequency difference between the two laser sources to the phase difference between the two laser sources. The frequency difference was measured and locked directly. The slave laser's resonator was disturbed by the master laser's resonator at a nearby frequency. When the coupling was strong enough by injecting carrier from the master laser to the slave laser, the resonator of the slave laser could capture the resonator of the master laser, causing the slave laser to have essentially identical frequency as the master laser. However, there was no connection between the phase of the master laser and the phase of the slave laser. Hence, although the frequency difference of the master laser and slave laser was constant, the phase difference of these two laser sources that was caused by the fluctuation of the carrier density inside the gain medium drift all the time and the two laser sources were not in phase. Because of the random phase noise of the two laser sources, the Brillouin interaction between these two laser sources was not coherent and the Brillouin spectrum obtained with laser source frequency locking had broad linewidth.

In next section, the difference between laser source phase locking and frequency locking and their impacts on the distributed Brillouin sensor will be studied through performing a numerical simulation based on an improved three wave coupled equations.

4.2 Theoretical Model and Numerical Simulation

The theoretical model used to simulate the Brillouin scattering in the sensing fiber is based on the following three-wave coupled wave equations with the slowly-varying amplitude approximation for the pump, probe, and acoustic waves [Agrawal 2007]:

$$(\frac{\partial}{\partial z}-\frac{n}{c}\frac{\partial}{\partial t})E_p = ig_1 Q E_s + \frac{1}{2}\alpha E_p \tag{4.2.1}$$

$$(\frac{\partial}{\partial z}+\frac{n}{c}\frac{\partial}{\partial t})E_s = -ig_1 Q^* E_p - \frac{1}{2}\alpha E_s \tag{4.2.2}$$

$$(\frac{\partial}{\partial t}+\Gamma)Q = -ig_2 E_p E_s^* \tag{4.2.3}$$

where E_p, E_s, and Q denote the fields of the CW pump, pulsed Stokes, and acoustic wave respectively, g_1 and g_2 represent the photon-phonon coupling coefficients, α is the attenuation factor of the fiber, $\Gamma = \Gamma_1 + i\Gamma_2$ with $\Gamma_1 = \frac{1}{2\tau_{ph}}$ representing the damping rate with phonon lifetime, τ_{ph}~10 ns for silica fiber, and Γ_2 denotes the detuning frequency.

Equations (4.2.1-4.2.3) are solved by applying the numerical method in Ref

[Chu *et al.* 1992] and the simulation code is written in FORTRAN 95. The boundary conditions are input pump power P at one fiber end ($z = L$) and input Stokes pulse at the other end ($z = 0$). The input Stokes pulse at the output of EOM is described by:

$$E_s(0,t) = A_{out}\{\cos\theta \exp[i\eta\phi(t)] + \sin\theta \exp[-i(1-\eta)\phi(t)]\} \qquad (4.2.4)$$

with $A_{out} = \sqrt{\frac{I_{in}}{2}} \exp[iwt + i\varphi(t)]$ and $\phi(t) = \phi_0 + \phi_{\max} \exp\{-(\ln 2)[\frac{2(t-t_0)}{\tau}]^m\}$ specifying the m[th] order super Gaussian pulse. $\phi(t)$ is the phase difference between the optical waves in the two arms of the EOM and it contains the modulation information. ϕ_0 is the actual bias phase difference. $\phi_{\max}$ denotes the maximum possible phase difference produced by applied modulation voltage of EOM. $\eta \in [0, 1]$ denotes the ratio of the voltage induced phase in the upper arm of EOM to the total phase $\phi(t)$. $\theta = \arctan\frac{A_2}{A_1}$, where A_1 and A_2 represent the amplitudes of the optical waves in the two arms of EOM. $\varphi(t)$ represents the laser phase noise, which is the rapid, short-term, random fluctuations in the phase of the optical wave and is related to the bandwidth of the laser source. In order to compare the Brillouin spectra from phase locked laser sources with those from only frequency locked laser sources, the parameter $\varphi(t)$ is chosen as the following: for phase locked laser sources, because the phase of the beat signal is locked, the phase noise $\varphi(t)$ is considered as a constant all along the fiber, which is the same as the analysis presented in Ref [Zou *et al.* 2005, Bao *et al.* 2005]; for laser sources that are only frequency locked, because the phase of the beat signal drifts all the time, the phase noise $\varphi(t)$ is simulated by a coloured Gaussian noise [Fox *et al.*

1988, Zhu *et al.* 1986], whose correlation function is an exponential decay function with de-correlation time associated with the inverse laser bandwidth. The simulation code for generating the coloured Gaussian noise in written in FORTRAN 95 and it is shown in the Appendix.

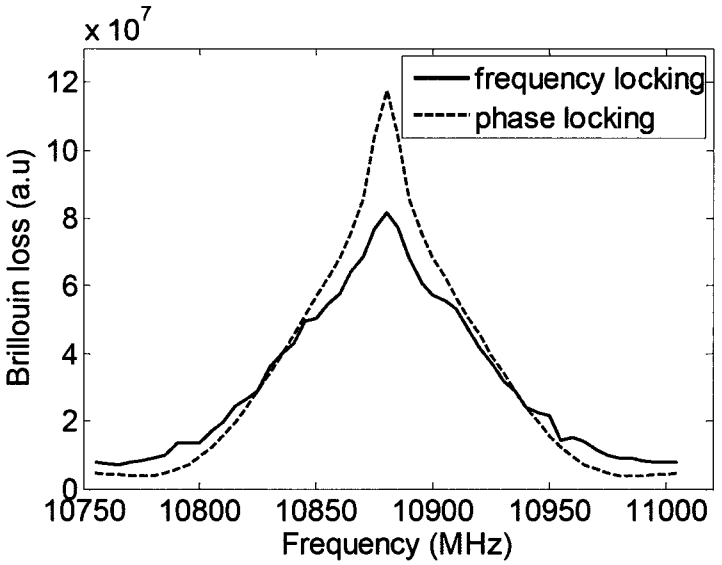

Fig. 4.2.1: Simulated Brillouin spectrum for10 m fiber and10 ns pulse with 24 dB extinction ratio). Dash line (FWHM~57 MHz), solid line (FWHM~100 MHz).

In the simulation, single mode fiber with Brillouin frequency of 10880 MHz under room temperature was used. Fig.4.2.1 shows the averaged Brillouin loss spectra in the middle of a 10 m sensing fiber for a 10 ns probe pulse with 24 dB extinction ratio. The dashed line represents the spectrum calculated by setting the phase noise $\varphi(t)$ as a constant, which is equivalent to infinite correlation time, all along the fiber.

The FWHM of the spectrum denoted by the dashed line is 57 MHz. The solid line is the spectrum calculated when the phase noise $\varphi(t)$ is considered as a coloured Gaussian noise with 10 ns correlation time, which represents the case when two laser sources are not phase locked together but only the frequency difference of them is kept at the Brillouin frequency of the sensing fiber. The FWHM of the spectrum denoted by the solid line is around 100 MHz. Based on the comparison of these two spectra, it is found that by decreasing the correlation time of the phase noise, the gain of the Brillouin scattering decreases and the FWHM of the Brillouin spectrum increases for pulses that have the same width and the same ER.

The gain reduction and the spectrum broadening are caused by the phase mismatch between the pump and probe waves induced by the laser phase noise in the case of only frequency locking. Under this condition, the interaction among the pump, probe, and acoustic waves is thus intensity added which leads to the Brillouin gain decreasing and the linewidth of the Brillouin spectrum increasing. When two phase-locked laser sources are used, the pump, probe, and acoustic waves are all in phase. These waves generate coherent Brillouin scattering with maximum Brillouin gain within the linewidth of the natural spectrum due to the optical field adding, while outside the linewidth of the Brillouin spectrum, the Brillouin amplification is much weaker since the phase and frequency matching conditions are not both fulfilled. As a result, a narrowed and higher Brillouin gain spectrum is obtained.

4.3 Experimental Results and Discussion

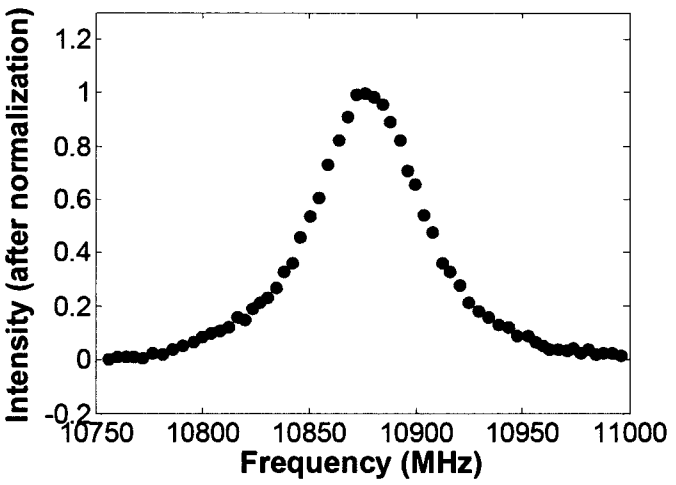

(a)

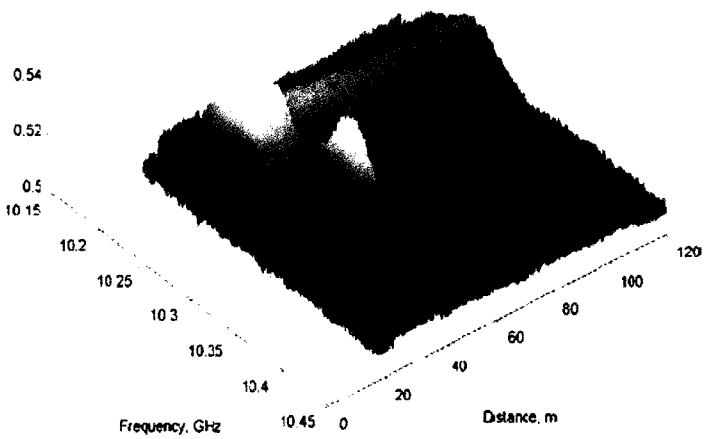

(b)

Fig. 4.3.1: Measured Brillouin spectrum with 10 ns pulse

(a) Phase locking (FWHM~52 MHz) (fiber length 2 km)

(b) Injection locking (FWHM~110 MHz) (Ref. [Thévenaz *et al.* 2004]), the same as simulated result in Fig.1.

In Fig.4.3.1, the Brillouin spectrum measured with the phase locking technique is compared with the spectrum measured with the injection locking technique [Thévenaz *et al.* 2004] using 10 ns pulse. With the phase locking technique, the FWHM of the Brillouin spectrum measured with a 24 dB ER pulse along 2 km fiber is 52 MHz, which is very close to the calculated FWHM (~50 MHz) in Fig.4.3.2 (a). The FWHM of the Brillouin spectrum measured with 2 km fiber in Fig.4.3.2 (a) is a little bit smaller than that measured with 10 m fiber due to the integrated DC contribution. However, in the injection locking technique, the frequency change is tuned through the mismatching of the laser mode and no phase is detected. The two laser sources are only frequency locked at the Brillouin frequency by a laser side mode. The linewidth of the Brillouin gain spectrum becomes comparable to the pulse spectral width. Thus, the Brillouin interaction between pump wave and probe wave via acoustic wave is not as efficient as that under the phase locked condition. Even with a commercial EOM that usually has a 20 dB ER, the FWHM of the Brillouin spectrum without laser source phase locking can increase to over 110 MHz, which is very close to the 10 ns pulse spectrum width and the calculated Brillouin spectrum line width in Fig.4.2.1.

Furthermore, it is found that there exists an optimized pump and probe power to ensure the narrowest linewidth of the Brillouin spectrum and highest SNR for the distributed fiber sensor. Above this optimized power level, the increased pump or probe power leads to decreased SNR and broadened Brillouin spectrum even for a

uniform fiber. Fig.4.3.2 shows the relationship between the FWHM/SNR of the Brillouin spectrum and the input pump power. By phase locking pump and probe waves to perform coherent Brillouin scattering, the Brillouin spectrum with narrow FWHM and high SNR can only be achieved within the working range of pump power from 8 dBm to 14 dBm when using DFB lasers with a 2 km sensing fiber. The pump power that is higher than 14 dBm will induce gain saturation, distort the Brillouin spectrum, and decrease the SNR. When high pump power is used, the peak frequency reaches the maximum gain and then becomes saturated, which results in prolonged phonon lifetime and distorted Brillouin spectrum [Bao *et al.* 2006]. When low pump power (around 8 dBm in Fig. 4.3.2 (a)) is used, the linewidth (42MHz) of the Brillouin spectrum with fiber laser sources that has 1 kHz phase locking bandwidth is narrower than the linewidth (55MHz) of the Brillouin spectrum with DFB laser sources that has 250 kHz phase locking bandwidth. However, the optimum working range that is from 8 dBm to 12 dBm with fiber laser sources is smaller than the optimum working range that is from 8 dBm to 14 dBm with DFB laser sources in Fig. 4.3.2 (a). This is because under narrower phase locking bandwidth, the Brillouin gain is higher, thus the gain saturation effect can occur at lower pump power. The similar linewidth of the Brillouin spectrum for DFB lasers with 2 MHz laser bandwidth and for fiber laser with 5 kHz laser bandwidth proves that the linewidth of the Brillouin spectrum in BOTDA sensor is not determined by the laser bandwidth. The better the phase locking quality of the pump and probe lasers, the fewer the phase noises between the pump and probe lasers

are. Thus, the phonon field generated by the phase locked pump and probe lasers is enhanced and coherent Brillouin interaction can be obtained. The coherent Brillouin interaction ensures the achievement of narrow linewidth Brillouin spectrum. Hence, the phase locking quality of the pump and probe lasers, which is the phase locking bandwidth and which determines the enhanced phonon field generated by the phase locked pump and probe lasers, plays an important role in determining the linewidth of the Brillouin spectrum in the coherent Brillouin scattering.

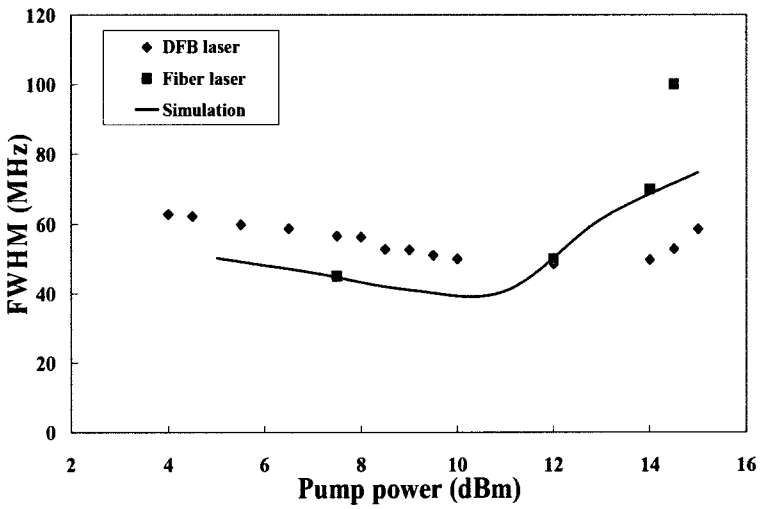

(a)

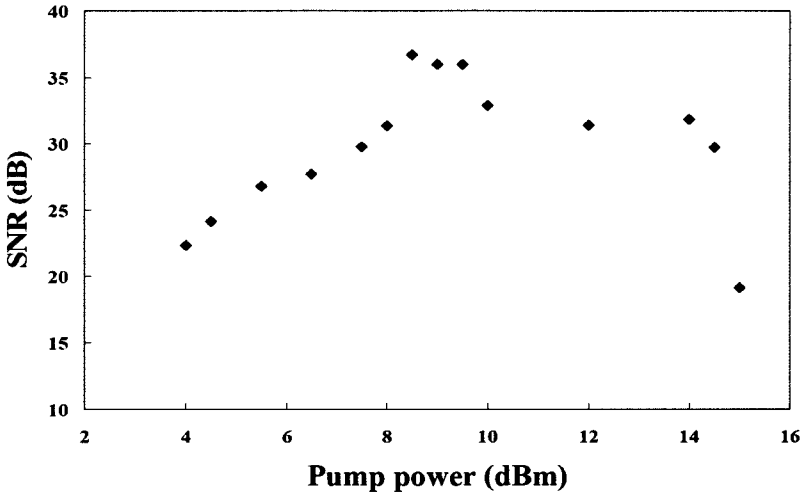

(b)

Fig. 4.3.2: (a) FWHM of the Brillouin spectrum change with pump power
(Fiber length: 2km; laser line width in simulation: 2MHz)
(b)) SNR of the Brillouin spectrum change with pump power
(Fiber length: 2km).

Our theoretical and experimental results show the following: 1) two phase locked laser sources give a narrow Brillouin spectrum for nanosecond pulses even when the DC base of the pulse is kept at the minimum level; 2) if the pump wave, probe wave, and acoustic wave are not in phase, the linewidth of the Brillouin spectrum can be increased up to the pulse spectral linewidth; 3) the phase locking technique can apply not only to laser sources with kHz bandwidth, such as fiber lasers, but also to laser sources with MHz bandwidth, such as DFB lasers, to reduce the linewidth of the Brillouin spectrum; 4) the Brillouin scattering with the phase locking technique requires much lower pump and probe power than the Brillouin scattering with the frequency locking technique because the enhanced phonon field is in phase

with the pump and probe waves. The better the phase locking quality of the pump and probe lasers, that is the smaller phase locking bandwidth, the lower the maximum pump and probe power can be applied.

4.4 Conclusion

Applying low ER optical pulses in a BOTDA sensor system gives the advantages of a narrow Brillouin spectrum linewidth and a relatively high Brillouin signal; however, it has the drawback of distorted Brillouin spectra [Bao *et al.* 2006] caused by gain saturation, especially for a kilometres-long sensing fiber. The advantages of obtaining narrow Brillouin spectrum by applying high ER nanosecond pulse with phase locked laser sources are as the following: 1) the minimum DC base prevents Brillouin spectrum distortion caused by the gain saturation when the long length sensing fiber is used; 2) the pulse distortion due to the prolonged phonon relaxation time [Bao *et al.* 2006] can be minimized, thus the correct location information can be guaranteed; 3) the centimeter spatial resolution in the time domain BOTDA can be achieved with high strain and temperature measurement accuracy over kilometres-long sensing length with low pump and probe power.

In conclusion, the phase effect in the Brillouin spectrum narrowing phenomenon has been studied with phase locked DFB lasers in a BOTDA system. It has been shown theoretically and experimentally that two laser sources that are not phase locked can

contribute to a broadening of the Brillouin spectrum up to pulse spectral width. Under the conditions of nanosecond pulse with minimum DC leakage in the phase locked BOTDA system with fiber laser sources or DFB laser sources, the Brillouin spectrum is much narrower than the pulse spectrum. This research provides an efficient and simple way to build a sensor system that has high spatial resolution, high frequency resolution, relatively low power, and long sensing length.

Chapter 5

High Spatial and Frequency Resolution Brillouin Sensor with Different Pulse Width Pair BOTDA Technique

The distributed Brillouin sensor with offset locking technique described in chapter 3 and 4 can obtain 1m spatial resolution with ~ 60MHz Brillouin spectrum linewidth over a 2km long testing fiber. In order to identify the early crack and deformation of the civil structures, higher spatial and strain resolutions are required, which means the pulse that have a smaller than 5ns pulse width, which is equivalent to higher than 0.5m spatial resolution, should be used. However, the narrow pulse brings two severe problems to the distributed Brillouin sensors: 1) the narrow pulse corresponds to a broader spectrum than the natural Brillouin spectral linewidth (~35MHz), and this means that the detected Brillouin loss or gain spectrum via the interaction of the pump, probe and acoustic waves in fibers will be broadened, which results in low Brillouin peak frequency detection accuracy and low strain and/or temperature resolution; 2) the narrow pulse width means the short interaction length for the pump, probe and acoustic waves, and the low Brillouin loss signal, hence the low strain resolution. To overcome the above problems, people use pre-pumping approach to further increase the DC base of the probe pulse

[Zou *et al.* 2005]. The DC base of the probe beam interacts with the pump beam over the entire sensing fiber, while the interaction between the pulsed part of the probe beam and the pump beam provides the spatial information of the temperature or strain change. These two parts are added coherently to get narrow spectrum and high spatial resolution. However, the required DC level varies with the sensing length and optical power. When the sensing length is very long, for example a few kilometers, it will be difficult to control the amount of the DC portion of the probe signal. There exists a trade-off between the DC leakage of pre-pumping and the Brillouin spectrum narrowing, because the interaction between the pump and the probe via DC base of the pulse can be much stronger than the Brillouin loss signal at a specific small and short strain section via the pulse part interaction. Hence, the small strain cannot be detected [Wang *et al.* 2008]. In field applications such as the nerve system in the smart materials, the distributed Brillouin sensor is required to detect many closely (less than 1m) located strain sections. Because of the short (10ns) phonon relaxation time and the short (less than 1m) separation length between two strain sections, the Brillouin signal from the first strain section would overwhelm the Brillouin signal from the second small strain section. Thus, the minimum detectable frequency shift for the detection of short and small strain sections in the conventional BOTDA sensor equals to the linewidth of the Brillouin spectrum, especially when the strain sections are closely located. Moreover, when the testing fiber length is over tens of kilometers the pre-pumping technique will cause gain saturation and spectrum distortion that will induce the strain measurement error.

In this chapter, a novel different pulse width pair BOTDA (DPP-BOTDA) sensor proposed by our group will be described [Li *et al.* 2008a]. The DPP-BOTDA is capable of detecting small strain and/or temperature changes over centimeter fiber section by using long duration (tens of nanosecond) pulses over kilometer sensing length. The idea is to use a pair of same shaped broad pulses ($\tau_1 = \tau$ and $\tau_2 = \tau+\delta\tau$) to generate time domain BOTDA signal one after another, and then calculate the difference of the two time domain waveforms at the same frequency to obtain the differential Brillouin gain signal at each position of fiber. Because of the small pulse width difference of the pulse pair, the difference in Brillouin loss signal is negligible for the same strain or temperature fibers. When the strain or the temperature varies at a specific fiber location, the difference of the Brillouin losses at this location will be quite different, because the relative Brillouin gain or loss within τ and $\tau+\delta\tau$ at this position are different. As a result, the DPP-BOTDA sensor can show the difference for the small and short strain sections at the zero signal background while the BOTDA sensor shows the difference for the small and short strain sections at a nonzero signal background that corresponds to the non-strained fiber section. The ultimate spatial and strain resolution in the DPP-BOTDA sensor will also be studied experimentally and theoretically in this chapter by examining two short and small strain sections and then comparing the performance with that of the BOTDA sensor whose pulse width equals the pulse width difference of the pulse pair in the DPP-BOTDA sensor system.

5.1 Working Principle and Demonstration of the DPP-BOTDA Sensor

The DPP-BOTDA sensor employs two separate long (a few tens of nanoseconds) pulses with a small (a few nanoseconds) pulse-width difference to map the Brillouin gain spectrum of the sensing fiber. When two temporal Brillouin gain signals are obtained by injecting a pair of pulsed light with different pulse-width τ and $\tau+\delta\tau$ to the fiber, the subtraction of those two signals removes the common term, such as equal temperature or strain portion, and retains the difference [Li *et al.* 2008a]. Actually, in the DPP-BOTDA sensor, the signal that is obtained is the differential Brillouin gain caused by the pulse-width difference rather than the Brillouin gain caused by long period pulses. This differential process is shown schematically in the following Fig. 5.1.1, where $I(0,t,\tau)$ and $I(0,t,\tau+\delta\tau)$ denote the temporal Brillouin gain signals obtained at $z=0$ by using two probe pulses with different pulse widths τ and $\tau+\delta\tau$ at a particular detuning frequency, $I(0,\delta\tau)$ represents the gain difference between them. For a small strained section at position z of the testing fiber, its relative position as well as the Brillouin gain within the pulse width τ and $\tau+\delta\tau$ are different. The subtraction of these two Brillouin signals allows detecting such a difference signal at zero background. Hence, the DPP-BOTDA is capable of detecting tiny strain and/or temperature change

within a length equals to $\frac{1}{2}\upsilon\delta\tau$, where υ is the light velocity inside the fiber. By tuning the frequency difference between the pump wave and the probe wave, measuring the time domain Brillouin signals with the probe pulse pair, and then subtracting the two Brillouin signals, the differential Brillouin gain spectra can be mapped out along the testing fiber. The spatial resolution of such DPP-BOTDA sensor is related to the pulse width difference of the probe pulse pair.

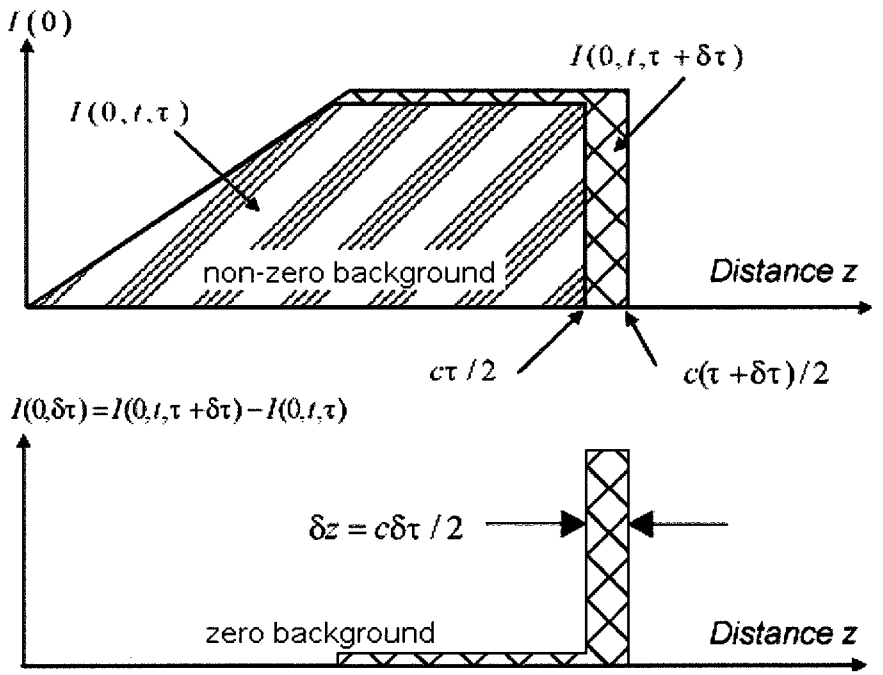

Fig. 5.1.1: working principle of DPP-BOTDA [Li *et al.* 2008a]

The experimental demonstration of the DPP-BOTDA sensor is made by Wenhai Li in our group [Li *et al.* 2008a]. The experimental setup is based on the conventional

BOTDA system. Light sources are two Nd:YAG lasers whose operation wavelengths are 1320nm. The beat frequency of the two laser sources is locked and tuned by a frequency counter. The peak power of the probe pulse is around 12mW and the pump power is around 4mW. The length of the testing fiber is 1km with two 0.5m strain sections that have 1m separation. The strain applied to the two strain sections is around 2000 με and 3000 με respectively. Fig. 5.1.2 shows the 3-dimensional Brillouin spectra. Fig. 5.1.2 (a) is the one obtained by the conventional BOTDA sensor with 50ns probe pulse. It is illustrated that the two 0.5m strain sections occurring at position 5m are overlapping over a length of around 9m. Due to the 5m spatial resolution, the two 0.5m strain sections cannot be discriminated. The linewidth of the Brillouin gain spectrum is around 30MHz because of the tens of nanosecond probe pulse used. Fig. 5.1.2 (b) is the one obtained by the DPP-BOTDA sensor with 50/45ns probe pulse pair. Even though the pulse widths are 50ns and 45ns, the two 0.5m strain sections can be clearly resolved and the linewidth of the Brillouin spectrum is still around 30MHz.

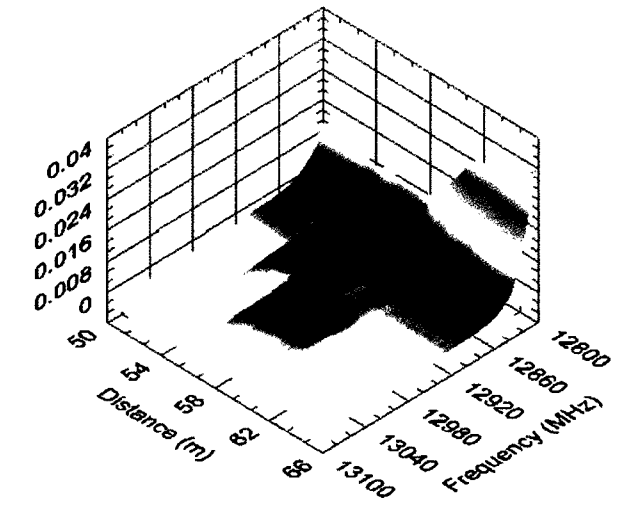

(a)

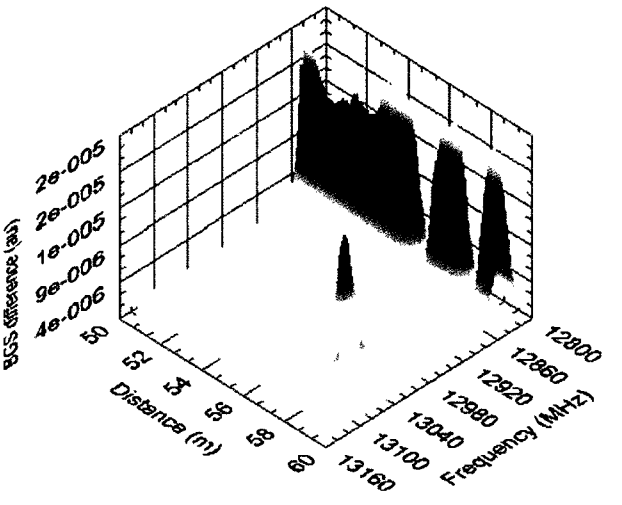

(b)

Fig. 5.1.2: 3-dimensional Brillouin spectrum (a) conventional BOTDA sensor with 50ns probe pulse. (b) DPP-BOTDA sensor with 50/45ns probe pulse pair. [Li *et al.* 2008a]

The DPP-BOTDA sensor has the following advantages over the conventional BOTDA sensor: 1) narrow (< 35MHz) linewidth Brillouin gain spectrum and high (< 1m) spatial resolution can be obtained simultaneously due to the long duration probe pulses used and subtraction of the two Brillouin signal, which enhances the

measurement accuracy of the Brillouin frequency shift and strain and/or temperature location; 2) high (> 30dB) extinction ratio pulses can be used without the need of pre-pumping for long sensing length that is over a few kilometers, so the effect of the prolonged phonon lifetime and gain saturation can be avoided; 3) the differential Brillouin gain spectrum provides stronger signal intensity and thus higher SNR than those of the BOTDA sensor that directly uses narrow pulse width when the pulse width difference of the pulse pair equals the narrow pulse width.

5.2 Measurement Accuracy of the DPP-BOTDA Sensor

In section 5.1, it is demonstrated that high spatial resolution and strain resolution can be obtained at the same time with the DPP-BOTDA technique. In the following, the ultimate spatial and strain resolution in DPP-BOTDA sensor is demonstrated experimentally and theoretically by examining two short and small strain sections that are closely located. The performance of the DPP-BOTDA sensor will be compared with that of the conventional BOTDA sensor whose pulse width equals to the pulse width difference of the applied probe pulse pair in the DPP-BOTDA sensor.

The experimental setup is the DFB laser offset locking based distributed Brillouin sensor described in Chapter 3. As shown in Fig. 5.2.1, in order to reduce the gain fluctuation caused by the polarization dependent Brillouin gain, a 5 meters PM fiber is used as the sensing section. Two polarization beam splitters are connected to

both ends of the PM fiber to ensure the pump and probe light aligned at the same Principal State of Polarization (PSP) of the PM fiber. The Brillouin frequency of loose PM fiber at room temperature is ~10.59GHz for 1550nm operation wavelength and the strain is applied over a length of ~20 cm.

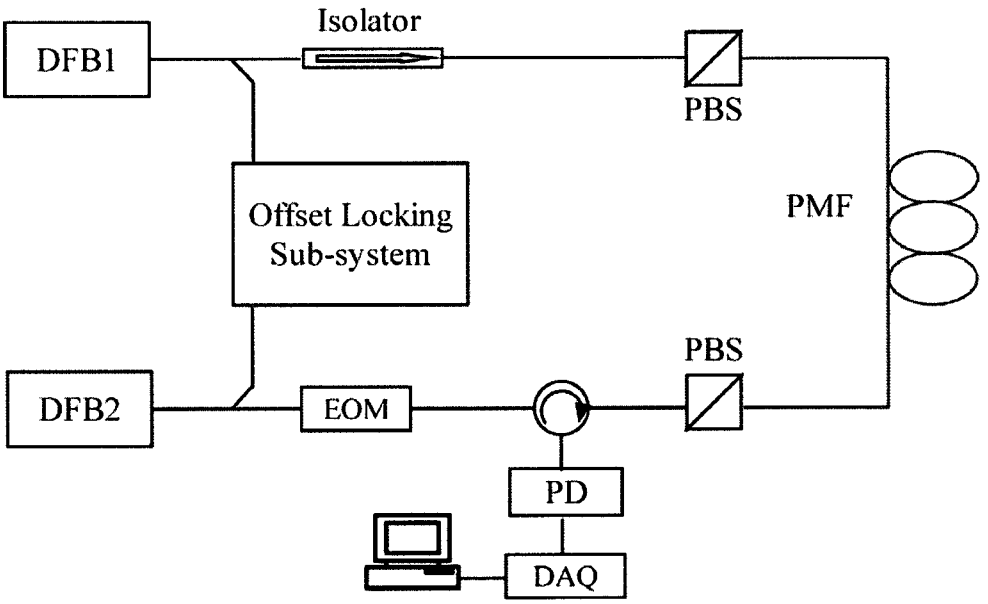

Fig. 5.2.1: Experimental Setup: DFB: Distributed Feedback Laser, EOM: Electro-optic Modulator, PMF: Polarization Maintaining Fiber, PBS: Polarization Beam Splitter, PD: Photo detector, DAQ: Data Acquisition Card

The theoretical model used to simulate the sensing fiber in the DPP-BOTDA sensor is based on the following three-wave coupled equations for the pump, probe, and acoustic waves with the slowly-varying amplitude approximation [Agrawal 2003]:

$$(\frac{\partial}{\partial z}-\frac{n}{c}\frac{\partial}{\partial t})E_p = ig_1 Q E_s + \frac{1}{2}\alpha E_p \tag{5.2.1}$$

$$(\frac{\partial}{\partial z}+\frac{n}{c}\frac{\partial}{\partial t})E_s = -ig_1 Q^* E_p - \frac{1}{2}\alpha E_s \tag{5.2.2}$$

$$(\frac{\partial}{\partial t}+\Gamma)Q = -ig_2 E_p E_s^* \tag{5.2.3}$$

where E_p, E_s, and Q denote the fields of the CW pump, pulsed Stokes, and acoustic wave respectively. g_1 and g_2 are the photon-phonon coupling coefficients, α represents the fiber attenuation, $\Gamma = \Gamma_1 + i\Gamma_2$ with $\Gamma_1 = \frac{1}{2\tau_{ph}}$ being the damping rate with phonon lifetime τ_{ph}~10 ns for silica fibers, and $\Gamma_2 = 2\pi(\nu_p - \nu_s - \nu_B)$ denoting the detuning angular frequency between the pump and probe waves away from local Brillouin frequency ν_B. Equations (5.2.1-5.2.3) are solved through applying the numerical method in Ref [Kalosha *et al.* 2006a, Kalosha *et al.* 2006b]. The boundary conditions are input pump power P at one fiber end $z = L$ and input Stokes pulse at another end $z = 0$. The input Stokes pulse is described by the two-kink profile function $A(t) = \left[\frac{(\tanh t_1 - \tanh t_2)}{2}\right]^{1/2}$, where $t_{1,2} = (t \pm \frac{\tau_s}{2})/a$ and τ_s is the pulse duration. The rise time is defined as a time interval between pulse power levels 0.1 and 0.9 of the peak power at leading and tailing edges, and then it is related to the parameter a as $t_{rise} = a/0.45$.

5.2.1 Strain Location Determination

In the DPP-BOTDA sensor with a different pulse width pair, by subtracting the Brillouin gain of the larger pulse from that of the narrower pulse, the strain location, which is defined as the central position of the applied strain, is shifted by $\tau_2 + \frac{\tau_1 - \tau_2}{2} - \frac{tt}{2}$ from that in the BOTDA sensor as shown in Fig. 5.2.2, where τ_1 is the pulse duration of the longer pulse of the pulse pair, τ_2 is the pulse duration of the narrower pulse of the pulse pair, and tt is the rise/fall time of the optical pulse. The strain location of the experimental result is shifted by 1.93m for 20/19ns pulse pair with 0.67ns pulse rise time, which is close to $\tau_2 + \frac{\tau_1 - \tau_2}{2} - \frac{tt}{2}$. The strain location shift $\tau_2 + \frac{\tau_1 - \tau_2}{2} - \frac{tt}{2}$ is a constant that relates to the duration and rise time of the pulse pair, thus in real field test, in order to obtain the correct strain location, people only need to subtract this constant from all the location information.

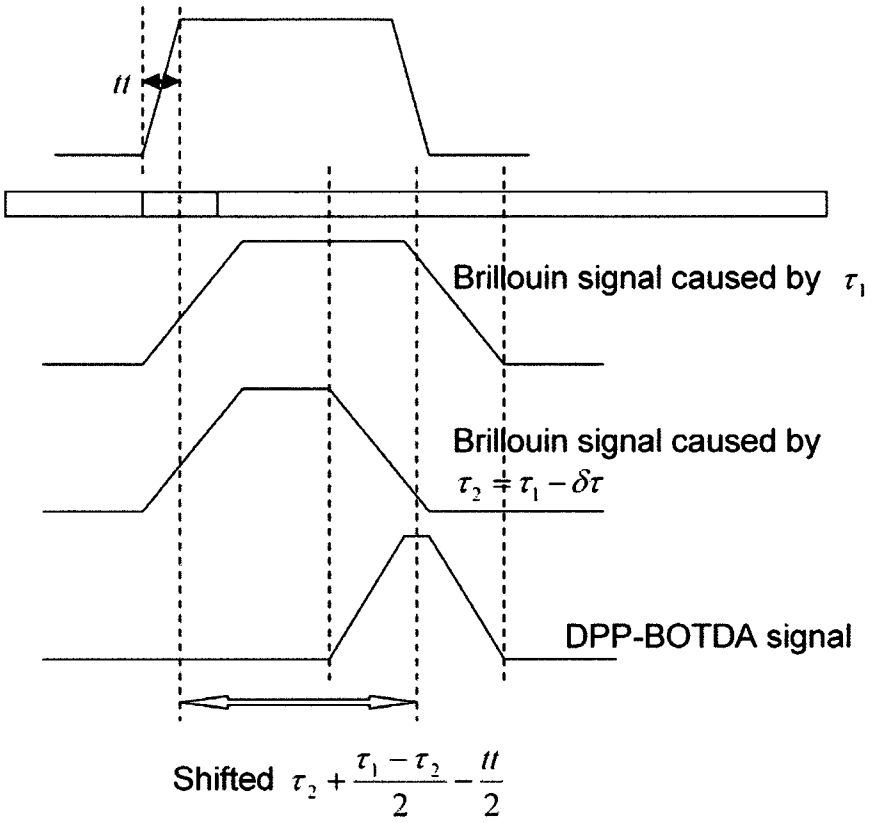

Fig. 5.2.2: Time domain Brillouin signal in DPP-BOTDA sensor

5.2.2 Spatial Resolution Determination

The spatial resolution of a distributed fiber sensor can be defined as 1) the probe pulse width if the bandwidth of the detection system is larger than the pulse spectrum [Horiguchi *et al.* 1995] and the spatial resolution is limited by the phonon lifetime [Fellay *et al.* 1997] or 2) the rise time during which the Brillouin signal increases from 10% to 90% of its peak value. Since the DPP-BOTDA sensor detects the differential

Brillouin gain rather than the Brillouin gain itself, the spatial resolution can be much smaller than the probe pulse width; here we use the second definition.

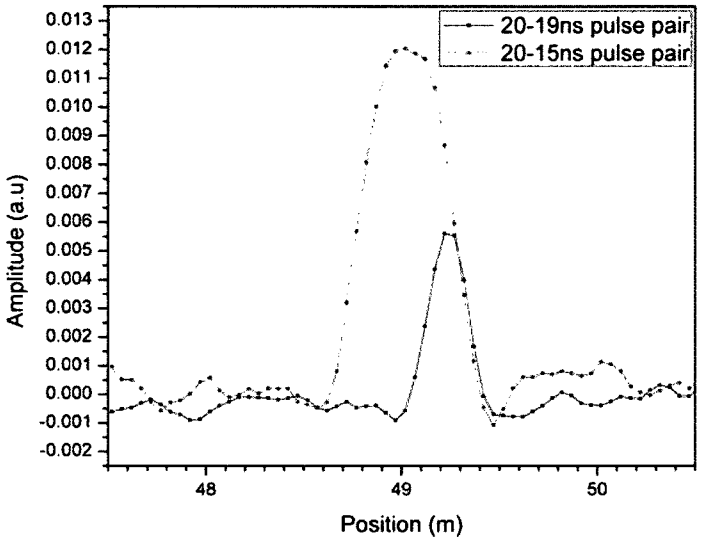

Fig. 5.2.3: DPP-BOTDA signal change with pulse width difference of pulse pair

The spatial resolution of the DPP-BOTDA sensor is determined by the pulse width difference of the pulse pair. Fig. 5.2.3 shows the time domain DPP-BOTDA sensor signals when the pulse pairs are 20/19ns and 20/15ns, the rise/fall time of both pulse pairs are 0.67ns. With 20/19ns pulse pair, the spatial resolution is 0.12m that is shorter than that (0.26m) with the 20/15ns pulse pair. This is the results of the high pass filtering effect in DPP-BOTDA sensors. In the DPP-BOTDA sensor the subtraction of Brillouin signal from two nearly equal width pulses can be considered as

a high pass filtering process. The DPP-BOTDA sensor emphasizes the differential Brillouin gain rather than the Brillouin gain itself for the small strain section that is experienced by two different pulses at the same location. The cutoff frequency f of this high pass filtering process is inversely proportional to the pulse width difference of the pulse pair, which can be expressed as $f \propto \frac{1}{\Delta\tau}$, where $\Delta\tau$ is the pulse width difference of the pulse pair. Small signal fluctuations or high frequency components can be more easily detected with smaller pulse width difference. Hence, in order to obtain high spatial resolution, the pulse width difference of the applied pulse pair should be as small as possible. However, there exists a trade-off between the spatial resolution and the SNR that is proportional to strain resolution. When the pump power is 5mW, the SNR for 20/19ns pulse is 36.78dB that gives the strain resolution of 85με and the SNR for 20/15ns pulse is 41.70dB that is equivalent to 64με strain resolution.

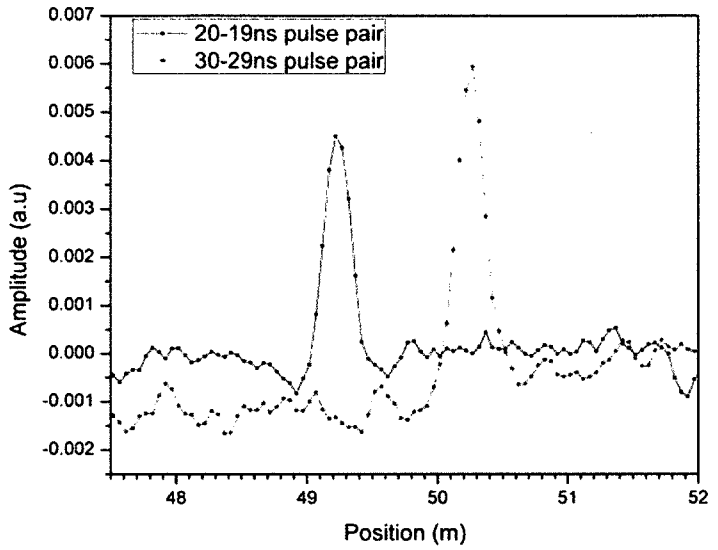

Fig. 5.2.4: DPP-BOTDA signal change with absolute pulse width of pulse pair

Next, the spatial resolution for the DPP-BOTDA sensor with pulse width difference of 1ns over different pulse pairs of 30/29ns and 20/19 ns is examined. Fig.5.2.4 shows the detected Brillouin signals in the DPP-BOTDA sensor with 30/29ns and 20/19ns pulse pairs for the same pulse rise time of 0.67ns respectively. The spatial resolution of 20/19ns pulse pair is 0.12m, which is very close to the 0.18m spatial resolution obtained by 30/29ns pulse pair. However, the detected differential signal in the DPP-BOTDA sensor with 30/29ns pulse pair is greater than that with 20/19ns pulse pair. This means higher SNR in the DPP-BOTDA sensor for the pulse pair with larger pulse widths and thus higher strain resolution. The higher SNR for the pulse pair with

larger pulse widths is caused by the nonlinear amplification property of the Brillouin interaction. Due to the nonlinear process of the Brillouin interaction, the gain difference between 30ns and 29ns pulse pair is greater than the gain difference between 20ns and 19ns pulse pair.

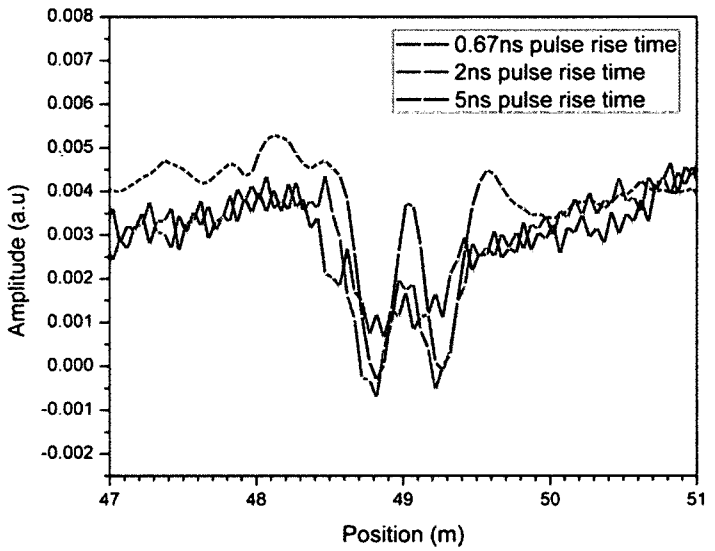

(a)

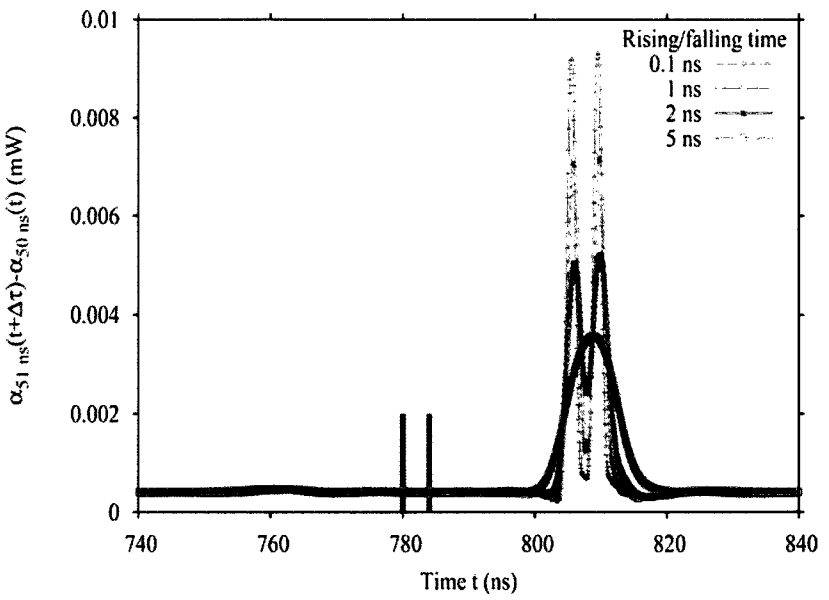

(b)

Fig. 5.2.5: Spatial resolution of DPP-BOTDA with pulse pair of 20/19ns at different pulse rise time for the two stress sections (marked by two vertical lines in (b)) separated by a 20cm loose fiber section for the experimental (a) and simulated (b) results. Note the time shifted phenomenon discussed for DPP-BOTDA in (b)

The pulse rise time t_{rise} also plays an important role in determining the spatial resolution of the DPP-BOTDA sensor. Fig 5.2.5 (a) is the experimental result of the time domain DPP-BOTDA sensor signal when the optical pulse rise/fall time was changed from 0.67ns to 5ns. There are two strain sections (frequency shift ~ 75MHz) along the testing fiber. The fiber length of each strain section is 20cm and the two strain sections are separated by a 20cm loose fiber. When the rise time of the optical pulse is 0.67ns, the two strain sections can be easily detected; however, the two strain sections can not be discriminated with the optical pulse of 5ns rise/fall time. The same result is also demonstrated by the simulation that is shown in Fig 5.2.5 (b). During the

Brillouin interaction the sharp strain and/or temperature variation can be detected only if a rise/fall time shorter than the strain length is used.

Thus, the ultimate spatial resolution in the DPP-BOTDA sensor is defined as $\Delta l = \upsilon \cdot t_{rise}$, where t_{rise} is the optical pulse rise/fall time and υ is the light velocity inside the optical fiber. The spatial resolution in the conventional BOTDA sensor is defined as $\Delta l = \frac{1}{2}\upsilon \cdot \tau$, where τ is the pulse width and υ is the light velocity inside the optical fiber. In the DPP-BOTDA sensor experiment, the rise time of the optical pulse is 0.67ns that corresponds to ~13cm spatial resolution, while in the conventional BOTDA sensor, the spatial resolution is 20cm by using 2ns probe pulse. The spatial resolution in the DPP-BOTDA sensor is even shorter than that in conventional BOTDA sensor with the same power and short pulse width that equals the pulse width difference of the pulse pair in the DPP-BOTDA sensor.

Therefore, the spatial resolution of the DPP-BOTDA sensor is independent of the absolute pulse width; it is determined by the pulse width difference of the pulse pair if the rise/fall time of the pulse is shorter than the equivalent strain length and the pulse width difference. Furthermore, the limitation of the spatial resolution of the DPP-BOTDA sensor is the optical pulse rise time. While in the BOTDA sensor the ultimate spatial resolution is limited by the phonon life time (~10ns) that corresponds to 1m spatial resolution for high extinction ratio pulse (>30dB).

5.2.3 Strain Resolution Determination

The strain resolution in the DPP-BOTDA sensor is determined by the SNR and FWHM of the measured Brillouin spectrum as

$$\delta\upsilon = \frac{\Delta\upsilon_B}{\sqrt{2}(SNR)^{1/4}} \qquad (5.2.4)$$

where $\Delta\upsilon_B$ is the FWHM of the convolution between the natural Brillouin spectrum and the pulse spectrum, and the SNR is the electrical signal-to-noise power ratio [Horiguchi *et al.* 1995]. For the pulse width pair that has bigger absolute pulse width, the measured Brillouin spectrum is narrower and the SNR is higher, thus the strain resolution is higher. For the pulse width pair that has the same absolute pulse width, the greater the pulse width difference of the pulse pair, the higher the SNR, thus the higher the strain resolution.

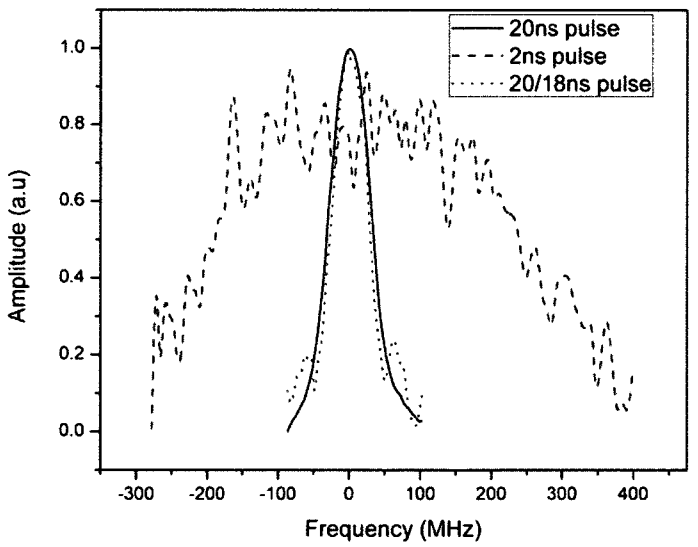

Fig. 5.2.6: Brillouin spectra of BOTDA with 2ns and 20ns pulses, DPP-BOTDA with 20/18ns pulse pair.

Fig.5.2.6 compares the Brillouin spectrum obtained under the same power by the DPP-BOTDA sensor with 20/18ns pulse pair and the BOTDA sensor with 2ns and 20ns pulses. In the DPP-BOTDA sensor, $\Delta\upsilon_B$ is around 50MHz by applying 20/18ns pulse pair, while in the BOTDA sensor it is around 400MHz by adopting 2ns probe pulse. Because of the spectral width difference between the DPP-BOTDA sensor and the BOTDA sensor, the strain resolution in the DPP-BOTDA sensor is eight time higher than that in the BOTDA sensor. Moreover, the measured SNR of the DPP-BOTDA sensor is 36.78dB for 20/18ns pulse pair with a 10dBm pulse peak power and the measured SNR of the conventional BOTDA sensor is 18.72dB for 2ns pulse with the same peak power. The SNR is greatly increased in the DPP-BOTDA sensor in optical domain and the increase is around 18dB after the data processing.Thus, the strain resolution of the DPP-BOTDA sensor is 85με and that of the BOTDA sensor is 2000με. The strain resolution is increased by more than 13dB by the DPP-BOTDA sensor.

In summary, the measurement accuracy of the strain location, the spatial resolution, and the strain resolution in a novel DPP-BOTDA sensor system is studied. High spatial resolution, high frequency resolution and high SNR can be achieved by utilizing pulse pairs that have large absolute pulse width, small pulse width difference, and short pulse rise/fall time in the DPP-BOTDA sensor. The ultimate measurement

accuracy in the DPP-BOTDA sensor is determined by the combination of the system bandwidth, system SNR, absolute pulse width, pulse width difference, and the rise/fall time of the pulse.

5.3 Conclusion

In conclusion, a novel DPP-BOTDA sensor that can measure distributed strain and/or temperature with high spatial resolution of 0.12m over kilometer long testing fiber has been demonstrated in this chapter. The DPP-BOTDA technique can obtain narrow Brillouin spectrum by using long pulse width and can achieve high spatial resolution by the subtraction of the two Brillouin signals that are obtained with two different probe pulse widths. By choosing proper pulse width pair and their rise/fall time, a spatial resolution of <0.2m and Brillouin frequency accuracy of 2-3MHz for kilometer long fiber is demonstrated. The proposed technique is suitable for static and quasi-static measurement such as civil structural health monitoring and perimeter applications that require high measurement and spatial resolution over long sensing length.

Chapter 6

High Spatial and Frequency Resolution Brillouin Sensor with Optical Differential Parametric Amplification Technique

With the DPP-BOTDA technique that is described in previous chapter, it is possible to obtain high spatial resolution and high SNR at the same time. However, the DPP-BOTDA technique requires sweeping the frequency twice to obtain two signal traces, which increases the measurement time. In this chapter, a new approach, the coherent interaction of the Brillouin gain and loss via optical differential parametric amplification (ODPA) in a single mode fiber, will be described. Simultaneous Brillouin gain and loss processes on the CW sensing field can be created through two large pulses at the Stokes and anti-Stokes wavelengths interacting with two counter-propagating acoustic waves. The simultaneous Brillouin gain and loss processes inside the sensing fiber maintain the shorter measurement time in the ODPA-BOTDA sensor than that in the DPP-BOTDA sensor. The narrow Brillouin spectrum as that in the DPP-BOTDA sensor is guaranteed because of the large pulse used. The coherent interaction between the Brillouin gain and loss at the CW sensing field creates a small pulse proportional to the pulse width difference of the Stokes and

anti-Stokes waves, which makes high spatial resolution possible. More importantly, both the DPP-BOTDA sensor and the ODPA-BOTDA sensor use photodetector to collect the data. Because of the limited dynamic range of the photodetector, the higher the signal intensity, the easier the photodetector will become saturated. In the DPP-BOTDA sensor, normal Brillouin signal is detected by the photodetector and the subtraction of the two Brillouin signals is performed after the photodetector. Thus, it will be easier for the photodetector to become saturated with large signal when the fiber length is long. While in the ODPA-BOTDA sensor, the signals have been subtracted in the optical field before reaching the photodetector and the ODPA-BOTDA sensor detects the difference of the signal directly. Thus, the photodetector in the ODPA-BOTDA sensor is less likely to become saturated and longer sensing length is possible. Because of the large pulse applied for both Brillouin gain and loss process, this ODPA process maintains low saturation to the gain and low depletion to the loss, hence the sensing length is longer than that in the normal BOTDA sensor.

6.1 Theoretical Study of the ODPA-BOTDA Sensor

In this section, we will describe the working principle of the ODPA-BOTDA sensor. A novel theoretical model dealing with the ODPA-BOTDA sensor will be derived and the simulation results will be presented.

6.1.1 Working Principle of the ODPA-BOTDA Sensor

In the scheme of the ODPA-BOTDA shown in Fig. 6.1.1, the anti-Stokes pulse and Stokes pulse are launched into the sensing fiber simultaneously with different pulse widths of τ and $\tau + \Delta\tau$ working in the Brillouin loss regime. Two related SBS processes are occurring in the same region of the sensing fiber at the same time. For the SBS process between anti-Stokes pulse and CW sensing wave, the CW sensing wave receives Brillouin gain and generates a counter-propagating acoustic wave; while for the SBS process between Stokes pulse and CW sensing wave, the CW sensing wave gives energy to the Stokes pulse as a pump, which acts as Brillouin loss, and the enhanced acoustic wave has the opposite direction of the previous generated acoustic wave via anti-Stokes pulse. Because the CW wave acts as pump for Stokes and probe for the anti-Stokes, and we detect this wave in the distributed sensor, we call it "CW sensing wave".

If the Stokes and anti-Stokes pulses are carefully chosen, at the overlapping region of the two pulses, the Brillouin gain and loss of CW sensing wave could counterbalance each other, where the energy is first transferred from anti-Stokes pulse to the CW wave and then is transferred from the CW wave to Stokes pulse, and the CW wave power is unchanged. The differential process of the ODPA-BOTDA sensor is realized in optical domain, while this process is performed in electric domain in the

DPP-BOTDA sensor through subtraction [Li *et al.* 2008a, Dong *et al.* 2009]. The effective pulse width is the differential pulse width of the anti-Stokes and Stokes pulses, such as $\Delta\tau$, which determines the spatial resolution of the ODPA-BOTDA sensor and the starting time of sensing fiber is the trailing edge of the smaller pulse of the pulse pair. The narrow differential parametric Brillouin gain spectrum can be obtained by long anti-Stokes and Stokes pulses. In order to well balance the Brillouin gain and Brillouin loss, the anti-Stokes and Stokes pulses should have the same power and polarization, and their leading edge should be launched into the sensing fiber simultaneously.

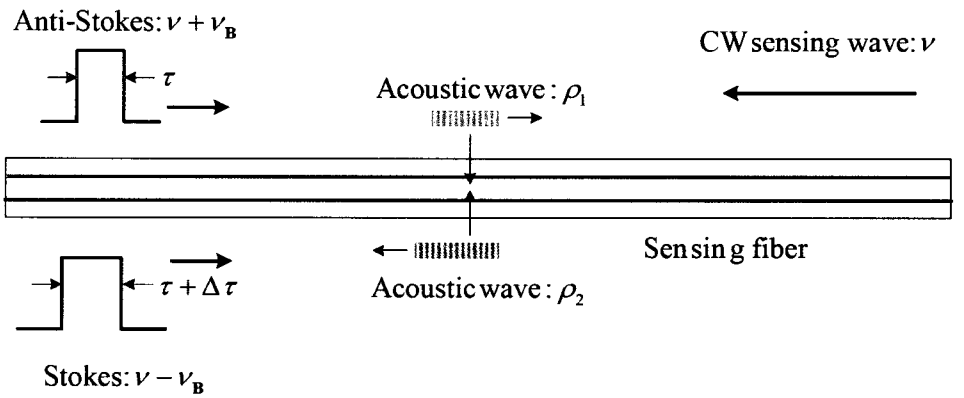

Fig. 6.1.1: Schematic diagram of the ODPA-BOTDA

6.1.2 Theoretical Model of the ODPA-BOTDA Sensor

As shown in Fig. 6.1.1, the optical fields inside the optical fiber can be written as [Boyd 2003]:

$$E_1 = A_1(z,t)e^{i(-k_1 z-\omega_1 t)} + c.c. \tag{6.1.1}$$

$$E_2 = A_2(z,t)e^{i(k_2 z-\omega_2 t)} + c.c. \tag{6.1.2}$$

$$E_3 = A_3(z,t)e^{i(k_3 z-\omega_3 t)} + c.c. \tag{6.1.3}$$

where A_1, A_2, and A_3 are the complex slowly varying amplitude of the light waves respectively, ω_1 is the carrier frequency of the CW sensing wave, which is affected by both the anti-Stokes pulse and the Stokes pulse, and ω_2 and ω_3 are the carrier frequencies of the two pulsed Stokes and anti-Stokes waves. The pulsed Stokes and anti-Stokes fields of E_2 and E_3 propagate along the positive z directions while the CW sensing field E_1 propagates along the negative z direction. Similarly, the acoustic fields are described in terms of the material density distribution as the following:

$$\tilde{\rho}_1 = \rho_0 + [\rho_1(z,t)e^{i(-q_1 z-\Omega_1 t)} + c.c.] \tag{6.1.4}$$

$$\tilde{\rho}_2 = \rho_0 + [\rho_2(z,t)e^{i(q_2 z-\Omega_2 t)} + c.c.] \tag{6.1.5}$$

In the above acoustic field distributions, ρ_0 denotes the mean density of the material and $\Omega_1 = \omega_1 - \omega_2$, $\Omega_2 = \omega_3 - \omega_1$, $\mathrm{q}_1 = k_1 + k_2$, $\mathrm{q}_2 = k_3 + k_1$. The acoustic field $\tilde{\rho}_1$ propagates along the negative z direction while the acoustic field $\tilde{\rho}_2$ propagates along the positive z direction.

It is assumed that the material densities obey the acoustic wave equation:

$$\frac{\partial^2 \tilde{\rho}}{\partial t^2} - \Gamma' \nabla^2 \frac{\partial \tilde{\rho}}{\partial t} - v^2 \nabla^2 \tilde{\rho} = \vec{\nabla} \cdot \vec{f} \tag{6.1.6}$$

in which υ is the velocity of sound, Γ' is a damping parameter, and $\vec{f}$ is the force per unit volume caused by electrostriction [Boyd, 2003]. The spatial evolutions of the optical fields are described by the wave equation [Boyd 2003]:

$$\frac{\partial^2 E_i}{\partial z^2} - \frac{n^2}{c^2}\frac{\partial^2 E_i}{\partial t^2} = \frac{4\pi}{c^2}\frac{\partial^2 \tilde{P}_i}{\partial t^2} \qquad i = 1,2,3 \tag{6.1.7}$$

After simplifying the optical wave equations and these acoustic wave equations, we can get the following coupled five wave equations:

$$\begin{cases} -\frac{\partial A_1}{\partial z} + \frac{n}{c}\frac{\partial A_1}{\partial t} = \frac{i\omega_1 \gamma_e}{2nc\rho_0}\rho_1 A_2 + \frac{i\omega_1 \gamma_e}{2nc\rho_0}\rho_2^* A_3 - \frac{1}{2}\alpha A_1 \\ \frac{\partial A_2}{\partial z} + \frac{n}{c}\frac{\partial A_2}{\partial t} = \frac{i\omega_2 \gamma_e}{2nc\rho_0}\rho_1^* A_1 - \frac{1}{2}\alpha A_2 \\ \frac{\partial A_3}{\partial z} + \frac{n}{c}\frac{\partial A_3}{\partial t} = \frac{i\omega_3 \gamma_e}{2nc\rho_0}\rho_2 A_1 - \frac{1}{2}\alpha A_3 \\ (-2i\Omega_1 + \Gamma_B)\frac{\partial \rho_1}{\partial t} + (\Omega_B^2 - \Omega_1^2 - i\Omega_1\Gamma_B)\rho_1 = \frac{\gamma_e q_1^2}{4\pi} A_1 A_2^* \\ (-2i\Omega_2 + \Gamma_B)\frac{\partial \rho_2}{\partial t} + (\Omega_B^2 - \Omega_2^2 - i\Omega_2\Gamma_B)\rho_2 = \frac{\gamma_e q_2^2}{4\pi} A_3 A_1^* \end{cases} \tag{6.1.8}$$

Here α is the attenuation coefficient of the fiber, and Γ_B is the inverse phonon lifetime. In the parametric amplification process, the interaction between optical fields E_1, E_2, and acoustic field $\tilde{\rho}_1$ is a Brillouin loss process. E_1 also interacts with E_3 via acoustic field $\tilde{\rho}_2$, which is a Brillouin gain process. The effect of Brillouin loss process and Brillouin gain process on optical field E_1 is a coherent process of field addition rather than intensity addition. In Equation (6.1.8) it is clear that in equation for

A_1, E_1 is associated with E_2 via A_2 and E_3 via A_3 simultaneously. Due to the well balanced energy transfer between the Brillouin gain process and the Brillouin loss process, the Brillouin spectral width will not be the same as the gain process or the loss process alone.

6.1.3 Numerical Simulation and Results Discussion

The performance of the ODPA-BOTDA sensor was simulated by the coupled five wave theoretical model described in section 6.1.2. The simulation code is written in FORTRAN95, excerpt of which is shown in the Appendix. In the simulation, the power of continuous wave E_1 was 3.3dBm, the peak power of the Stokes and anti-Stokes pulses were 6.9dBm and the extinction ratio of the two optical pulses were over 30dB. The pre-pumping effect can be neglected because of the high ER pulses used [Zou *et al.* 2005]. The Stokes pulse width was 20ns and the anti-Stokes pulse width was 19ns. A 50cm-long strain section was made in the middle of the testing fiber and the Brillouin frequency shift induced by the strain was 5MHz that corresponds to 85με. The computations were performed for a 10m-long fiber and a linear loss coefficient of 0.2dB/km.

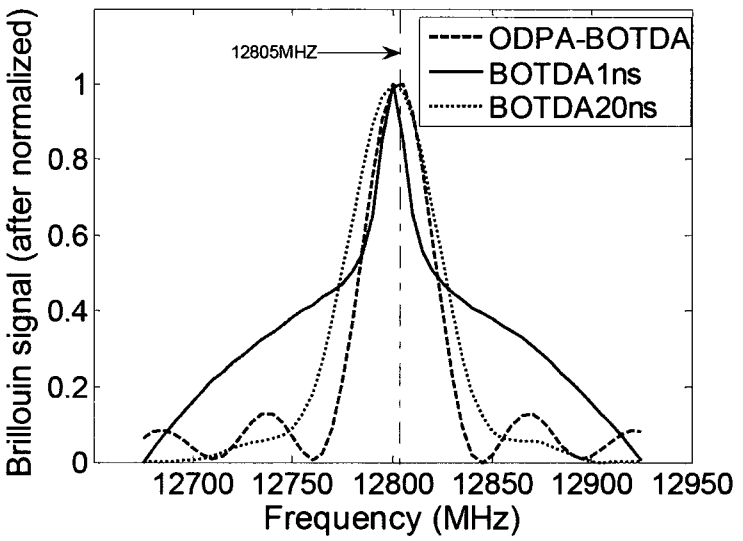

(a)

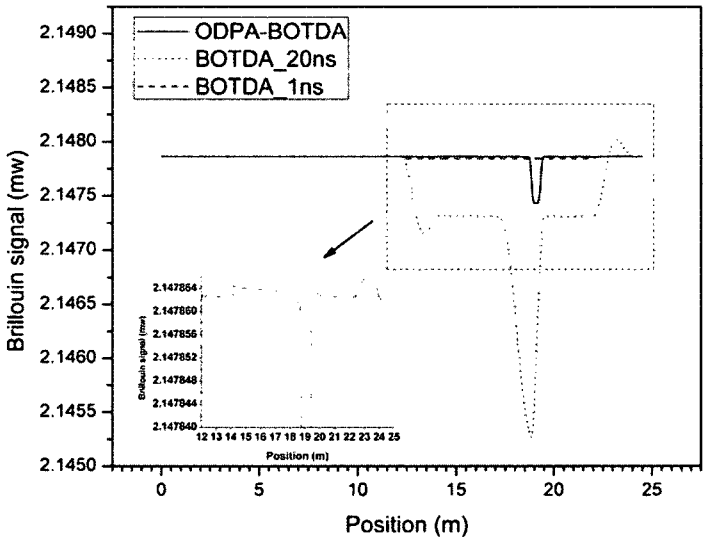

(b)

Fig. 6.1.2: (a) Brillouin spectrum comparison between the BOTDA sensor with 20ns pulse, the BOTDA sensor with 1ns pulse, and the ODPA-BOTDA sensor with 20/19ns pulse pair (Simulation).

(b) Time domain signal comparison between the BOTDA sensor with 20ns pulse, the BOTDA sensor with 1ns pulse, and the ODPA-BOTDA sensor with 20/19ns pulse pair (Simulation).

Fig. 6.1.2 demonstrates that the spatial resolution and frequency resolution of the ODPA-BOTDA technique are better than those of the BOTDA technique. Fig. 6.1.2 (a) shows the Brillouin spectra at the strain location for the ODPA-BOTDA sensor with 20/19ns pulse pair and the BOTDA sensor with 20ns and 1ns probe pulses. For the ODPA-BOTDA technique, it is clearly shown that the peak Brillouin frequency shifts 5MHz while for the BOTDA technique the Brillouin frequency shift cannot be discriminated. Fig. 6.1.2 (b) is the time domain sensing signal at the Brillouin frequency shift of 50MHz for 1ns pulse of the BOTDA sensor and 1ns pulse width difference of the ODPA-BOTDA sensor. Since 5MHz Brillouin frequency shift can't be detected by the BOTDA sensor due to the low power used for the Stokes, the anti-Stokes, and the CW sensing waves, we increase the Brillouin frequency shift to 50MHz. In the BOTDA sensor with 20ns pulse, we see a strain length of 2m and a detected sensing fiber length of 12m, which equals L+δL, where L is the real fiber length and $\delta L = \tau\upsilon$, τ is the probe pulse width and υ is the light velocity inside the fiber; and the detected sensing length is greater than the real sensing length of 10m. While in the ODPA-BOTDA sensor, the 50cm strain section can be illustrated clearly because of the instantaneous counterbalance between the Brillouin gain and the Brillouin loss processes. Moreover, in the ODPA-BOTDA sensor the effective probe pulse is the differential pulse, for example it is 1ns for the 20/19ns pulse pair used in the simulation, so that the spatial resolution is determined by 1 ns differential pulse and

the start time is the trailing edge of 19ns pulse. This is why the strain location has a 1.9m shift compared with that in the BOTDA sensor with 1ns pulse. The shift of the strain location in the ODPA-BOTDA sensor is correspondent to 19ns pulse of the 20/19ns pulse pair. However, this is a constant shift along the sensing fiber and the location information can be correctly determined by simply subtracting this constant shift. In addition, in the ODPA-BOTDA sensor the signal strength at the strain section is 24dB higher than that at the loose fiber section, while in the BOTDA sensor with 20ns pulse this contrast is only 6dB and in the BOTDA sensor with 1ns pulse this contrast is only 0.1dB, which indicates that small strain section can be more easily detected in the ODPA-BOTDA sensor. Apparently the signal contrast between the stressed fiber and loose fiber in the ODPA-BOTDA sensor with 20/19ns pulse pair is higher than that in the BOTDA sensor with either 1ns or 20ns pulse width. Moreover, because of the counterbalance between the Brillouin gain process and the Brillouin loss process in the ODPA-BOTDA sensor, it is less likely for the sensing signal to become saturated in the ODPA-BOTDA sensor than in the BOTDA sensor when long length sensing fiber is used. Thus, the ODPA-BOTDA technique can be used to build distributed Brillouin sensor that has kilometer-long length.

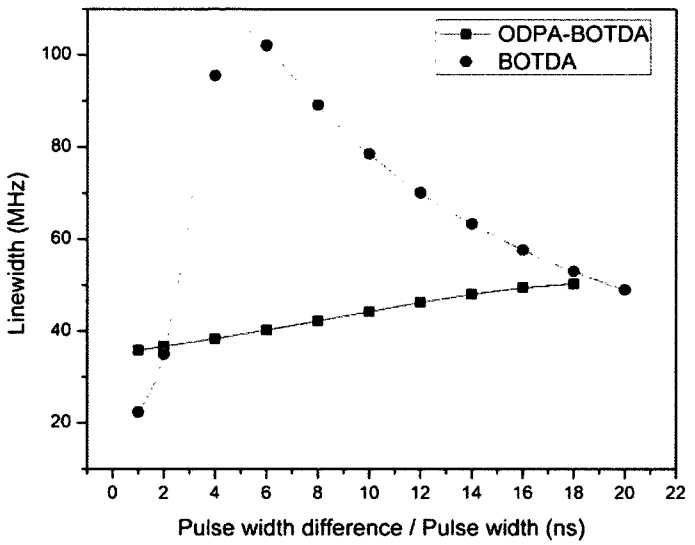

Fig. 6.1.3: Linewidth of the Brillouin spectrum vs. the pulse width different in the ODPA-BOTDA sensor and vs. the pulse width in the BOTDA sensor (Simulation).

The linewidth of the Brillouin spectrum versus the pulse width difference in the ODPA-BOTDA sensor and the linewidth of the Brillouin spectrum versus the pulse width in the BOTDA sensor are presented in Fig. 6.1.3. The ER of the pulses in the simulation equals 30dB. The linewidth of the Brillouin spectrum in the ODPA-BOTDA sensor increases as the pulse width difference increases, which implies that the ODPA-BOTDA sensor works better at smaller pulse width difference. While in the BOTDA sensor, because of the combination of the CW-pulse interaction and CW-CW leakage interaction, the linewidth of the Brillouin spectrum first increases and then decreases as the pulse width decreases. Furthermore, the linewidth of the Brillouin spectrum in the ODPA-BOTDA sensor with 20/19ns pulse pair is around 36MHz

which is even smaller than the linewidth of the Brillouin spectrum in the BOTDA sensor with 20ns pulse. That the linewidth of the Brillouin spectrum in the ODPA-BOTDA sensor is narrower than that in the BOTDA sensor is further investigated in the following.

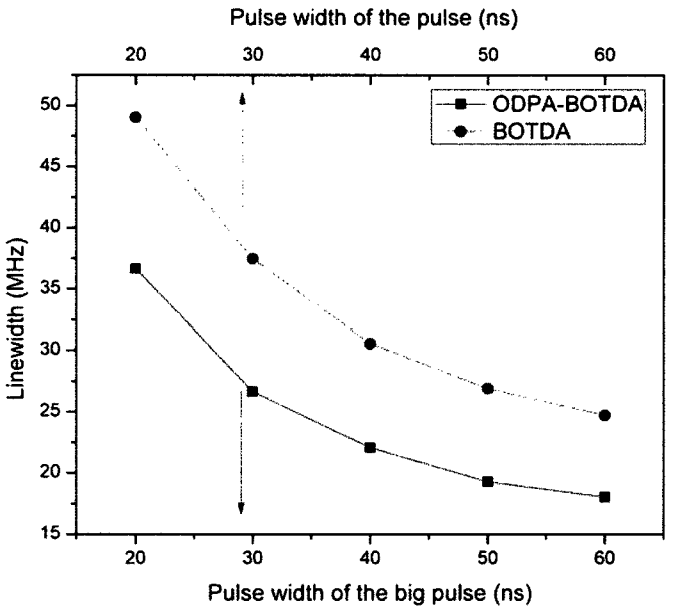

(a)

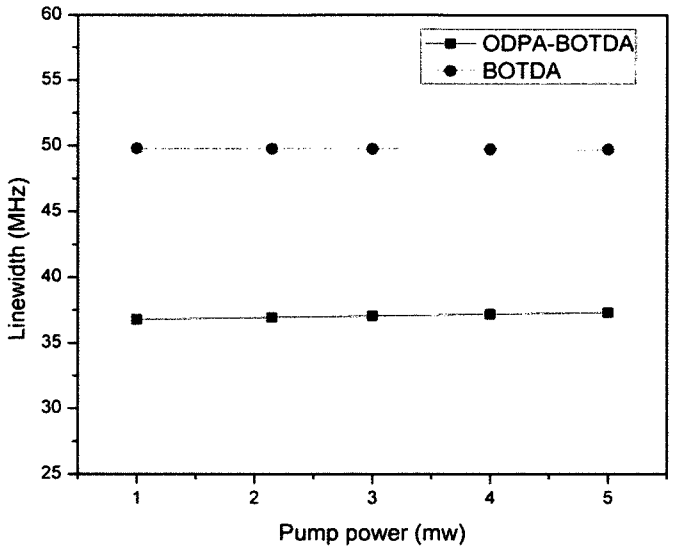

(b)

Fig 6.1.4: Linewidth of the Brillouin spectrum comparison between the BOTDA sensor and the ODPA-BOTDA sensor (Simulation).

(a) Linewidth vs. pulse width in the BOTDA sensor and linewidth vs. pulse width of the big pulse in the ODPA-BOTDA sensor.

(b) Linewidth vs. pump power in the BOTDA sensor and the ODPA-BOTDA sensor (pulse width is 20ns in the BOTDA sensor and the pulse pair is 20/18ns in the ODPA-BOTDA sensor).

More simulations results were presented to compare the linewidth of the Brillouin spectrum in the ODPA-BOTDA sensor with that in the BOTDA sensor. Fig. 6.1.4 (a) shows how the linewidth of the Brillouin spectrum changes with the pulse width in the BOTDA sensor and how the linewidth of the Brillouin spectrum changes with the pulse width of the bigger pulse of the pulse pair in the ODPA-BOTDA sensor. The pulse width difference between the big pulse and small pulse in the

ODPA-BOTDA sensor is 2ns. Fig. 6.1.4 (b) shows how the linewidth of the Brillouin spectrum changes with the pump power in both the ODPA-BOTDA sensor and the normal BOTDA sensor. Apparently, for different pulse widths or different pump powers, the linewidth of the Brillouin spectrum in the ODPA-BOTDA sensor is always narrower than the linewidth of the Brillouin spectrum in the normal BOTDA sensor. The narrow Brillouin spectrum in the ODPA-BOTDA sensor is a result of the differential parametric amplification process. In the ODPA-BOTDA sensor the transferred energy in the Brillouin gain process is well-balanced with that in the Brillouin loss process when the pulse width difference is small, thus narrow Brillouin spectrum is obtainable. That the linewidth of the Brillouin spectrum in the ODPA-BOTDA sensor is narrower than that in the BOTDA sensor indicates that the ODPA-BOTDA sensor has higher frequency resolution than the BOTDA sensor.

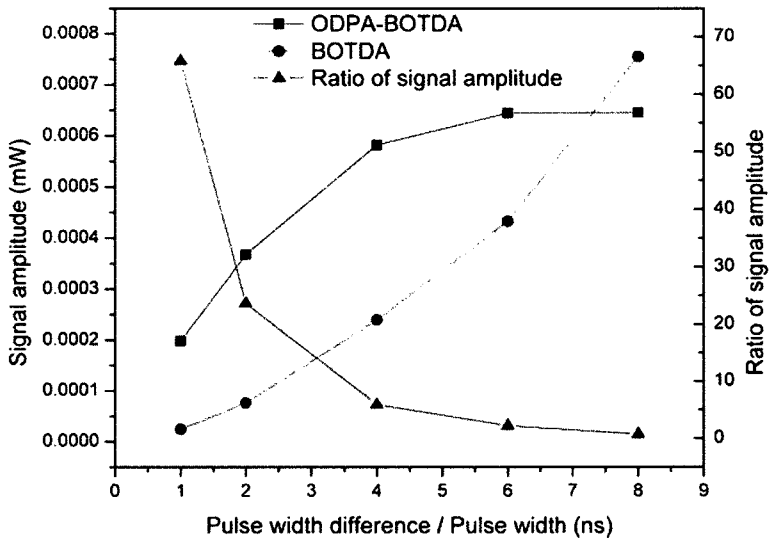

Fig. 6.1.5: Signal amplitude of ODPA-BOTDA and BOTDA vs. pulse width difference / pulse width.

Fig. 6.1.5 includes the following: 1) the signal amplitude versus the pulse width difference in the ODPA-BOTDA sensor, 2) the signal amplitude versus the pulse width in the BOTDA sensor, 3) the ratio of the signal amplitude, which is defined as the signal in the ODPA-BOTDA sensor over the signal in the BOTDA sensor, versus the pulse width. The sensing signal in the ODPA-BOTDA sensor with pulse pair that has 7ns pulse width difference is comparable with that in the BOTDA sensor with pulse that has 7ns pulse width. The sensing signal in the ODPA-BOTDA sensor with pulse pair that has 1ns pulse width difference is 64 times larger than that in the BOTDA sensor with pulse that has 1ns pulse width. Because high spatial resolution corresponds to narrow pulse width in the BOTDA sensor and narrow pulse width difference in the ODPA-BOTDA sensor, thus, the ODPA-BOTDA sensor performs better than the

BOTDA sensor when high spatial resolution is required because the signal in the ODPA-BOTDA sensor with less than 7ns pulse width difference is greater than the signal in the BOTDA sensor with less than 7ns pulse width.

6.2 Experimental Study of the ODPA-BOTDA Sensor

6.2.1 Generation and Separation of the Stokes and Anti-Stokes Waves

The generation of the Stokes and anti-Stokes waves is achieved simply by applying a microwave signal on the EOM [Niklès *et al.* 1996]. This creates sidebands in the laser spectrum as shown in Fig. 6.2.1. When the modulation frequency f_m equals the Brillouin frequency shift ν_B, the first upper side band works as anti-Stokes waves and interacts with the CW sensing wave through Brillouin gain process; the first lower side band works as Stokes waves and interacts with the CW sensing wave through Brillouin loss process. As a matter of fact, by simply sweeping the modulation frequency f_m and recording the intensity of the CW sensing wave, one can determine the Brillouin gain spectrum of the ODPA-BOTDA process. The carrier frequency component is irrelevant to the measurement after the EOM modulation and even has a negative effect on the Stokes and anti-Stokes pulse profile due to the interference between the carrier frequency component and the upper or lower side band frequency component. Thus, the carrier frequency component should be suppressed by adjusting

the DC bias setting of the EOM at the zero transmission point.

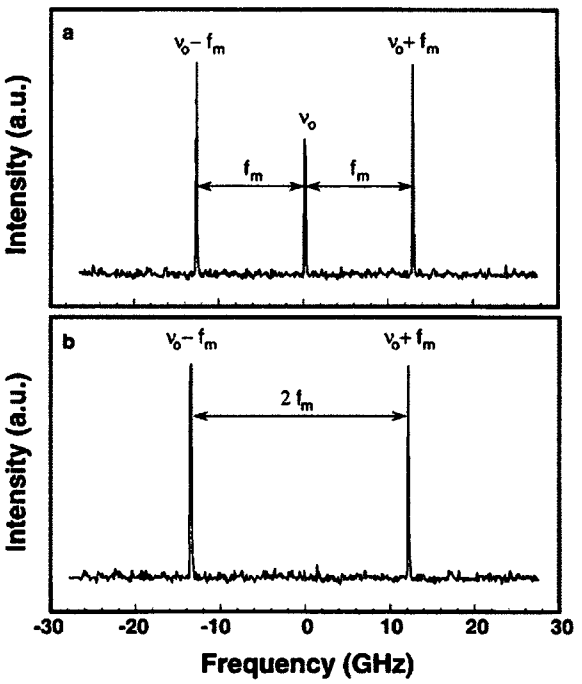

Fig. 6.2.1: Optical spectra of a single frequency laser modulated by: a. an electro-optic carrier and first order sidebands and b. suppression of the carrier by setting the DC bias of the modulator at the zero transmission point. [Niklès *et al.* 1996].

The separation of the Stokes and anti-Stokes waves was achieved by using a fiber Bragg Grating (FBG) [Othonos *et al.* 1999] based narrow band filter and an optical circulator. The configuration of separating the Stokes and anti-Stokes waves is shown in Fig. 6.2.2. The transmitted frequency of the FBG based narrow band filter matches well with the anti-Stokes wave. Thus, the anti-Stokes wave can be transmitted by passing through the FBG based narrow band filter while the Stokes wave is reflected back through an optical circulator.

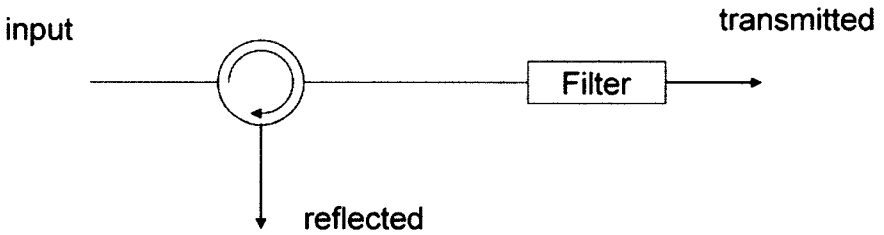

Fig. 6.2.2: Configuration of separating the Stokes and anti-Stokes waves.

Fig. 6.2.3 gives the laser spectrum measured using HP 86142A optical spectrum analyzer before and after the FBG based narrowband filter. The central frequency of the laser source is 1548.98nm. The two side bands generated by using EOM can be clearly seen in Fig. 6.2.3 (a). The contrast between the central frequency component and the side band frequency component is higher than 12dB through adjusting the DC bias setting of the EOM. Fig. 6.2.3 (b) and Fig. 6.2.3 (c) show the reflected and transmitted spectrum after passing the FBG based narrowband filter. The Stokes component and anti-Stokes component are well separated.

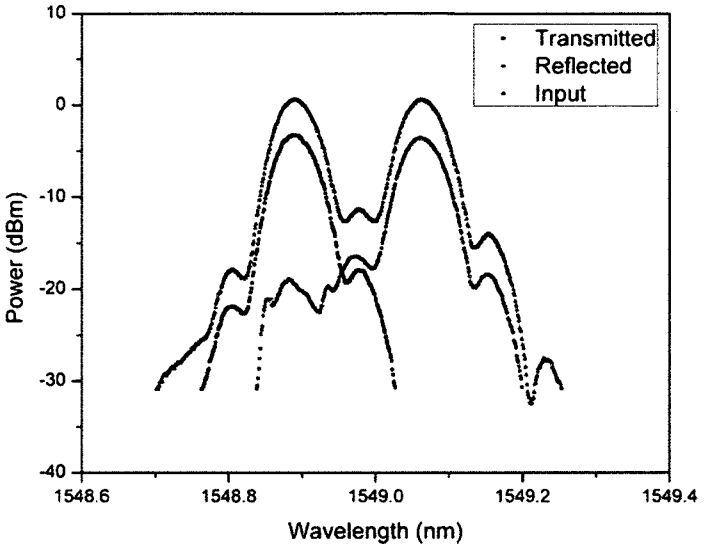

Fig. 6.2.3: (a) laser spectrum with two side bands
(b) Reflected spectrum
(c) Transmitted spectrum

6.2.2 Sensor Configuration

The sensor configuration is shown in Fig. 6.2.4. A DFB laser with a wavelength at 1550nm and an output power at 20mW was used as the laser source. The output light from the DFB laser was split into two parts by a 3dB fiber coupler. One part worked as CW sensing field and was sent to the testing fiber directly. The other part was modulated by an EOM to generate two side bands with the optical carrier suppressed [Niklès *et al.* 1996]. A FBG with a 3dB bandwidth of 2GHz was applied to separate the upper side band and lower side band as described in section 6.2.1. Two optical pulses

with different carrier frequencies and slightly different pulse widths were generated by two EOMs after the FBG. The pulse widths of the two pulses were 20ns and 15ns for anti-Stokes and Stokes signal. After the generation of the Stokes and anti-Stokes pulses, a 3dB fiber coupler was adopted to combine the two pulses together. The combined Stokes and anti-Stokes pulses were then sent to the testing fiber via a circulator. An AC coupled photo detector was used to detect the sensing signal. During the experiment, a PM fiber was used as the testing fiber in order to reduce the signal fluctuation caused by the polarization dependent gain. A 2m strain section with around 1500με, which corresponds to 90MHz Brillouin frequency shift, was made in the middle of the PM fiber.

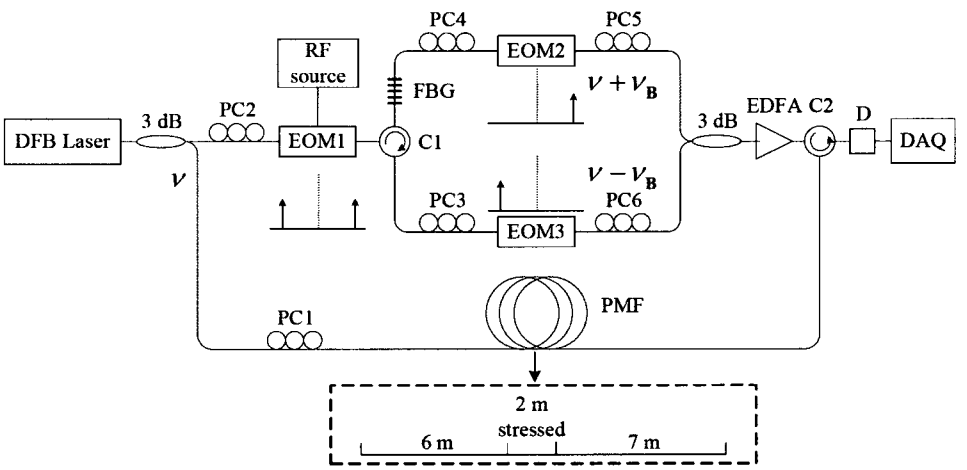

Fig. 6.2.4: Experimental setup of ODPA_BOTDA, C: circulator, PMF: Polarization Maintaining Fiber; EOM: Electro-Optic Modulator, FBG: Fiber Bragg Grating, PC: polarization controller DAQ: Data Acquisition.

6.2.3 Sensor performance

The effectiveness of the spatial and frequency resolution improvement of the ODPA-BOTDA technique is proved in Fig. 6.2.5. Fig. 6.2.5 (a) compares the measured time domain sensing signal of the ODPA-BOTDA sensor with that of the BOTDA sensor. The 2m strain section can be clearly seen in this figure. With the ODPA-BOTDA technique the strain section is shifted by 1.5m that corresponds to the 15ns pulse of the 20/15ns pulse pair. In real field tests, in order to get the correct distributed location information we can simply subtract an amount that is correspondent to the smaller pulse width of the used pulse pair from all the location information. The spatial resolution of the ODPA-BOTDA sensor with 20/15ns pulse pair, which corresponds to the time during which the signal increases from 10% to 90% of its peak value, is around 0.5m and is much smaller than the 2m spatial resolution of the BOTDA sensor with 20ns probe pulse that is measured in the same way as the ODPA-BOTDA sensor. The spatial resolution of the BOTDA sensor with 5ns probe pulse is comparable to that of the ODPA-BOTDA sensor with 20/15ns pulse pair; however the signal amplitude of the ODPA-BOTDA sensor with 20/15ns pulse pair is 5 times greater than that of the BOTDA sensor with 5ns pulse. Because the Brillouin gain increases very slowly during the acoustic wave establishing procedure, 5 ns pulse in the BOTDA sensor can only get very small direct Brillouin gain. However, for 20/15 ns pulse pair with much longer interaction than the phonon lifetime (~10 ns)

in optical fiber, two acoustic waves can be completely built up, so a larger differential gain is expected. The linewidth of the Brillouin gain spectrum in the BOTDA sensor with 5ns pulse is larger than 100 MHz with a relatively large frequency uncertainty because of low SNR. Fig. 6.2.5 (b) gives the measured differential parametric Brillouin gain spectrum of the stressed fiber using the ODPA-BOTDA sensor with 20/15 ns pulse pair. The measured central frequency is 10969MHz that corresponds to the applied strain of around 1500με in the ODPA-BOTDA sensor. The FWHM of the detected Brillouin spectrum in the ODPA-BOTDA sensor is 52MHz which is even narrower than that (~69MHz) in the BOTDA sensor with 20ns probe pulse. This difference is attributed by the parametric amplification of the Brillouin gain and loss simultaneously. Moreover, by doing a Lorentzian fitting to the measured Brillouin spectra, the measured frequency uncertainty of the ODPA-BOTDA sensor is only 0.29MHz, which corresponds to a strain accuracy of 6 με.

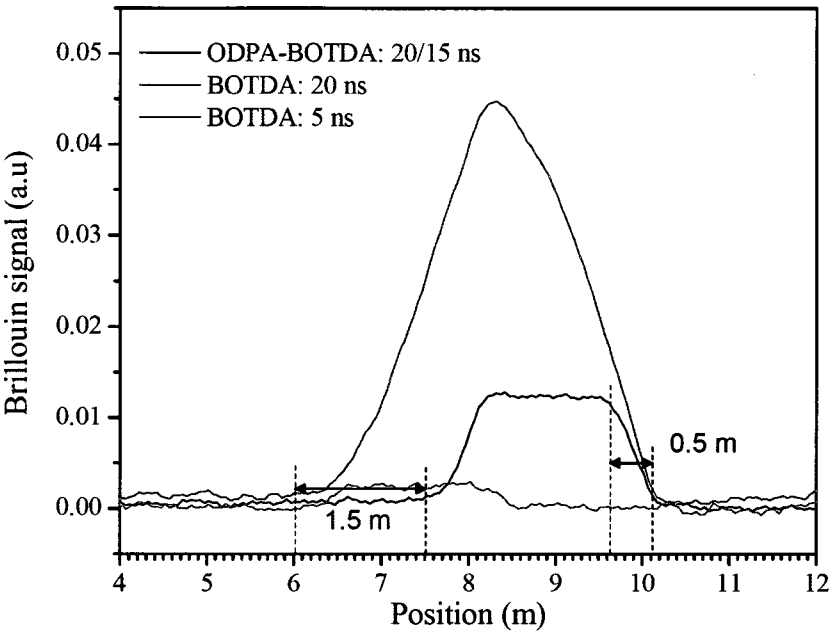

(a)

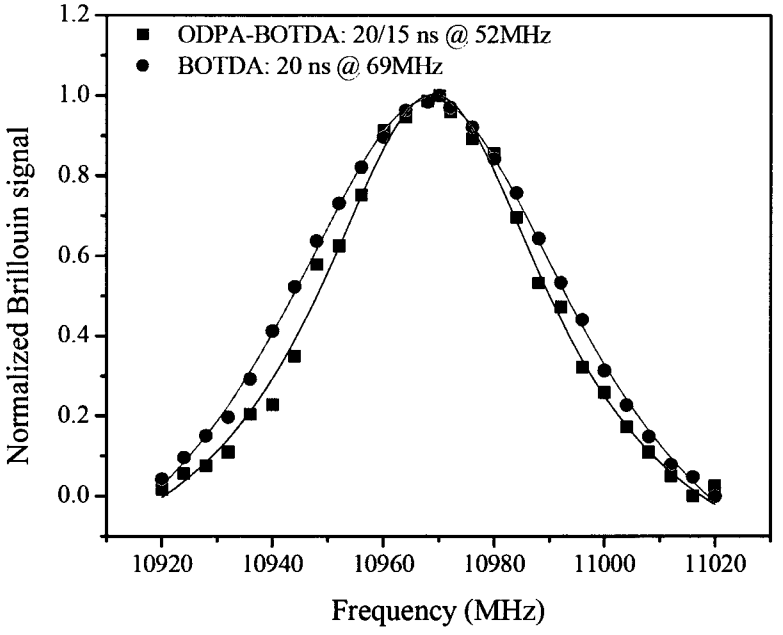

(b)

Fig. 6.2.5: Experimental results: (a) time domain signal of ODPA-BOTDA vs. BOTDA

(b) Brillouin spectrum of ODPA-BOTDA vs. BOTDA

6.3 Conclusion

In conclusion, a novel ODPA-BOTDA sensor is proposed to measure distributed strain and/or temperature changes. This method exhibits high spatial resolution and high frequency resolution simultaneously, while the measurement time and noise is half of that in the DPP-BOTDA sensor. An experiment is successfully realized to justify the proposal in a PM fiber with a spatial resolution of 0.5 m and a strain accuracy of 6 με. Due to the bias drifting of the EOM, the Brillouin gain and loss can not be balanced completely all the time, which can introduce a noise and reduce the SNR. A high spatial resolution and high frequency accuracy can be obtained by precisely controlling the bias and extinction ratio of EOM.

Chapter 7

Conclusion

7.1 Thesis Outcomes

My research mainly focused on improving the spatial and frequency resolution of the distributed fiber sensor based on Brillouin scattering.

We have built a novel distributed Brillouin sensor based on offset locking of two DFB lasers. This offset locking frequency stabilization technique that made use of laser heterodyne source and optical delay line was used to lock and tune the beat frequency of two DFB lasers. A lock-in amplifier was adopted to stabilize the bias drift of EOM. The offset locking based distributed Brillouin sensor that uses cheap and widely adopted devices presents a simple frequency locking method, large tuning range, high SNR, and fast tuning speed. The spatial resolution obtained with this system so far is 1 m with 1 °C temperature resolution. It is therefore promising for the future development of the distributed Brillouin sensor.

From the experimental results of the offset locking based distributed Brillouin sensor, it is evident that the linewidth of the Brillouin spectrum with phase locking technique is narrower than the linewidth of the Brillouin spectrum with only frequency

locking technique. In other words, the frequency resolution of the distributed Brillouin sensor with laser sources phase locked together is higher than the frequency resolution of the distributed Brillouin sensor with laser sources only frequency locked together. A theoretical model has been built and a numerical simulation has been made to prove the capability of narrowing the linewidth of Brillouin spectrum with laser sources phase locking technique.

In order to further increase the spatial resolution and frequency resolution, our group proposed a DPP-BOTDA technique. With the DPP-BOTDA technique, high spatial resolution (<1m) and narrow linewidth of the Brillouin spectrum (<35MHz) can be obtained simultaneously. Numerical simulation and experimental investigation have been performed to investigate the ultimate measurement accuracy in the DPP-BOTDA sensor. In the DPP-BOTDA sensor, high spatial resolution, high frequency resolution, and high SNR can be achieved by utilizing pulse pairs that have large absolute pulse width, small pulse width difference, and short pulse rise/fall time. The ultimate measurement accuracy in the DPP-BOTDA sensor system is determined by the combination of the system bandwidth, system SNR, absolute pulse width, and the pulse width difference.

For the first time to the best of our knowledge, we proposed and built a BOTDA sensor based on optical differential parametric amplification (ODPA) technique. This technique use two optical pulses with slightly different pulse width and different carrier frequency to simultaneously perform Brillouin gain process and Brillouin loss

process with CW pump wave inside the testing fiber. This method exhibits high spatial resolution and high frequency resolution simultaneously, while the measurement time and noise is half of those in the DPP-BOTDA sensor. A spatial resolution of 0.5m and a strain accuracy of 6 με have been obtained with a PM fiber in the experimental validation of this proposal.

7.2 Future Work

Some possible future research directions are presented as follows.

In the distributed Brillouin sensor based on offset locking technique described in chapter 3, a digitizer card and a desktop computer were employed to do the system control and process the data. As stated in chapter 3, the tuning and locking of the beat signal from two DFB laser sources were performed in the following way: the delay time of the optical delay line was changed by the control computer, and then the offset locking system locked the beat signal of the two DFB laser sources at a new frequency corresponding to the new optical delay time. Once the beat frequency was locked, the pump and probe waves performed Brillouin scattering inside the testing fiber. The digitizer card collected the CW pump signal and then sent them to the control computer. Based on our current setup, the measurement time is highly limited by the optical delay line and the digitizer card, and it needs a few minutes to finish one Brillouin spectrum scan. We believe that a fast Brillouin spectrum scan can be

achieved by using a high speed digitizer card, a customized microprocessor and a customized optical delay line, so that we can greatly reduce the tuning time of the optical delay line and the data collection time.

In the ODPA-BOTDA technique, how to obtain two narrow linewidth Stokes and anti-Stokes signals is the key for the system setup. We use a FBG and an optical circulator to separate the Stokes and anti-Stokes signal. The 3dB linewidth of the FBG is 2GHz, which ensures the narrow linewidth of the transmitting signal. However, the linewidth of the reflecting signal is not under control. Another transmitting FBG can be applied to guarantee the narrow linewidth property of the reflecting signal from the first FBG, which would mitigate the interference signal appearing inside the optical pulses due to the narrow linewidth of the Stokes and anti-Stokes waves. Moreover, the Brillouin gain and loss can not be balanced completely all the time because of the bias drifting of the EOM, which could introduce a noise and reduce the SNR. Higher spatial resolution and higher frequency accuracy can be obtained by precisely controlling the bias and extinction ratio of the EOM.

Bibliography

[Afshar 2003] S. V. Afshar, G. A. Ferrier, X. Bao, and L. Chen, "Effect of the finite extinction ratio of an electro-optic modulator on the performance of distributed probe-pump Brillouin sensor systems," *Optics Letters*, 28, 1418-1420 (2003)

[Agrawal 2002] G. P. Agrawal, *Fiber-Optic Communication Systems*, 3rd ed., John Wiley & Sons, Inc.(2002).

[Agrawal 2007] G. P. Agrawal, *Nonlinear Fiber Optics*, 4th ed., Academic Press (2007).

[Alasaarela 2002] I. Alasaarela, P. Karioja, and H. Kopola, "Comparison of distributed fiber optic sensing methods for location and quantity information measurements," *Optical Engineering,* 41, 181-189 (2002).

[Astrom 1995] K. Astrom and T. Hagglund, *PID Controllers: Theory, Design, and Tuning,* 2nd ed. Instrument Society of America (1995).

[Bao et al. 1993a] X. Bao, D. J. Webb, and D. A. Jackson, "22-km distributed temperature sensor using Brillouin gain in an optical fiber," *Optics Letters*, 18, 552-554 (1993).

[Bao *et al.* 1993b] X. Bao, D. J. Webb, and D. A. Jackson, "32-km distributed temperature sensor based on Brillouin loss in an optical fiber," *Optics Letters*, 18, 1561-1563 (1993).

[Bao *et al.* 1995] X. Bao, J. Dhliwayo, N. Heron, D. J. Webb, and D. A. Jackson, "Experimental and theoretical studies on a distributed temperature sensor based on Brillouin scattering," *Journal of Lightwave Technology*, 13, 1340-1348 (1995).

[Bao *et al.* 1999] X. Bao, A. Brown, M. DeMerchant, and J. Smith, "Characterization of the Brillouin-loss spectrum of single-mode fibers by use of very short (<10-ns) pulses," *Optics Letters*, 24, 510-512 (1999).

[Bao *et al.* 2001] X. Bao, M. DeMerchant, A. Brown, T. Bremner, "Tensile and compressive strain measurement in the lab and field with the distributed Brillouin scattering sensor," *IEEE Journal of Lightwave Technology*, 19, 1698-1704 (2001).

[Bao *et al.* 2005] X. Bao, Y. Wan, L. Zou, and L. Chen, "Effect of optical phase on a distributed Brillouin sensor at centimeter spatial resolution," *Optics Letters*, 30, 827-829 (2005).

[Bao *et al.* 2006] X. Bao, Q. Yu, V. P. Kalosha, and L. Chen, "Influence of prolonged phonon relaxation on the Brillouin loss spectrum for the nanosecond pulses," *Optics Letters*, 31, 888-890 (2006).

[Boyd 2003] R. W. Boyd, *Nonlinear Optics*, 2nd ed., Academic Press (2003).

[Boyd 2008] R. W. Boyd, *Nonlinear Optics*, 3rd ed., Academic Press (2008).

[Brown *et al.* 1999] A. W. Brown, M. D. DeMerchant, X. Bao, and T. W. Bremner, "Spatial resolution enhancement of a Brillouin-distributed sensor using a novel signal processing method," *IEEE Journal of Lightwave Technology*, 17, 1179-1183 (1999).

[Brown *et al.* 1999] A. W. Brown, J. P. Smith, and X. Bao, "Brillouin Scattering Based Distributed Sensors for Structural Applications," *Journal of Intelligent Material Systems and Structures*, 10, 340-349 (1999).

[Brown *et al.* 2005] A. W. Brown, B. G. Colpitts, and K. Brown, "Distributed Sensor Based on Dark-Pulse Brillouin Scattering," *IEEE Photonics Technology Letters*, 17, 1501-1503 (2005).

[Chiao *et al.* 1964] R.Y. Chiao, C.H. Townes, and B.P. Stoicheff, "Stimulated Brillouin Scattering and Coherent Generation of Intense Hypersonic Waves," *Physical Review Letters,* 12,592-595 (1964).

[Chu *et al.* 1992] R. Chu, M. Kanefsky, and J. Falk, "Numerical Study of Transient Stimulated Brillouin Scattering," *Journal of Applied Physics*, 71, 4653-4658 (1992).

[Culshaw 2004] B. Culshaw, "Optical fiber sensor technologies: opportunities and-perhapspitfalls," *IEEE Journal of Lightwave Technology*, 22: 39-50 (2004).

[Damzen *et al.* 2003] M. J. Demzen, V. I. Vlad, V. Babin, and A. Mocofanescu, *Stimulated Brillouin Scattering, Fundamentals and Applications*, Institute of Physics Publishing, Bristol and Philadelphia (2003).

[DeMerchant 2000] M. DeMerchant, "Distributed Strain Sensing for Civil Engineering Applications," Ph.D Thesis, University of New Brunswick (2000).

[Deventer *et al.* 1994] M. O. Deventer and A. J. Boot, "Polarization properties of stimulated Brillouin scattering in single-mode fibers," *Journal of Lightwave Technology,* 12, 585-590 (1994).

[Doi *et al.* 2001] Y. Doi, S. Fukushima, T. Ohno, and K. Yoshino, "Frequency stabilization of millimeter-wave sub carrier using laser heterodyne source and optical delay line," *IEEE Photonics Technology Letters*, 13, 1002-1004 (2001).

[Dong *et al.* 2009] Y. Dong, X. Bao, and W. Li, "Differential Brillouin gain for improving the temperature accuracy and spatial resolution in a long-distance distributed fiber sensor", *Applied Optics*, 48, 4297-4301 (2009).

[Fabelinskii, 1968] I. L. Fabelinskii, *Molecular Light Scattering*, Plenum Press, New York (1968).

[Fellay *et al.* 1997] A. Fellay, L. Thevenaz, M. Facchini, M. Nikles, and P. Robert, "Distributed sensing using Brillouin scattering: towards ultimate resolution," *12th International Conference on Optical Fiber Sensors*, 16, 324-327 (1997).

[Fellay *et al.* 2001] A. Fellay, S. Le Floch, M. Facchini, L. Thévenaz, W. Scandale, P. Robert, "Brillouin gain curve measurements in fibers at cryogenic temperatures (3K-140K)," *Proc. of the 6th Optical Fibre Measurement Conference*, Cambridge UK, 55-58 (2001).

[Fox *et al.* 1988] R. F. Fox, I. R. Gatland, R. Roy, and G. Vemuri, "Fast, accurate algorithm for numerical simulation of exponentially correlated colored noise," *Physical Review A*, 38, 5938-5940 (1988).

[Galtarossa *et al.* 2008] A. Galtarossa, L. Palmieri, M. Santaguistina, L. Schenato, and L. Ursini, "Polarized Brillouin Amplification in Randomly Birefringent and Unidirectionally Spun Fibers," *IEEE Photonics Technology Letters*, 20, 1420-1422 (2008).

[Garus *et al.* 1996] D. Garus, F. Schliep, K. Krebber, and T. Golgolla, "Distributed sensing technique based on Brillouin optical-fiber frequency-domain analysis," Optics Letters, 21, 1402-1404 (1996).

[Garus *et al.* 1997] D. Garus, T. Golgolla, K. Krebber, and F. Schliep, "Brillouin optical frequency-domain analysis for distributed temperature and strain measurements," *IEEE Journal of Lightwave Technology*, 15, 654-662 (1997).

[Horiguchi *et al.* 1989a] T. Horiguchi, T. Kurashima and M. Tateda, "Tensile strain dependence of Brillouin frequency shift in silica optical fibers," *IEEE Photonics Technology Letters*, 1, 107-108 (1989).

[Horiguchi *et al.* 1989b] T. Horiguchi and M. Tateda, "Optical-fiber-attenuation investigation using stimulated Brillouin scattering between a pulse and a continuous wave," *Optics Letters*, 14, 408-410 (1989).

[Horiguchi *et al.* 1989c] T. Horiguchi,, and T. Shimizu, T. Tateda, M. Tateda, and Y. Koyamada, "BOTDA-nondestructive measurement of single-mode optical fibers attenuation characteristics using Brillouin interaction: theory," *IEEE Journal of Lightwave Technology*, 7, 1170-1176 (1989).

[Horiguchi *et al.* 1995] T. Horiguchi, K. Shimizu, T. Kurashima, M. Tateda, and Y. Koyamada, "Development of a Distributed Sensing Technique Using Brillouin Scattering, " *IEEE Journal of Lightwave Technology*, 13, 1296-1302 (1995).

[Hotate *et al.* 1999] K. Hotate and T. Hasegawa, "Measurement of Brillouin gain spectrum distribution along an optical fiber with a high spatial resolution using a novel correlation-based technique," *13th International Conference on Optical Fiber Sensors*, Kyongju, Korea, *Proceedings of SPIE*, 3746, 337-340 (1999).

[Hotate *et al.* 2000] K. Hotate and T. Hasegawa, "Measurement of Brillouin gain spectrum distribution along an optical fiber suing a correlation-based technique-Proposal experimental and simulation," *IEICE Transactions on Electronics,* Vol. E83-C, 3, 405-412 (2000).

[Hotate *et al.* 2001] K. Hotate and M. Tanaka, "Correlation-based continuous-wave technique for optical fiber distributed strain measurement using Brillouin scattering with cm-order spatial resolution," *IEICE Transactions on Electronics,* Vol. E84-C, 12, 1823-1828 (2001).

[Hotate *et al.* 2002] K. Hotate and M. Tanaka, "Distributed fiber Brillouin strain sensing with 1-cm spatial resolution by correlation-based continuous-wave technique," *IEEE Photonics Technology Letters,* 14, 179-181 (2002).

[Hotate *et al.* 2003] K. Hotate and S. S. L. Ong, "Distributed dynamic strain measurement using a correlation-based Brillouin sensing system," *IEEE Photonics Technology Letters,* 15, 272-274 (2003).

[Izumita *et al.* 1996] H. Izumita, T. Sato, M. Tateda, Y. Koyamada, "Brillouin OTDR Employing Optical Frequency Shifter Using Side-band Generation Technique with High-Speed LN Phase-Modulator," *IEEE Photonics Technology Letters*, 8, 1674-1676 (1996).

[Jungerman *et al.* 1990] R. L. Jungerman, C. Johnsen, D. J. McQuate, K. Salomaa, M. P. Zurakowski, R. C. Bray, G. Conrad, D. Cropper, P. Hernday, "High-Speed Optical Modulator for Application in Instrumentation," *IEEE Journal of Lightwave Technology*, 8, 1363-1370 (1990).

[Kalosha *et al.* 2006a] V. P. Kalosha, E. Ponomarev, L. Chen, X. Bao, "How to obtain high spectral resolution of SBS-based distributed sensing by using nanosecond pulses," *Optics Express*, 14, 2071-2078 (2006).

[Kalosha *et al.* 2006b] V. P. Kalosha, L. Chen, X. Bao, "Slow and fast light via SBS in optical fibers for short pulses and broadband pump," *Optics Express*, 14, 12693-12703 (2006).

[Kalosha *et al.* 2008] V. P. Kalosha, W. Li, F. Wang, L. Chen, and Xiaoyi Bao, "Frequency-shifted light storage via stimulated Brillouin scattering in optical fibers," *Optics Letters*, 33, 2848-2850 (2008).

[Kersey 1996] A. D. Kersey, "A review of recent developments in fiber optic sensor technology," *Optical Fiber Technology*, 2, 291-317 (1996).

[Koyamada *et al.* 2007] Y. Koyamada, Y. Sakairi, N. Takeuchi, and S. Adachi, "Novel Technique to Improve Spatial Resolution in Brillouin Optical Time-Domain Reflectometry," *IEEE Photonics Technology Letters*, 19, 1910-1912 (2007).

[Kurashima *et al.* 1990] T. Kurashima, T. Horiguchi, and M. Tateda, "Distributed-temperature sensing using stimulated Brillouin scattering in optical silica fibers," *Optics Letters*, 15, 1038-1040 (1990).

[Kurashima *et al.* 1992] T. Kurashima, T. Horiguchi, H. Izumita, S. Furukawa, and Y. Koyamada, "Brillouin optical-fiber time domain reflectometry," Proceedings of *the International Quantum Electronics Conference*, Vienna, 42-44 (1992).

[Kurashima et al. 1993] T. Kurashima, T. Horiguchi, H. Izumita, S. Furukawa, and Y. Koyamada, "Brillouin optical-fiber time domain reflectometry," *IEICE Transactions in communications*, E76-B: 382-390 (1993).

[Lecoeuche *et al.* 2000] V. Lecoeuche, D. J. Webb, C. N. Pannell, and D. A. Jackson, "Transient response in high-resolution Brillouin-based distributed sensing using probe pulses shorter than the acoustic relaxation time," *Optics Letters*, 25, 156-158 (2000).

[Li *et al.* 2003a] G. L. Li and P. K. L. Yu, "Optical Intensity Modulators for Digital and Analog Applications," *IEEE Journal of Lightwave Technology*, 21, 2010-2030 (2003).

[Li *et al.* 2003b]Y. Li, F. Zhang, and T. Yoshino, "Wide-Range Temperature Dependence of Brillouin Shift in a Dispersion-Shifted Fiber and Its Annealing Effect," *Journal Lightwave Technologies,* 21, 1663-1667 (2003).

[Li *et al.* 2008a] W. Li, X. Bao, Y. Li, L. Chen, "Differential pulse-width pair BOTDA for high spatial resolution sensing," *Optics Express*, 16, 21616-21625 (2008).

[Li *et al.* 2008b] Y. Li, X. Bao, F. Ravet, E. Ponomarev, "Distributed Brillouin Sensor System Based on Offset Locking of Two DFB lasers," *Applied Optics*, 47, 99-102 (2008).

[Lounis 2007] Z. Lounis, "Aging Highway Bridges," *Canadian Consulting Engineer*, 48,30-34 (2007).

[Meade 1983] M. L. Meade, *Lock-in amplifiers: principles and applications*, Peter Peregrinus Ltd (1983).

[Mizuno *et al.* 2008] Y. Mizuno, W. Zou, Z. He, and K. Hotate, "Proposal of Brillouin optical correlation-domain reflectometry (BOCDR)," *Optics Express*, 16, 12148-12153 (2008).

[Mizuno *et al.* 2009] Y. Mizuno, Z. He, and K. Hotate, "One-End-Access High-Speed Distributed Strain Measurement with 13-mm Spatial Resolution Based on Brillouin Optical Correlation-Domain Reflectometry," *IEEE Photonics Technology Letters*, 21, 474-476(2009).

[Niklès *et al.* 1994] M. Niklès, L. Thèvenaz, and P. A. Robert, "Simple distributed temperature sensor based on Brillouin gain spectrum analysis," *Proceedings of OFS'94*, Glasgow, Scotland, 138-141 (1994).

[Niklès *et al.* 1996] M. Niklès, L. Thévenaz, and P. A. Robert, "Simple distributed fiber sensor based on Brillouin gain spectrum analysis," *Optics Letters*, 21, 758-760 (1996).

[Okawachi *et al.* 2005] Y. Okawachi, M. S. Bigelow, J. E. Sharping, Z. Zhu, A.

Schweinsberg, D. J. Gauthier, R. W. Boyd, and A. L. Gaeta, "Tunable all-optical delays via Brillouin slow light in an optical fiber," *Physical Review Letters*, 94, 153902 (2005).

[Othonos *et al.* 1999] Andreas Othonos and Kyriacos Kalli, "Fiber Bragg Gratings: fundamentals and application in telecommunications and sensing," Chapter 7 Fiber Bragg Grating Sensors, Artech House Publishers, Inc., 1999.

[Ravet *et al.* 2006] F. Ravet, X. Bao, L. Zou, Q. Yu, Y. Li, V. Kalosha, L. Chen, "Accurate strain detection and localization with Distributed Brillouin Sensor based on a phenomenological signal processing approach," *Proceedings of SPIE*, 6176, 61761C (2006).

[Ravet 2007] F. Ravet, PhD Thesis, University of Ottawa (2007).

[Smith *et al.* 1999] J. Smith, A. Brown, M. DeMerchant, X. Bao, "Pulse width dependence of the Brillouin loss spectrum," *Optics Communications*, 168, 393-398 (1999).

[Snoddy *et al.* 2007] J. Snoddy, Y. Li, F. Ravet, and X. Bao, "Stabilization of electro-optic modulator bias voltage drift using a lock-in amplifier and a proportional-integral-derivative controller in a distributed Brillouin sensor system," *Applied Optics*, 46, 1482-1485 (2007).

[Song *et al.* 2005] K. Y. Song, M. Herráez, L. Thévenaz, "Observation of pulse delaying and advancement in optical fibers using stimulated Brillouin scattering," *Optics Express*, 13, 82-88 (2005).

[Song *et al.* 2006] K. Y. Song, Z. He, and K. Hotate, "Distributed strain measurement with millimeter-order spatial resolutionbased on Brillouin optical correlation domain analysis," *Optics Letters*, 31, 2526-2528 (2006).

[Thévenaz *et al.* 2004] L Thévenaz, S. L. Floch, D. Alasia, and J. Troger, "Novel schemes for optical signal generation using laser injection locking with application to Brillouin sensing," *Measurement Science and Technology*, 15, 1519-1524 (2004).

[Thévenaz 2006] L. Thévenaz, "Review and progress in distributed fiber sensing," 18th International Conference on Optical Fiber Sensors OFS 2007, Cancun (Mexico), Technical Digest of the Optical Society of America, Paper ThC6, 23-27(2006).

[Thévenaz *et al.* 2008] L. Thévenaz, A. Zadok, A. Eyal, and M. Tur, "All-Optical

Polarization Control Through Brillouin Amplification," Proceeding OFC/NFOEC, paper OML7 (2008).

[Walker *et al.* 2008] D. R. Walker, M. Bashkansky, A. Gulian, F. K. Fatemi, and M. Steiner, "Stabilizing slow light delay in stimulated Brillouin scattering using a Faraday rotator mirror," *Journal of Optical Society of American B*, 25, C61-C64 (2008).

[Wang *et al.* 2008] F. Wang, X. Bao, L. Chen, Y. Li, J. Snoddy and X. Zhang, "Using pulse with dark base to achieve high spatial and frequency resolution for the distributed Brillouin sensor, " *Optics Letters*, 33, 2707-2709 (2008).

[Yu, 2006] Q. Yu, Ph.D Thesis, University of Ottawa (2006)

[Zadok *et al.* 2008]A. Zadok, E. Zilka, A. Eyal, L. Thévenaz, and M. Tur, "Vector analysis of stimulated Brillouin scattering amplification in standard single-mode fibers," *Optics Express*, 16, 21692-21707 (2008).

[Zeng *et al.* 2002] X. Zeng, X. Bao, C. Chhoa, T. Bremner, A. Brown, M. DeMerchant, G. Ferrier, A. L. Kalamkarov, A. V. Georgiades, "Strain measurement in a concrete beam using the Brillouin scattering based distributed fibers sensor with single mode fibers imbedded in GFRP rod and bonded to steel reinforcing bars," *Applied Optics*, 41, 5105-5114 (2002).

[Zhu *et al.* 1986] S. Zhu, A. W. Yu, and R. Roy, "Statistical Fluctuations in laser transients," *Physical Review A*, 34, 4333-4347 (1986).

[Zou *et al.* 2005] L. Zou, X. Bao, Y. Wan, and L. Chen, "Coherent probe-pump-based Brillouin sensor for centimeter-crack detection," *Optics Letters*, 30, 370-372 (2005).

Appendix

Excerpt of the simulation code for ODPA-BOTDA sensor in FORTRAN 95

```
!**********************************************************************
!SBS_ODPA.f95
!Created: Feb 3nd, 2009
!Author: Yun Li


PROGRAM SBS_ODPA

  implicit none

  real*8,parameter :: pi=3.141592653589793
  real*8,parameter :: &
        vg=0.2041,&
        alpha=0.0002/4.343,&
        !alpha=0,&
        a=1/vg,&
        b=alpha/2,&
        tao=10,&
        Gamma1=1/(2*tao),&
        gB=5E-14,&
        scal=1e-11,&
        sigma=1.414,&
        delta_t=0.005,&
        delta_z=vg*delta_t,&
        Length=10,&
        t0=2.5*Length/vg,&
        chi1=Gamma1*gB*delta_t*delta_z/4,&
        chi2=Gamma1*(-gB)*delta_t*delta_z/4,&
        A2_A1=0.99684,&
```

```
        pw1=20,&
        pw2=19,&
        Rx=30
  integer,parameter :: stepsize=2
  integer,parameter :: &
        Nmax=Length/delta_z,&
        Mmax=t0/delta_t+(2.5*Length*a)/delta_t,&
        nuB=12800,&
        StartOffset=0,&
        EndOffset=0,&
        numofFreq=(StartOffset+EndOffset)/stepsize+1
  complex*16,parameter :: &
        EpN=(0.1654e6,0.0),&
        Es0_top1=(0.2523e6,0.0),&
        Es0_base1=(0.0000e6,0.0),&
        Es0_top2=(0.2523e6,0.0),&
        Es0_base2=(0.0000e6,0.0)
!------------------------Single variable-------------------------------
  integer :: nu_tuning
  integer :: same
  integer,dimension(0:Nmax-1) :: nuBprofile
  complex*16,dimension(0:Nmax-1) :: Gamma
  integer :: m
  integer :: j
  integer :: which_Freq
  integer,dimension(1:numofFreq) :: Freq
!------------------------Array variable for
loss--------------------------------
  complex*16,dimension(0:Mmax) :: Es0_m1
  complex*16,dimension(0:Nmax-1) :: Ep0_n
  complex*16,dimension(0:Nmax-1) :: &
    phi_m1, &
    psi_m1
  complex*16,dimension(0:Nmax) :: Es_m1,v11,v12,v2
  complex*16,dimension(0:Nmax-1) :: Ep_m
!------------------------Array variable for
gain--------------------------------
  complex*16,dimension(0:Mmax) :: Es0_m2
  !Boundary values of the Es at z=0 at all time indices
  complex*16,dimension(0:Nmax-1) :: &
    phi_m2, &
```

```
    psi_m2
  complex*16,dimension(0:Nmax) :: Es_m2
!------------------------Matrix variable-------------------------------
  complex*16,dimension(0:Nmax-1) :: Q0
  complex*16,dimension(0:Mmax) :: Ep0=(0.0,0.0)
  logical :: new
  character*5 :: stringN
  character*150  :: nameString
  character*150, save :: filenameEp
!-----------------End of the variable declaration----------------------
!================The main program=====================================
!----------------Initiate variables at the very begining--------------
   call getFrequencies()
   call setEp0_n()
   call getnuBprofile()
   call setEs0_m1()
   call setEs0_m2()

   same=0
   new=.TRUE.
   LoopFreq: do which_Freq=1,numofFreq,1
      nu_tuning=Freq(which_Freq)
      call getGamma()

      filenameEp='/fiber_home/09051201'&
                 //nameString//'.dat'
      open(unit=12,file=filenameEp,status='new',action='write')
      call Initialization()

      LoopTime: do m=1,Mmax
         write(*,*) 'Now runs the m=',m,'loop at frequency:',nu_tuning
         Es_m1(0)=Es0_m1(m)
         Es_m2(0)=Es0_m2(m)
         do j=0,Nmax-1
            v2(j)=a*delta_z*Ep_m(j)/delta_t
         end do

         do j=Nmax-1,0,-1
            if(j==Nmax-1) then
Ep_m(j)=(EpN+v2(j)-chi1*phi_m1(j)*Es_m1(j)-chi2*phi_m2(j)*Es_m2(j)&
                    )/(1+a*delta_z/delta_t+b*delta_z+&
```

```
chi1*Es_m1(j)*conjg(Es_m1(j))+chi2*Es_m2(j)*conjg(Es_m2(j)))
              else
Ep_m(j)=(Ep_m(j+1)+a*delta_z*Ep_m(j)/delta_t-chi1*phi_m1(j)*Es_m1(j)&
-chi2*phi_m2(j)*Es_m2(j))/(1+a*delta_z/delta_t+b*delta_z+&
chi1*Es_m1(j)*conjg(Es_m1(j))+chi2*Es_m2(j)*conjg(Es_m2(j)))
              end if
           end do
           do j=0,Nmax-1
              v11(j)=a*delta_z*Es_m1(j)/delta_t
              v12(j)=a*delta_z*Es_m2(j)/delta_t
           end do
           do j=0,Nmax-1
Es_m1(j+1)=(1-a*delta_z/delta_t+chi1*Ep_m(j)*conjg(Ep_m(j))-b*delta_z)*
Es_m1(j)+v11(j)+chi1*psi_m1(j)*Ep_m(j)
Es_m2(j+1)=(1-a*delta_z/delta_t+chi2*Ep_m(j)*conjg(Ep_m(j))-b*delta_z)*
Es_m2(j)+v12(j)+chi2*psi_m2(j)*Ep_m(j)
           end do
           Ep0(m)=Ep_m(0)
           write(12,'(E24.12,1X)') abs(Ep0(m))**2
           if(m<Mmax) call updateAll(m)
        end do LoopTime
        close(12)
    end do LoopFreq
!=====================================================================
END PROGRAM TransientSBS_gainloss
```

The simulation code for generating the coloured Gaussian noise in FORTRAN 95

```
PROGRAM colorgauss
  real*8,allocatable :: eps(:,:)
  real*8 :: cgauss,mean
  real*8 :: dt,cortim,x
  integer :: nreal,nstep,i,j
  character*150, save :: filenameNo
  integer :: Openstatus, OutputStatus
```

```
   nreal=1
   nstep=20
   dt=1
   cortim=2.5

   filenameNo='/phase.dat'

open(unit=1,file=filenameNo,status='new',action='write',iostat=Openstat
us)
   allocate(eps(nreal,-1:nstep*2))

   call cgaus0(dt,cortim)

   do i=1,nreal
      do j=0,nstep*2
         eps(i,j)=cgauss()
         write(*,*) eps(i,j)
      end do
   end do

   npts=nstep*nreal
   do idly=0,nstep
      mean=0
      do i=1,nreal
         do j=0,nstep
            mean=mean+eps(i,j)*eps(i,j+idly)
         end do
      end do
      mean=mean/npts
   end do
   close(1)
   deallocate(eps)

END PROGRAM colorgauss
!=======================================================================
subroutine cgaus0(dt,cortim)
   real*8 :: cape,dt,me2,cgauss,cortim,x
   common /color/ me2,cape

   cape=exp(-dt/cortim)
```

```
   me2=-(1-cape*cape)*(2/cortim)
   x=cgauss()

   return
end subroutine cgaus0

!-----------------------------------------------------------------------
real*8 function cgauss()
   integer iset
   real*8 :: fac,gset,rsq,v1,v2,me2,h,cape,prev
   common /color/ me2,cape

   save iset,gset,prev
   data iset /0/
   data prev /0.0/

   if(iset .eq. 0) then
1     call random_number(v1)
      v1=2*v1-1
      call random_number(v2)
      v2=2*v2-1
      rsq=v1**2+v2**2
      if(rsq.ge.1 .or. rsq.eq.0) goto 1

      fac=sqrt(me2*log(rsq)/rsq)
      gset=v1*fac
      h=v2*fac
      iset=1
   else
      h=gset
      iset=0
   end if

   cgauss=h

   return
end function cgauss
```

Curriculum Vita

Full name Yun Li

Education

Ph.D 2004-2010

Department of physics, University of Ottawa, Canada
Supervisors: Dr.Xiaoyi Bao and Dr.Liang Chen

B.Sc 2000-2004
Department of Optoelectronic Engineering
Huazhong University of Sci. & Tech, China

List of Publications

Journal Papers

Li Yun; Bao Xiaoyi; Ravet Fabien; Ponomarev Evgueni, "Distributed Brillouin sensor system based on offset locking of two distributed feedback lasers," *Applied Optics*, 47, 99-102 (2008).

Snoddy Jeffrey; **Li Yun**; Ravet Fabien; Bao Xiaoyi, "Stabilization of electro-optic modulator bias voltage drift using a lock-in amplifier and a proportional-integral-derivative controller in a distributed Brillouin sensor system," *Applied Optics*, 46,1482-1485 (2007).

Wenhai Li, Xiaoyi Bao, **Yun Li** and Liang Chen, "Different pulse-width pair Brillouin optical time domain analysis (DPP-BOTDR) for high spatial resolution sensing," *Optics Express*, 16, 21616-21625 (2008).

Fabien Ravet, Xiaoyi Bao, **Yun Li**, Quinrong Yu, Alexandre Yale, Vladimir Kalosha, and Liang Chen, "Signal processing technique for the distributed Brillouin sensor at centimeter spatial resolution," *IEEE Journal of Lightwave Technology*, 25, 3610-3618 (2007).

Fabien Ravet, Xiaoyi Bao, Jeff Snoddy, **Yun Li**, Liang Chen, "Characterization of Brillouin fiber generator and amplifier for optimized working condition of distributed sensors," *Optical Fiber Technology*, 15, 304-309(2009).

Feng Wang, Xiaoyi Bao, Liang Chen, **Yun Li**, Jeffrey Snoddy and Xuping Zhang, "Using pulse with dark base to achieve high spatial and frequency resolution for the distributed Brillouin sensor," *Optics Letters*, 33, 2707-2709(2008).

Conference presentations

Yun Li, Xiaoyi Bao, Jeffrey Snoddy, and Liang Chen, "Brillouin spectrum narrowing in high extinction ratio nanosecond pulse from phase locked DFB lasers," *Photonic North, Proc. Of SPIE*, 7386, 73861F (2009).

Xiaoyi Bao, Wenhai Li, **Yun Li** and Liang Chen, "Distributed fiber sensors based on stimulated Brillouin scattering with centimeter spatial resolution," *International Conference of Optical Instrument and Technology (OIT'08)*, 7158-219(2008).

F. Wang, X. Bao, **Y. Li**, L. Chen, X. Zhang, "Reverse peak of Brillouin spectrum in BOTDA sensor," *International Conference of Optical Instrument and Technology (OIT'08)*, 7158-68 (2008).

Yun Li, Xiaoyi Bao, Lufan Zou, Fabien Ravet, "The distributed Brillouin sensor system based on offset locking two DFB lasers", *6th Asia-Pacific Conference, Proc.Of SPIE*, 6595, 65952T(1-6) (2007).

Xiaoyi Bao, **Yun Li**, Fabien Ravet, Evgieni Ponomarev, Lufan Zou, "The distributed Brillouin sensor based on offset locking of two DFB lasers," *1st World Forum on Smart Materials and Smart Structures Technology (SMSST '07)*(2007).

Jeff Snoddy, **Yun Li**, Ziyi Zhang, Wenhai Li, Xiaoyi Bao, "Polarization based fiber optic vibration sensor for structural health monitoring of civil structures," *ISIS*, poster presentation, Newfoundland, Canada (2007).

Yun Li, Fabien Ravet, Lufan Zou, Xiaoyi Bao, and Liang Chen, "1550nm distributed fiber optic Brillouin sensor system," *ISIS*, poster presentation, Calgary, Canada (2006).

Evgueni Ponomarev, **Yun Li**, Liang Chen, and Xiaoyi Bao, "Frequency stabilization of two 1550nm DFB lasers for distributed fiber optic Brillouin sensor system," *ISIS*, poster presentation, Ottawa, Canada (2005).

Patents

Xiaoyi Bao, Evgueni Ponomarev, **Yun Li**, Fabien Ravet, Lufan Zou, Omur M. Sezerman, "Distributed Brillouin sensor system based on DFB lasers using offset locking," United States Patent 7499151